"Effect of Combined Low Salinity and Surfactant Injection on Oil Recovery in Aged Bentheimer Sandstones at Different Temperatures"

Solveig Riisøen

Master Thesis
Petroleum Technology – Reservoir Chemistry

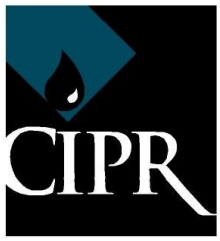

Department of Chemistry
Centre of Integrate Petroleum Research (Uni CIPR)
University of Bergen
June 2012

Acknowledgement

The experimental work present in this study has been carried out at the Centre of Integrated Petroleum Research (CIPR), at the University of Bergen, during 2010-2012. I want to acknowledge CIPR for providing both research facilities and knowledge sharing from CIPR employees.

I would like to express my gratitude towards my supervisor Professor Harald Høiland and co-supervisor Professor Arne Skauge, for their guidance and support during the work on this thesis.

Special thanks to Behruz Shaker Shiran for his support, discussions and counselling with both the experimental equipment and the writing process. I am also grateful for the advices and contributions from Jonas Solbakken.

Furthermore, many thanks to all my friends and graduate students at CIPR, especially Aina Marie Løkkevik, Katrine Bergøy, Katrine Slotnæs, Ragnhild Østensen and Jeelaja Kaliyugarasan, for being there for me, both socially and academically. A special appreciation goes to Elise Kvåle Perttamo for being an inspiration and contributor to a positive environment.

Finally, I would like to thank friends and family for all their support and encouragement through my years as a student. Especially thanks to my best friend Kristine Høstmark and my boyfriend Kristian Gundersen for their outstanding support and motivation.

Solveig Riisøen

Bergen, May 2012

Abstract

A moderate increase in crude oil recovery by reduction in salinity of the injection brine has been observed for numerous laboratory core flood experiments. The underlying mechanisms behind increased recovery by low salinity injection are not fully understood and are suggested to relate to complex crude oil/rock/brine interactions. Recent studies have also shown a positive effect by combining injection of low salinity brine and surfactant flooding.

In this study, core experiments were conducted in four aged Bentheimer cores; two experiments were performed at 23°C and two experiments at 90°C. During low salinity and low salinity surfactant injection pH of the effluent was measured. In addition, density, viscosity and interfacial tension of the fluids injected were analysed.

The results show a marginal potential of enhanced oil recovery by low salinity injection (less than 2 %OOIP). No fines or pH variation were observed during low salinity injection. The low potential of low salinity was suggested to be related to the small clay content and insufficient wettability alteration in the Bentheimer sandstone cores.

Combination of low salinity and surfactant injection resulted in significant increase in oil recovery (additional 26% OOIP). The effect of temperature gave lower recovery at 90°C. A reduction in pH was also observed, suggesting hydrolysis of the surfactant at elevated temperature.

Despite the insignificant response to low salinity brine, a combination with a surfactant may be more beneficial both to increase oil recovery and to be more economically than low salinity brine and surfactant flooding alone.

Nomenclature

Variables

μ	viscosity, Pa·s (1 Pa·s = 10^3 cP)
A	cross-sectional area, m^2
c	concentration, M
d	diameter, m
dP	differential pressure, Pa
E	displacement efficiency, dimensionless
F	force, N
g	the gravitational constant, 9.80665 m/s^2
I_{w-o}	wettability index, dimensionless
K	absolute permeability, m^2 (1 D = $0.98692 \cdot 10^{-12}$ m^2)
ke	effective permeability, m^2 (1 D = $0.98692 \cdot 10^{-12}$ m^2)
kr	relative permeability, dimensionless
L	length, m
m	mass, kg
M	mobility ratio, dimensionless
N	oil reserves, m^3
N_{vc}	capillary number, dimensionless
P	pressure, Pa (1 mmHg = 133.322 Pa)
P_c	capillary pressure, Pa
PV	pore volume, m^3
q	rate, m^3/s
R	radius, m
S	saturation, dimensionless
T	temperature, °C
T	period, s^{-1}
V	volume, m^3
z	ion charge, dimensionless
Θ	contact angle, °
λ	mobility, $m^2/(Pa \cdot s)$

ρ	density, g/m^3
σ	interfacial tension, N/m^2
τ	shear stress, Pa
ϕ	porosity, dimensionless
ω	velocity of rotation, rpm
$\dot{\gamma}$	shear rate, s-1

Subscript

0	end point
A	areal
b	bulk
c	critical
D	microscopic
dead	dead volume
H	head
HC	hydrocarbon
i	initial
i	ionic species
j	fluid phase
L	liquid
m	matrix
o	oil
p	pore
p	produced
r	residual
s	solid
V	vertical
Vol	volumetric
w	water
x	x-direction
y	y-direction

Abbreviations

AN	acid number of oil
B1	Bentheimer core sample 1
B2	Bentheimer core sample 2
B3	Bentheimer core sample 3
B4	Bentheimer core sample 4
BN	base number of oil
CDC	capillary desaturation curve
CMC	critical micelle concentration, M
COBR	crude oil/rock/brine system
CP	cone plate
cryo-SEM	cryo-scanning-electron-microscope
DC1	diluted crude oil conducted in B1 and B4
DC2	diluted crude oil conducted in B2 and B3
DG	double gap
DLVO	Deryaguin, Landau, Verwey and Overbeek
e.g.	for example (exempli gratia)
et al.	and others (et alli)
EOR	enhanced oil recovery
FW	fractionally wet
HSW	high salinity waterflood
i.e.	in other words (id est)
IFT	interfacial tension
IOR	increased/improved oil recovery
LS	low salinity
LSE	low salinity effect
LS-S	low salinity surfactant
LSW	low salinity waterflooding
MIE	multicomponent ionic exchange
MWL	mixed wet, large pores are oil-wet
MWS	mixed wet, small pores are oil-wet
OOIP	oil original in place
ppm	parts per million

PSD	pore size distribution
RB	reservoir brine
REV	representative elementary volume
rpm	rounds per minute
SARA	saturates, aromatic, resins and asphaltenes analysis
SSW	synthetic sea water
SWCTT	single well chemical tracer test
TDS	total dissolved solid
WBT	water break through
XRD	X-ray diffraction

Table of Contents

ACKNOWLEDGEMENT ..... **III**

ABSTRACT ..... **V**

NOMENCLATURE ..... **VII**

1 INTRODUCTION **1**

2 BASIC FLUID AND ROCK PROPERTIES **7**

2.1 Porosity 7
2.2 Absolute permeability, K 7
2.3 Interfacial tension (IFT) 8
2.4 Rock Wettability 9
2.5 Wettability alteration 13
2.6 Effective and relative permeability 14
2.7 Capillary pressure 16
2.8 Density 18
2.9 Fluid viscosity 18
2.10 pH 19
2.11 Ionic strength 20

3 ENHANCED OIL RECOVERY **21**

3.1 Mobility 23
3.2 Residual oil saturation 24
3.3 Capillary number and CDC 27

4 LOW SALINITY WATERFLOODING **29**

4.1 Proposed mechanisms for Low salinity effects 29
4.1.1 Wettability alteration 29
4.1.2 Fines migration 31
4.1.3 pH variation 31
4.1.4 Multicomponent ionic exchange (MIE) 32
4.1.5 Double layer expansion 34
4.2 Summary of field tests 35

5 SURFACTANT **37**

5.1 Properties and characteristics 37
5.2 Surfactant-Brine-Oil Phase behaviour 39
5.2.1 Type II (-) System: 39
5.2.2 Type II (+) System: 40
5.2.3 Type III System: 41
5.3 Hydrolysis 43

6 EXPERIMENTAL EQUIPMENT AND PROCEDURES 45

6.1 CHEMICALS, FLUIDS AND CORE MATERIAL 45
6.1.1 Bentheimer sandstone 45
6.1.2 Synthetic Sea Water (SSW) 48
6.1.3 Low Salinity water (LS) 48
6.1.4 Oils 48
6.1.5 Surfactant 49
6.2 PROCEDURES 50
6.2.1 Core preparations 50
6.2.2 Porosity measurements 51
6.2.3 Permeability measurements 51
6.2.4 Drainage 52
6.2.5 Aging (wettability alteration) 52
6.2.6 Synthetic sea water flooding (SSW) 53
6.2.7 Low salinity (LSW) and low salinity surfactant (LS-S) waterflooding 54
6.2.8 Volume estimations when using Fraction collector 55
6.2.9 S_{or} estimation by Mohr's titration after LS-S 56
6.3 EXPERIMENTAL APPARATUS AND EQUIPMENT 57
6.3.1 Rheometer 57
6.3.2 Densitometer 60
6.3.3 Spinning drop tensiometer 61
6.3.4 pH meter 63
6.3.5 Other experimental equipment 64

7 MAIN RESULTS AND DISCUSSION 67

7.1 FLUID AND ROCK PROPERTIES 67
7.1.1 Density results 68
7.1.1 Interfacial tension results 68
7.1.1 Viscosity results 69
7.1.1 Rock properties 69
7.2 PRODUCTION PROFILES 70
7.3 SYNTHETIC SEA WATER (SSW) FLOODING 73
7.3.1 Observations 73
7.4 LOW SALINITY (LS) WATERFLOODING 75
7.4.1 Oil recovery from LS 75
7.4.2 Observations 75
7.5 LOW SALINITY SURFACTANT (LS-S) FLOODING 78
7.5.1 Residual saturation after LS-S 78
7.5.2 Oil recovery 78
7.5.3 Observations 79
7.5.4 Capillary Desaturation Curve 81

8 CONCLUSION 83

9 FURTHER WORK 85

10 REFERENCES 87

APPENDICES 93

A.1 DENSITY DATA 93
A.2 INTERFACIAL TENSION DATA 94
A.3 VISCOSITY DATA 95
A.4 LENGTH AND DIAMETER OF THE CORE SAMPLES 97
A.5 MOHR'S TITRATION 97
A.6 WATERFLOODING EXPERIMENTAL DATA 98

1 Introduction

Waterflooding is the most widely applied method for oil recovery from petroleum reservoirs. In the past, not much attention has concerned the salinity and the ion composition of the injection water. In recent years, evidences (both laboratory and field tests) have shown that a reduction in the salinity of the injection water, may have impact on the oil recovery [1-26]. Numerous experimental studies have been carried out in order to compare low salinity waterfloods (LSW) to high salinity waterfloods (HSW), see Morrow and Buckley [11] and references cited therein. In secondary waterflood, LSW commence at initial water saturation, S_{wi}, whereas in tertiary waterfloods a LSW follows a conventional HSW.

Early reported observations of the important effects of brine composition in oil recovery dates back to Martin in 1959 [27]. Martin observed an increase in oil recovery by injection of fresh water compared to sea water injection in sandstone core samples. He suggested the increased recovery was due to migration of clay particles.

Almost 10 years later, Bernard (1967) [26] presented results from laboratory experiments showing increased oil recovery by reduction of the salinity of the injection brine. In these experiments, Berea sandstone cores were used, and favourable salinity was found in the range of 0.1-1.0 wt% NaCl. The suggested mechanisms were presented as clay swelling and migration. Unfortunately, this work did not capture the attention of the petroleum industry.

In 1990, Jadhunandan [28] showed that the waterflood oil recovery was dependent on the wettability state of the rock. Based on this, Jadhunandan and Morrow [29] stated that adjustment of the injection brine composition for mature waterflood offers a possible and economically feasible approach to increasing oil production by wettability alteration. Their results were based on more than 50 laboratory waterfloods conducted on Berea sandstone cores using brine with varying salt concentrations.

In 1996, Yildiz and Morrow [9] published their work based on the influence of brine composition on oil recovery in aged Berea sandstone cores. They used two different brines, 4% NaCl + 0.5% CaCl2 (brine 1) and 2% CaCl2 (brine 2). Waterfloods were conducted using either the same brine as both connate and injection water (standard waterflood) or changing the brines during the experiments (mixed-brine waterfloods). Standard waterflood showed higher oil recovery by brine 2 than brine 1 and also a less water-wet condition by using brine 2. Wettability was measured by spontaneous imbibition (Amott method [30]). The highest oil recovery was achieved by mixed-brine waterfloods; initially saturate the cores with brine 2, thereafter using brine 1 as primary injection brine and brine 2 as secondary injection brine.

Extensive research on the effect of brine composition on oil recovery using aged Berea sandstone was carried out by Tang and Morrow [2-7] from 1996-2002. They performed displacement test using different crude oils and diluted the reservoir brine (RB) by factors of 10 and 100. They observed significant increase in oil recovery by reducing the brine composition. Additionally it was observed a wettability alteration by spontaneous imbibition. Based on these results, low salinity effect (LSE) appears to be correlated to the system becoming more water-wet. A 12% reduction in S_{or} was established by secondary LSW in comparison with HSW.

Since the classification of LSW as an improved oil recovery (IOR) process at the SPE/DOE Symposium on IOR in Tulsa in 2006 [11], there has been growing interest of understanding the underlying LSE. This emerging trend has resulted in an increase in experimental work, single well tracer tests and log inject log which in turn resulted in a series of publications, as can be seen in Figure 1.1. Prior to injection of low salinity (LS) water in field tests, an extensive experimental analysis of the reservoir is needed. By conducting laboratory experiments on reservoir cores at reservoir conditions (e.g. temperature and pressure with live fluid), the prospect of LSW may be evaluated. Many of the on-going LSW laboratory and field projects within the oil industry are not reported in the public literature [11].

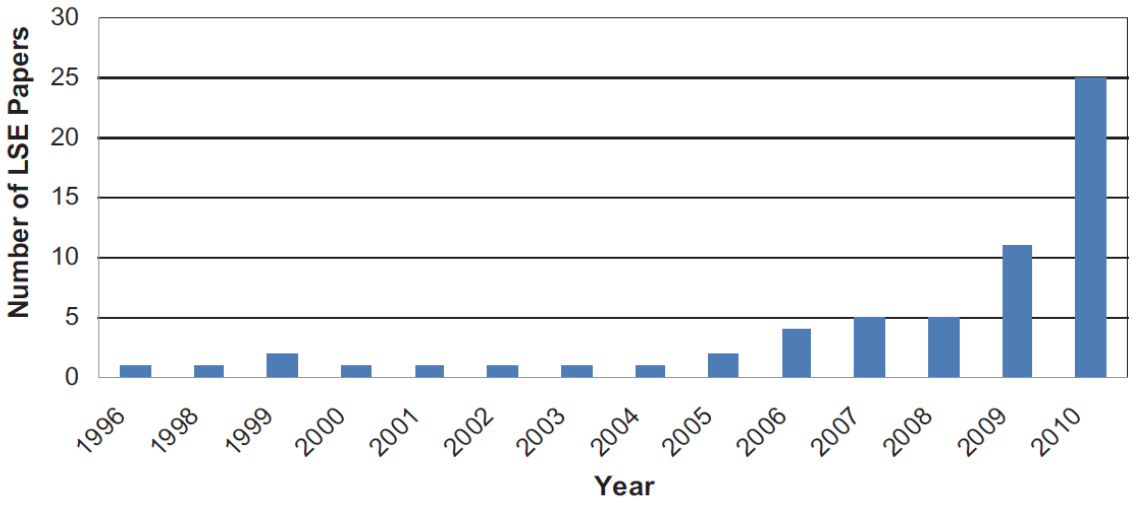

Figure 1.1 **Interest in LSW has increased as indicated by the number of publications and presentations focused on LSE [11]**

A comparison of secondary and tertiary LS recovery in outcrop Berea and reservoir sandstone were conducted by Zhang and Morrow [8]. Both secondary and tertiary LS increased oil recovery was observed. Zhang and Morrow concluded that the rock properties are important aspect in controlling the increase in recovery by injection of low salinity (LS) brine. Another important factor examined was the variation in initial water saturation, S_{wi}. Oil recovery generally increased with S_{wi} for secondary recovery by injection of LS brine. Reservoir core samples showed better respond to LSW compared to outcrop cores. Tertiary LSW on reservoir rock showed a 12% increase in oil originally in place (OOIP).

Zhang et al. [12] studied the effect of injecting LS brine (1500 ppm of RB) and two different concentrations of sodium chloride (8000 ppm and 1500 ppm) into consolidated reservoir sandstone. Each core was tested with two crude oils and one mineral oil. An increase in oil recovery by injection of LS brine was observed for both secondary and tertiary mode (Figure 1.2). There was little or no mineral oil recovery from a mixed wet core by injection of LS brine. Lack of response to injection of 8000 ppm NaCl showed removal of divalent ions and reduction in brine salinity was not sufficient for

tertiary recovery. Injection of 1500 ppm and later addition of divalent ions resulted in sharp increase in oil recovery and pressure drop.

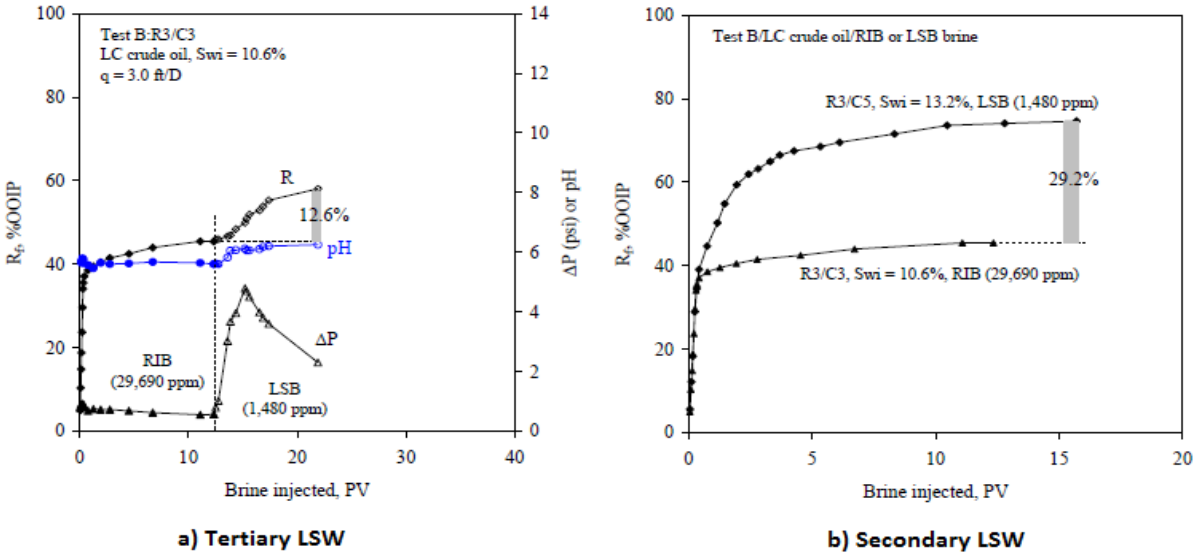

Figure 1.2 **LSW recovery on reservoir sandstone core sample a) Tertiary mode LSW b) Comparison of secondary mode LSW and HSW [12]**

Fully interpreted water/oil relative permeability derived at reservoir conditions comparing HSW and LSW tests with different live oil and brine were presented by Webb et al. [13, 23]. Both secondary and tertiary modes LSW were performed. The core materials applied were selected from several of producing basins across the world. A reduction in oil saturation, S_{or}, was observed in both secondary LSW (a reduction of 21% OOIP compared to HSW) and tertiary LSW (an incremental reduction of 7.5% OOIP). The end point water relative permeability data did not vary significantly between HSW and LSW, in secondary or tertiary modes, except an additional reduction in the oil saturation with LSW.

In 2012, Shiran et al. [25] investigated the effect of wettability on tertiary mode LSW in both Berea and Bentheimer sandstones. LSW experiments showed no increased oil recovery in strongly water-wet Bentheimer core samples and only modest increase in aged Bentheimer core samples. Insignificant oil recovery was observed by LSW in Berea sandstone.

In the abovementioned research the focus has been LS injection in sandstone material. The potential for carbonate reservoirs has been investigated and some reported studies have excluded carbonates from achieving positive LSE [17, 31]. However, in 2008, Saudi Aramco initiated a research program tagged “SmartWater Flood” to explore the potential of increased oil recovery in carbonates by tuning the properties of the injected water. Several studies have been conducted by Yousef et al. [32-37] in which an increase in oil recovery by the use of LS in carbonates was observed. The coreflood experiments were performed at reservoir conditions on Saudi carbonate rocks which showed a 9%

decrease in S_{or} by secondary LSW compared to HSW. In addition a substantial tertiary oil recovery was achieved by stepwise decreasing the salinity of the injection brine. A total decrease in S_{or} was as high as 11.4%. A wettability alteration towards more water-wet after LSW was observed by contact angle measurements.

Based on previous laboratory experiments, LSW may give an increase in oil recovery as high as 42% OOIP depending on crude oil/brine/rock system (COBR) [38]. An incremental oil recovery of 18% OOIP in tertiary mode conducted on sandstone material has been observed [17]. It seems that oil recovery during LSW is higher in secondary mode waterflood compared to tertiary mode [38]. It appears that a more favourable LSE is observed in reservoir rock compared to outcrop rock [8].

Even though some of the necessary conditions for LSE in sandstone are known (stated by Morrow and Buckley [11]) these conditions are not sufficient; many outcrop sandstones meeting these conditions showed no increase in oil recovery during LSW [39, 40]. The fundamental understanding of the mechanisms behind the LSE is not fully recognized, and further research is needed to be able to obtain a better prediction on LSW. Some of the proposed and most accepted mechanisms are further discussed in section 4.1.

Surfactant injection is a common EOR method to obtain an increased oil recovery. By injection of surfactants, the interfacial tension (IFT) between oil and water is reduced, thus leading to mobilization of capillary trapped oil and/or preventing oil from being capillary trapped. The effectiveness of surfactant is based on several factors such as brine concentration (see section 5.2). Another concept of the surfactant process is the economic issues. Surfactants that give low IFT at low salinity are more readily available and less expensive than those utilized in HSW [20]. Moreover, the surfactant retention increases with increasing brine salinity [41].

Based on this, Alagic et al. [18-20] presented a hybrid EOR process combining the effect of LS water injection and surfactant flooding in a low salinity surfactant (LS-S) injection process. The idea is that a more efficient oil recovery process can be obtained by combining destabilisation of oil layers during a LSW with a low IFT environment that prevents re-trapping of these oil layers. Several experiments were conducted on Berea core plugs. The highest recovery was obtained by a tertiary oil recovery of 94.4% of OOIP by LS-S injection, see Figure 1.3. A change in S_{or} from 0.30 (LS) to less than 0.05 (LS-S) was observed. In addition a significantly higher oil recovery was achieved when surfactant solution was introduced into a pre-established LS environment compared to high salinity environment.

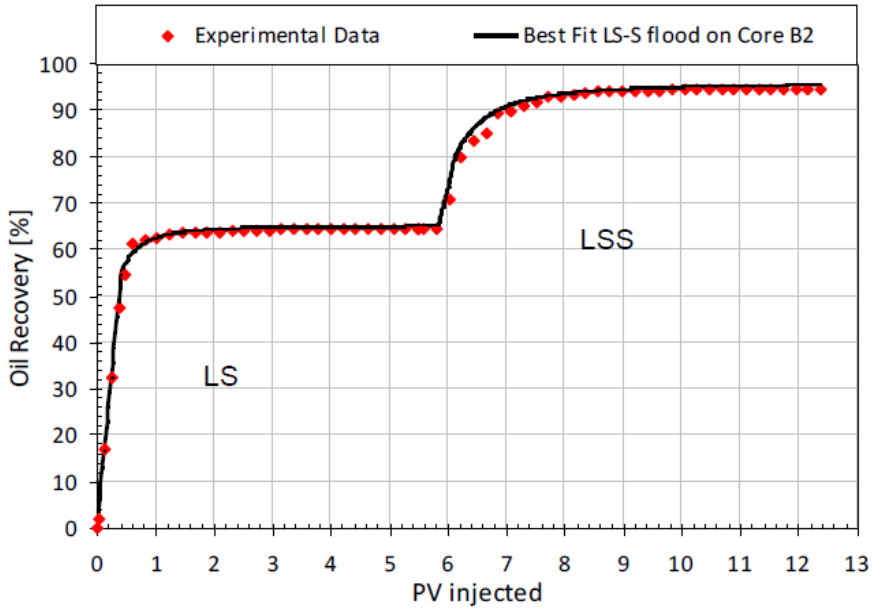

Figure 1.3 **Increased oil recovery by LS and LS-S [19] both experimental data and simulation data.**

The present study compares the effect of combined low salinity and surfactant injection on oil recovery in four aged Bentheimer cores. Tertiary mode LSW was conducted on the core samples, followed by LS-S injection. The waterflooding was carried out at different temperatures (23°C and 90°C). In addition to the main experiments, a thoroughly analysis (density, viscosity and IFT) of the fluid utilized was conducted in order to provide a greater insight to the experiments and a better understanding of the concepts behind waterflooding.

2 Basic fluid and rock properties

In order to understand fluid flow in porous medium, basic concepts and definitions of rock and fluid properties should be investigated. The topics emphasised in this chapter are highly relevant in order to understand the underlying mechanisms behind this study.

2.1 Porosity

The porosity, ϕ, of a rock is defined as the void space of the total volume of the rock. Porosity is of interest in the oil industry because the porosity indicates the possible volume of hydrocarbons present in the reservoir. The porosity can mainly be divided into effective or absolute porosity. Absolute porosity takes into account the total void space (including closed pores). Whereas the effective porosity only consider the interconnected pores as void space. In this thesis the effective porosity is referred to as the porosity and is defined as

$$\phi = \frac{V_p}{V_b}, \qquad \textbf{Equation 2.1}$$

where V_p is the total volume of interconnected pores and V_b is the bulk volume.

Typical for sandstone rocks the porosity is in the range 10-40%, depending on several factors, such as the rock type, its grain size range, grain packing and orientation (fabric), cementation, weathering, leaching and the type, content and hydration of clay [1].

2.2 Absolute permeability, K

The absolute permeability of a porous medium is the mediums capability to transmit fluids through its network of interconnected pores [1]. The absolute permeability is a rock property and is denoted K and is defined through Darcy law (simple form):

$$q = -\frac{K \cdot A}{\mu} \cdot \frac{dP}{L}, \qquad \textbf{Equation 2.2}$$

where q is the flow rate, K is the absolute permeability, A is the cross-sectional area, μ is the viscosity of the fluid, dP is the differential pressure (pressure gradient) and L is the length, see Figure 2.1 .

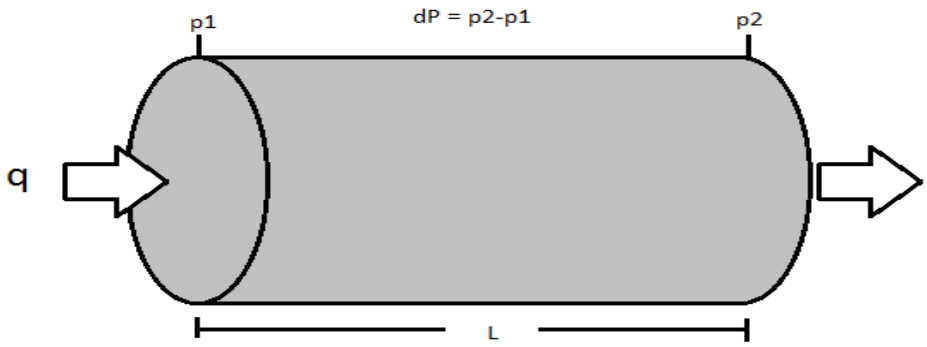

Figure 2.1 **Flow in porous media**

For Darcy law (Equation 2.2) to be valid, the following basic conditions have to be satisfied:

- 100% saturated with only one fluid
- The fluid have to be incompressible (valid for fluids at low pressures)
- The fluid flow have to be laminar (valid assumption for low flow rates) and stationary
- No chemical reaction between the fluid and rock
- Horizontal position of fluid flow (i.e. eliminate the force of gravity)

Rearranging Equation 2.2, the absolute permeability is given as followed:

$$K = -\frac{q \cdot \mu}{A} \cdot \frac{L}{dP}, \qquad \textbf{Equation 2.3}$$

2.3 Interfacial tension (IFT)

Interfacial tension (IFT) occurs between two immiscible phases in contact with each other because a molecule near an interface has different molecular interactions than an equivalent molecule within the bulk phase. A molecule at the surface will also have higher potential energy because of the anisotropy of intermolecular attractions and dynamic interactions. Energy or work is required to move a molecule from the bulk phase to the surface to increase the surface area, A. The surface area is proportional to the potential energy, minimum Gibbs free energy, which means that the surface area of the fluid phase will always be minimized [1].

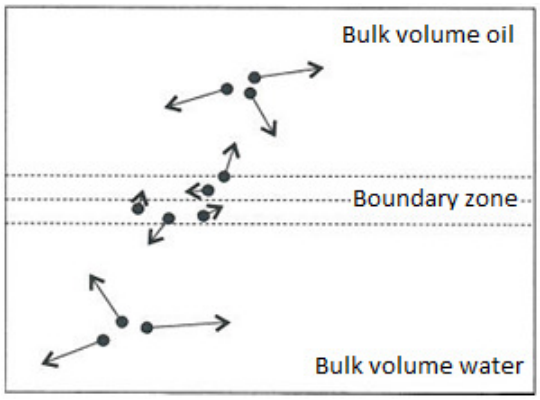

Figure 2.2 **Schematic diagram of a water-oil contact, showing that motion of the molecules in the boundary zone is more limited than the bulk molecules [1]**

For a two-phase fluid system with constant temperature, T, pressure, P, and mass, m, IFT can be defined as:

$$\sigma = \left(\frac{\partial G}{\partial A}\right)_{T,P,m_{1,2}}, \qquad \textbf{Equation 2.4}$$

where G is Gibb's free energy and A is the surface area.

2.4 Rock Wettability

The wettability of a rock can be defined as the tendency of one fluid to spread on or adhere to a solid surface in the presence of other immiscible fluids [42]. When two immiscible fluids are present at the same time near a solid surface, there will be an adhesive force between the molecules in the fluid and the molecules in the solid surface. The fluid with the strongest adhesive force to the solid will be the wetting fluid.

Wettability is an important factor concerning core analysis because it is effecting capillary pressure, relative permeability, waterflood behaviour, dispersion, oil displacement, irreducible water saturation, reducible oil saturation and simulated EOR [1, 43-45].

Classification of reservoir wettability may roughly be divided in to three categories, hence water-wet, oil-wet and intermediate wet. The intermediate-wet can further be divided into three sub-classes based on the fraction of oil wet pores and their distribution, hence fractionally-wet (FW), mixed-wet large (MWL) and mixed-wet small (MWS) [46].

In a strongly water-wet reservoir the water will stick to the solid surface of the pores, and the oil will occupy the centres of the larger pores and only water will occupy the smallest pores (Figure 2.3a). For an oil-wet reservoir oil will preferentially stick to the walls of the pores (Figure 2.3b). Production from a strongly water-wet rock will only produce oil before water break through (WBT) and nearly only water after. For an oil-wet rock there will be a long tail production (long economic two-phase production) after WBT.

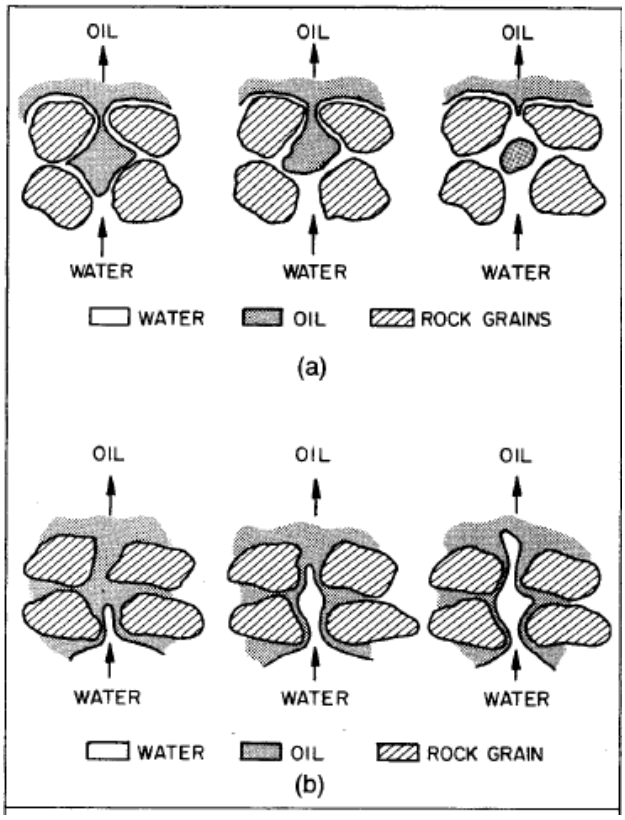

Figure 2.3 **Water displacing oil from a pore during a waterflood: (a) strongly water-wet rock, (b) strongly oil-wet rock [47]**

In a FW system the wettability would be reflected as spot like oil-wet sites on the surface, where the oil-wet pores are uncorrelated to the pore size (Figure 2.4b). The cause of this wetting state could be precipitation and variation in mineralogy and surface shape [46]. One literature example of the existence of FW state was conducted by Jerauld and Rathmell [48] on Prudhoe Bay rock material. From cryo-SEM they observed Dalmatian wettability where there are both oil- and water-wet regions in the same pore. Maximum oil recovery for Prudhoe Bay was found for wettability index, $I_{w\text{-}o}$, equal to zero (neutral-wet).

In a MWL system the largest pores are oil-wet (Figure 2.4c). An literature example of the existence of MWL is the studies of Hamon [49]. He found a weak trend between the amount of clays and

wettability: the larger the clay amount, the more water-wet rock and also the smaller the pores. This indicates a MWL system.

In a MWS system the smallest pores are oil-wet (Figure 2.4a). MWS is regarded as a more unconventional mixed-wet state [46]. An experimental evidence of the existence of MWS was found by Rueslåtten et al. [50] conducting North Sea cores. From Cryo-SEM observations they found remaining oil saturation in small pores and preferentially associated with kaolinite. The highest remaining oil saturation is seen for MWS cases which can be explained by the high capillary forces trapping the oil in the small pores.

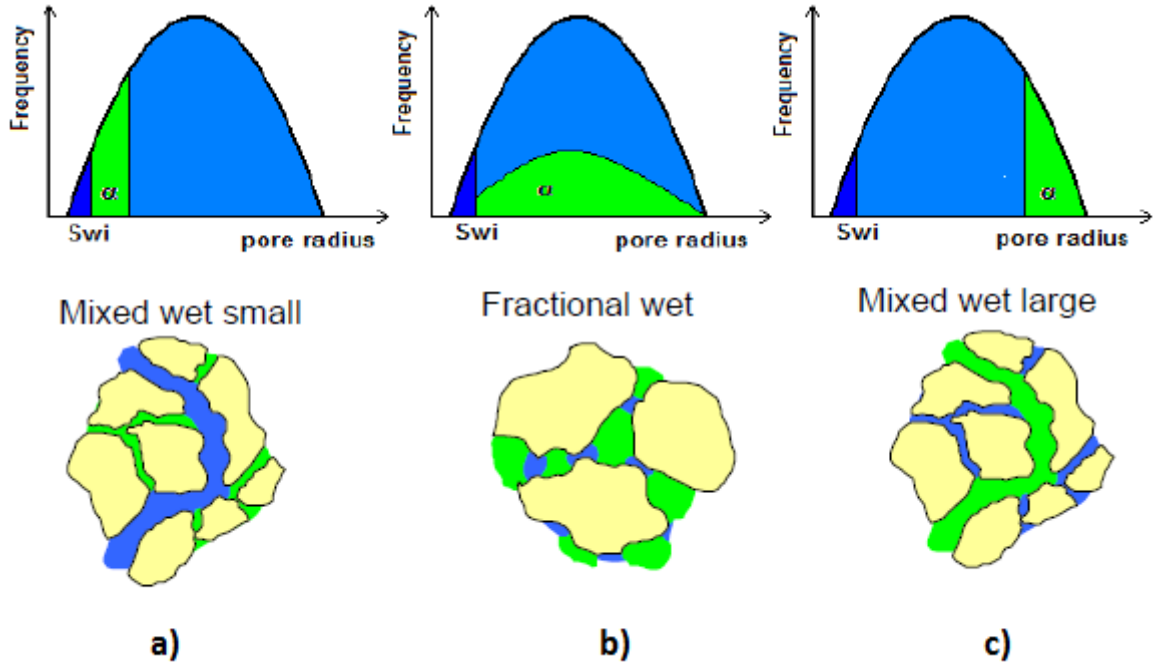

Figure 2.4 **Illustration of the intermediate sub-classes, α is the fraction of oil-wet pores a) mixed-wet small, b) fractional-wet, c) mixed-wet large [51]**

Several laboratory studies have been conducted regarding the effects of wettability on residual oil saturation, S_{or}, during waterflooding. Early studies by Amott [30] indicate that low oil recovery was obtain at both strongly water wet and strongly oil wet, and that higher oil recoveries are obtain in weakly water-wet to neutral wettability conditions. Later studies by Jadhunandan and Morrow [29] presents similar results that a maximum oil recovery is obtained on the weakly water-wet side of neutral (wettability index of 0.2), see Figure 2.5. Jadhunandan and Morrow stated that the higher recovery at near-neutral wettability has intuitive appeal because it can be argued that capillary forces are minimized. Similar studies were also carried out by Skauge and Ottesen [52] and more recently by Ashraf [53]. They showed that the oil recovery peaked at neutral-wet conditions regardless of the injection brines.

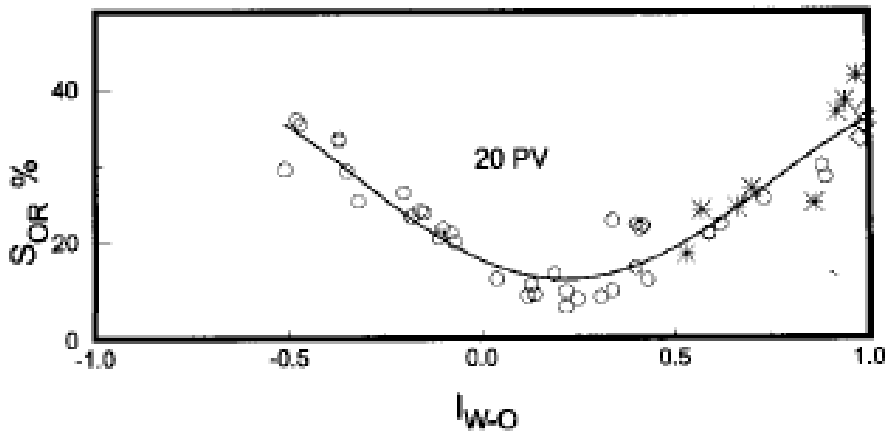

Figure 2.5 **Residual oil saturation as function of wettability index after 20 PV injected. The x-axis represent the wettability index which indicates the wettability state of the system (e.g. I_{w-o}=-1 represents strongly oil-wet, I_{w-o}=0 represents neutral-wet and I_{w-o}=1represents strongly water-wet) [29]**

Another important consideration concerning the effect of wettability on oil recovery is the amount of water injected before reaching the residual oil saturation. It can be seen from Figure 2.6 that oil-wet rock has a longer tail production than a water-wet rock.

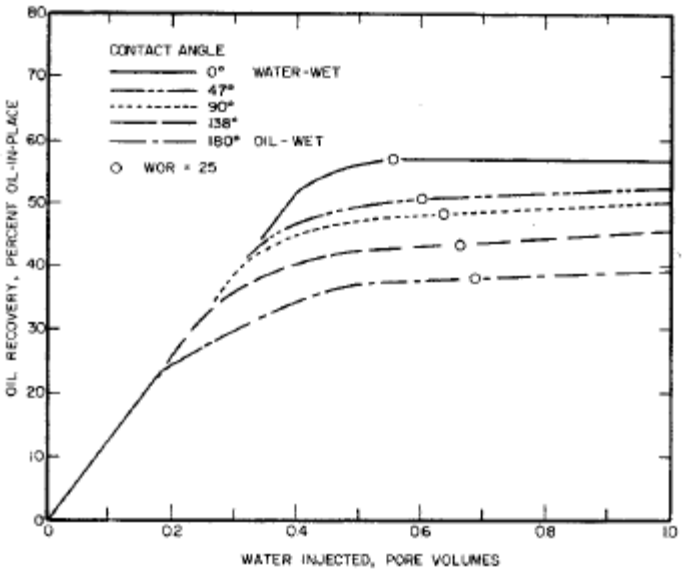

Figure 2.6 **Effect of wettability on waterflood performance calculations [54]**

2.5 Wettability alteration

The wettability of all petroleum reservoirs is initially strongly water-wet, but following migration of oil into the reservoir, the reservoir rock can change from strongly water-wet condition to more oil-wet conditions [43]. It is therefore of interest to establish a wettability condition close to that found in the reservoir.

The wettability alteration of crude oil is due to polar crude oil components being adsorbed on the mineral surface of the rock [43]. The degree of wettability alteration depends on several factors, such as the chemical composition of the oil (the amount of polar components), the brine initially present in the reservoir (amount, composition and pH), the injected brine (composition and pH) and also the lithology of the rock. The composition of the crude oil is important to the wetting alteration in two ways; polar (surface active) components present in the crude oil (especially asphaltenes and resins) and the ability of the oil to be a solvent for the surface active components [55].

Interfaces between crude oil and brine are electrically charged. The charge is depending on the oil components available and the composition of the brine [55]. Buckley et al. [55] reported several mechanisms describing the COBR interactions:

- *Polar interaction* (predominate in the absence of water film between oil and solid). Adsorption of asphaltenes directly from oil onto mineral surfaces (clay mineral). Important factors are the type of clay, nitrogen content of the oil and the ability of oil to be the solvent for the surface active components. Figure 2.7 (a).

- *Surface precipitations*. Dependent mainly on crude oil solvent properties with respect to the asphaltenes. If the oil is a poor solvent for the asphaltenes, the wetting alteration may be enhanced, Figure 2.7 (b).

- *Acid/base interactions*. In the presence of water, both the oil and the mineral interfaces become charged. Polar functional groups belonging to both the mineral and the crude oil phases can behave as acids (giving up a proton and becoming negatively charged) and bases (gaining a proton and becoming positively charged) [55]. Figure 2.7 (c).

- Ion binding. When Ca^{2+} ions are present, several interactions are possible:

  1) oil—Ca^{2+}—oil
  2) mineral—Ca^{2+}—mineral
  3) oil—Ca^{2+}—mineral, see Figure 2.7 (d)

  1) and 2) can limit wettability alteration, whereas 3) can promote it.

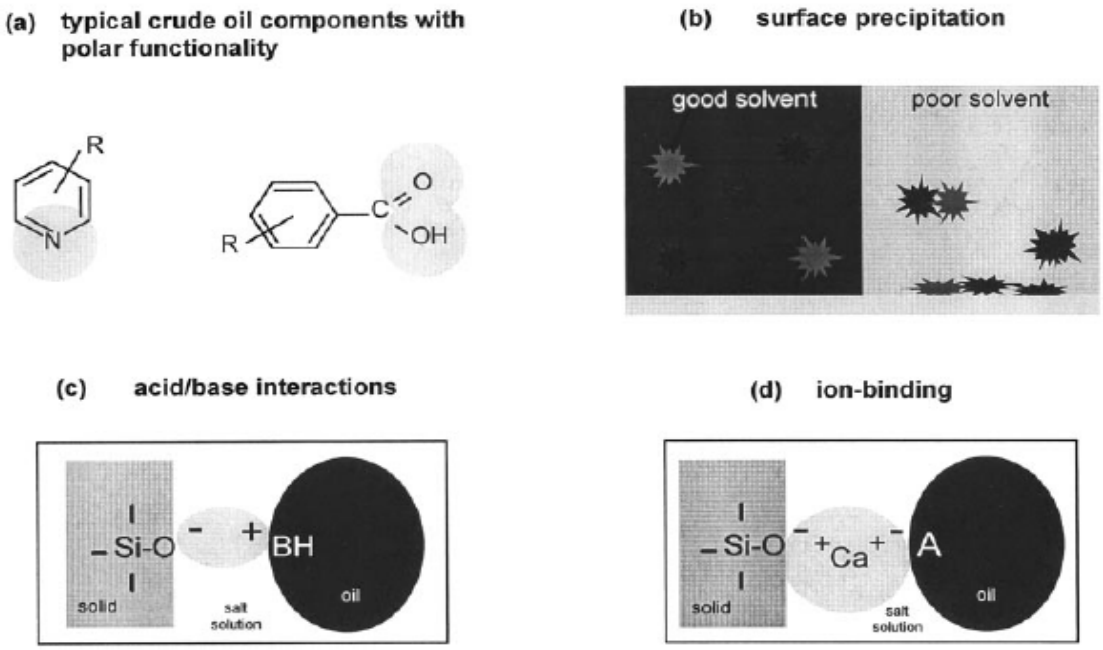

Figure 2.7 **Mechanisms of interaction between crude oil components and solid surfaces [55]**

A systematic study of the effect of initial water saturation, S_{wi}, on wetting behaviour induced by aging core samples in crude oil was performed by Jadhunandan [28]. As indicated by imbibition rate test, the wetting behaviour was influenced by brine composition and S_{wi}. The degree of water-wetness decreased as S_{wi} decreased.

2.6 Effective and relative permeability

In multiphase flow the term effective and relative permeability becomes important concepts. When two or more immiscible fluids are present in the system each of the fluid phase will have its own permeability, i.e. effective permeability. The effective permeability will mainly be dependent on the saturation of the fluid and the location of the other fluids in the rock [56]. In multiphase flow, the Darcy law can be written as followed [1]:

$$q_j = -\frac{k_{ej} \cdot A}{\mu_j} \cdot \frac{dP_j}{L}, \qquad \textbf{Equation 2.5}$$

where j denotes the fluid phase and k_{je} is the effective permeability of phase j.

The relative permeability, k_{rj}, is the ratio of the effective permeability to absolute permeability:

$$k_{rj} = \frac{k_{ej}}{K}, \qquad \textbf{Equation 2.6}$$

where k_{rj} is the relative permeability of phase j, k_{ej} is the effective permeability of phase j, and K is the absolute permeability of the rock.

The relative permeability can be defines as “A direct measurement of the ability of the porous system to conduct one fluid when one or more fluids are present” [42]. The relative permeability is a strong function of saturation (Figure 2.8), but also a function of rock properties and wettability. The wettability of the rock will strongly affect the relative permeability because it controls the location, flow and distribution in a porous medium. Relative permeability is not a strongly influenced by the fluid properties, though when certain properties (e.g. IFT) change drastically, relative permeability can be affected [57].

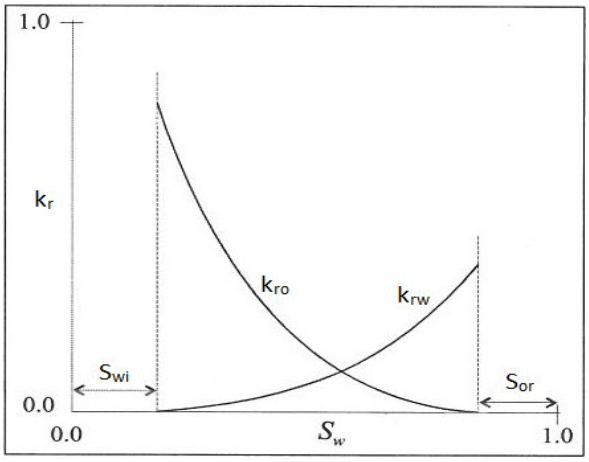

Figure 2.8 Relative permeability curve for a system of oil and water [1]

The structure of typical relative permeability curves are dominated by the wettability of the porous medium. By looking at typical water-oil relative permeability curves for strongly water-wet (left) and strongly oil-wet (right) formations in Figure 2.9, evident differences exists in the two apposite curves:

1. The irreducible water saturation, S_{wi}, is much lower for the strongly oil-wet case. As mentioned, this S_{wi} influence on wetting alteration was also illustrated by Jadhunandan [28].

2. The saturation at which oil and water permeability are equal (crossover saturation) is less than 50% of the water saturation for oil-wet case, and much greater than 50% for the water-wet case.

3. The residual oil saturation, S_{or}, is lower for the strongly water-wet case.

4. Relative permeability to water at maximum water saturation, i.e. endpoint relative permeability to water at residual oil saturation, $k_{rw,Sor}$, is approximately 0.1 and on the other hand for the oil-wet case it is approximately 0.8.

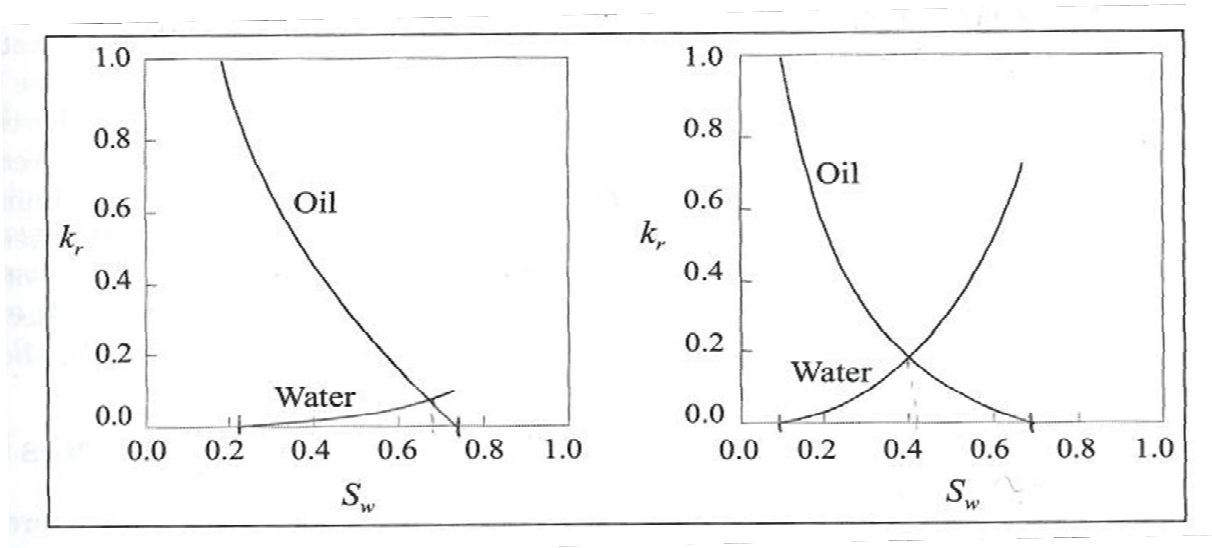

Figure 2.9 **Relative permeability curves. Strongly water-wet system (left) and strongly oil-wet system (right) [1]**

The endpoint relative permeability to water, $k_{rw,Sor}$, are usually less than one and can be used as an indication of the wettability of the system. The non-wetting phase at residual saturation will occur as trapped isolated globes in the centre of the larger pores and will therefore be an obstacle for the wetting phase flow, se Figure 2.3(a). This explains the low relative permeability to water at S_{or}.

In some cases, when a thin irreducible water film covers the pore wall and reduces the friction of the oil flow, the end point relative permeability to oil may exceed one. This concept is also known as the "lubricating" effect [58].

2.7 Capillary pressure

When two immiscible fluids are in contact in the pore networks of a porous medium, a discontinuity in pressure exist across the interface separating them. This pressure difference across the interface is called capillary pressure, P_c, and can be defined by the following equation:

$$P_c = P_{non-wetting} - P_{wetting}, \qquad \textbf{Equation 2.7}$$

Capillary pressure is also the pressure causing fluid to rise in a capillary tube when immersed in the fluid, see Figure 2.10. The capillary pressure can then be defined as

$$P_c = \frac{2 \cdot \sigma \cdot \cos\theta}{R}, \qquad \textbf{Equation 2.8}$$

where σ is the IFT between the two phases in contact, Θ is the wetting angle between the solid surface and the tangent to the interface between the two phases in contact and R is the radius of the capillary tube.

Capillary pressure can also be defined as:

$$P_c = (\rho_w - \rho_o) \cdot g \cdot h = \Delta\rho \cdot g \cdot h, \qquad \textbf{Equation 2.9}$$

where ρ_w and ρ_o is the density of water and oil, respectively and g is the gravitational constant, and h is the height of the fluid rise.

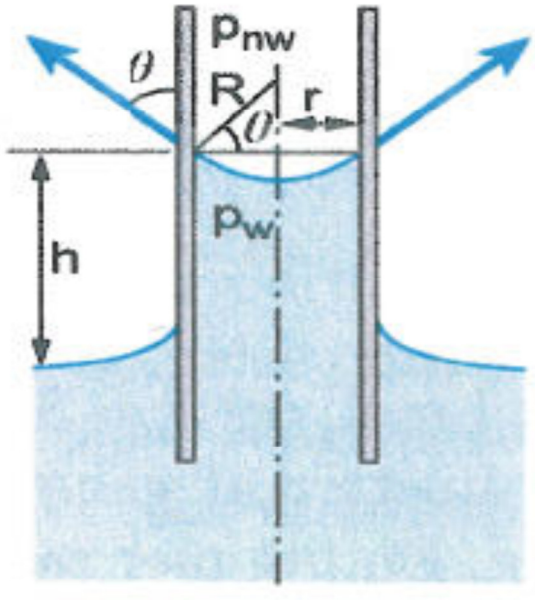

Figure 2.10 Capillary tube submerged in a vessel filled with two immiscible fluids [59]

2.8 Density

Density, ρ, is defined as the mass of the fluid, m_{fluid}, per unit volume,V,

$$\rho = \frac{m_{fluid}}{V}, \qquad \textbf{Equation 2.10}$$

Density normally increases with increasing pressure and decreasing temperature [60].

2.9 Fluid viscosity

Viscosity is defined as the internal resistance of fluid to flow. This study only uses Newtonian fluids, which means that the viscosity is independent of shear rate and that the shear stress is proportional to the shear rate, hence Figure 2.11.

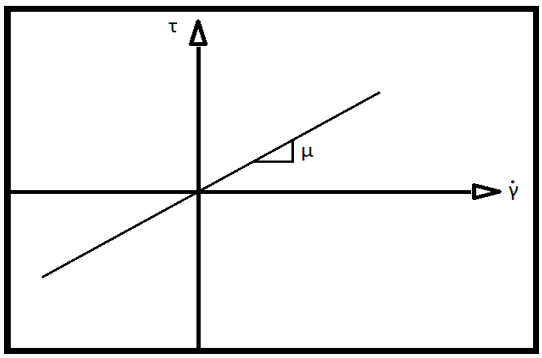

Figure 2.11 Shear stress, τ, versus shear rate, $\dot{\gamma}$, for a Newtonian fluid.

The basic equation of deformation of Newtonian fluid is given by the equation:

$$\tau = \frac{F}{A} = \mu \cdot \dot{\gamma} = \mu \cdot \frac{\partial v_x}{\partial y} \qquad \textbf{Equation 2.11}$$

where τ is the shear stress, F is the force the liquid is exposed to, A is the contact area, μ is the fluid viscosity, $\dot{\gamma}$ is the shear rate defined as $\delta v_x/\delta y$ (the change of fluid velocity in the x-direction and with respect to the y-direction), see Figure 2.12. The term τ can be defined as F/A where F is the force

required keeping the upper plate moving at constant velocity, v, in the x- direction and A is the area of the plate in contact with the fluid. By fluid viscosity, the force is transmitted through the fluid to the lower plate in such a way that the x-component of the fluid velocity linearly depends on the distance from the plate [61].

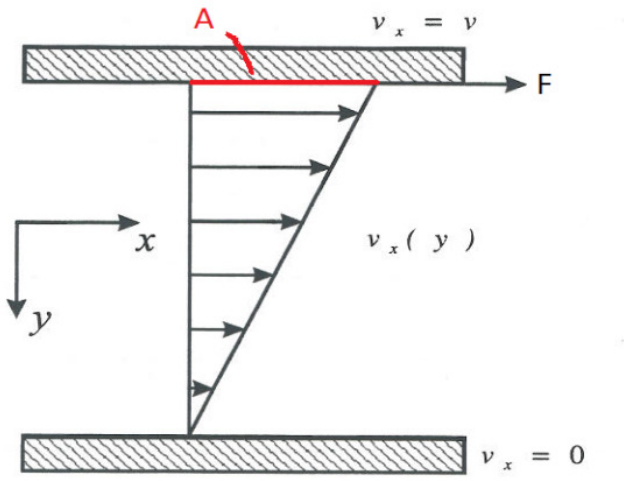

Figure 2.12 Velocity profile between two parallel plates

The fluid viscosity varies with temperature and pressure. A decrease in temperature causes the fluid viscosity to increase. The pressure on the other hand is different. A pressure increase with constant temperature will normally increase the viscosity, with some exceptions (e.g. water).

2.10 pH

The pH of an aqueous solution is a measure of acidity and can be defined as the negative logarithm of the hydrogen ion concentration:

$$\mathrm{pH} = -\log_{10}\left[\mathrm{H_3O^+}\right] \qquad \textbf{Equation 2.12}$$

The pH is always a positive, dimensionless number ranging from 1 (Acidic) to 14 (basic) and 7 is neutral.

2.11 Ionic strength

The ionic strength, I, of a solution is defined as:

$$I = \frac{1}{2}\sum_{i=1}^{n}\left(c_i \cdot z_i^2\right) \qquad \textbf{Equation 2.13}$$

where c_i is the concentration of the ion i, z_i is the charge of the ion and n is the sum of ionic species present in the solution.

3 Enhanced Oil Recovery

Oil recovery can be divided into three steps; primary, secondary and tertiary recovery. Primary recovery is spontaneously production of oil due to the natural pressure that exists in the reservoir (pressure depletion). The recovery factor after a primary recovery is usually low (5 % or less of the OOIP). The secondary recovery is defined as improving oil recovery normally by the injection of water or gas. The objective is to maintain or restore the pressure and to flood the reservoir. After secondary recovery a large amount of oil is still trapped in the reservoir due to capillary forces and unfavourable reservoir characteristics. The tertiary recovery, which is the recovery of remaining oil by the use of sophisticated techniques after a field has been exploited by primary and secondary recovery [62].

Enhanced oil recovery (EOR) can be defined as "oil recovery by the injection of material not normally present in the reservoir" [63]. Several EOR methods and techniques exist, among others polymer injection, surfactant injection, gel, foam and microbial increased oil recovery (MIOR). It could also be a combination of the different methods (defined as hybrid EOR).

The recovery factor, E_R, can be defined as [63]

$$E_R = \frac{N_P}{N} = E_D \cdot E_{vol} = E_D \cdot E_v \cdot E_A \qquad \textbf{Equation 3.1}$$

where N_p is the produced reserves, N is the total reserves, E_D, E_{vol}, E_V and E_A are the microscopic, volumetric, vertical and areal displacement efficiency, respectively. These concept are illustrated in Figure 3.1.

The microscopic displacement efficiency, E_D, and the volumetric displacement efficiency, E_{vol}, can further be defined as:

$$E_D = \frac{\text{Volume oil displaced}}{\text{Volume oil contacted}} \qquad \textbf{Equation 3.2}$$

$$E_{vol} = \frac{\text{Volume oil contacted}}{\text{Volume oil in place}} \qquad \textbf{Equation 3.3}$$

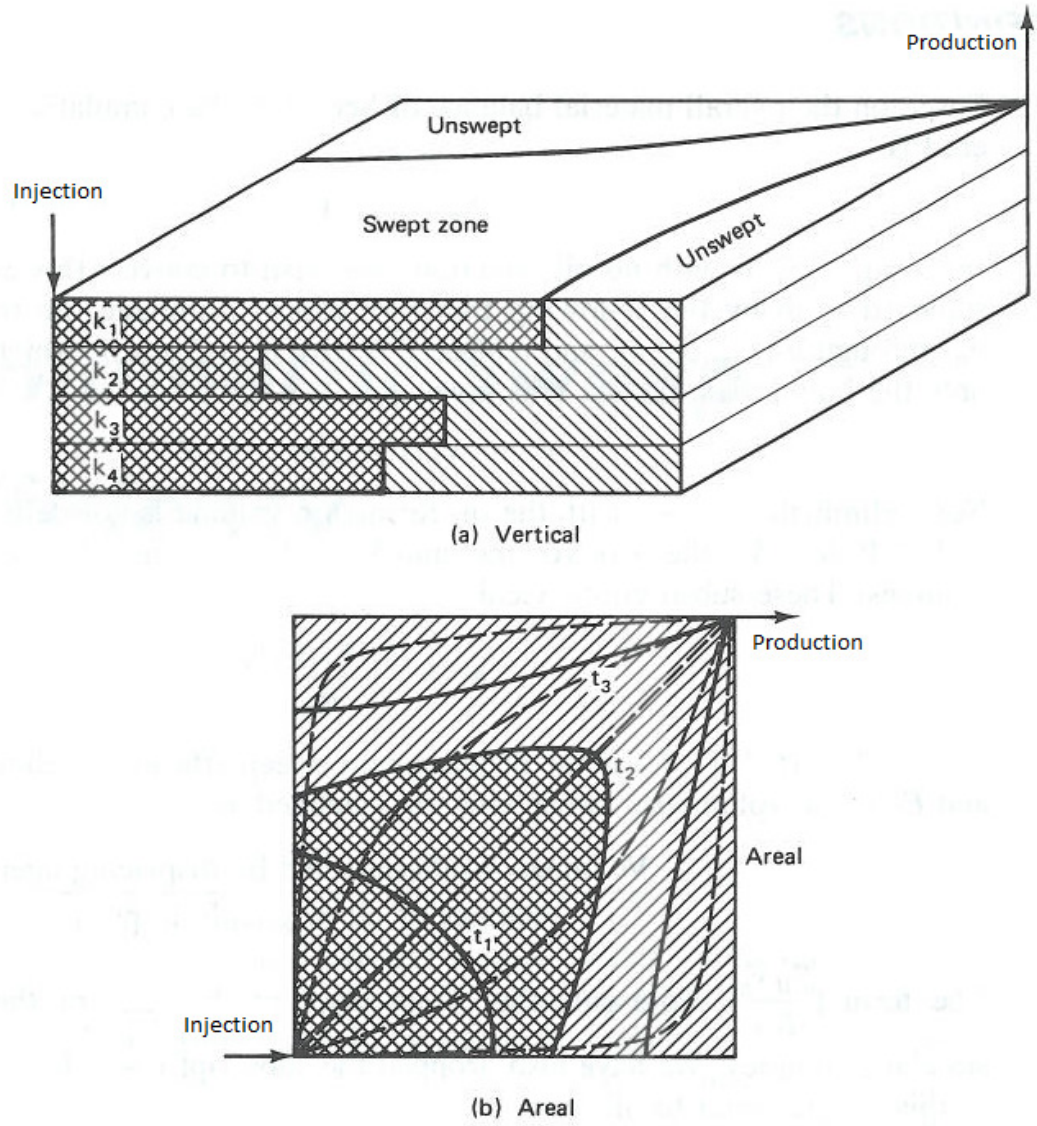

Figure 3.1 **Schematic E_{vol} (a) E_V (b) E_A [64]**

The aim of increasing the microscopic displacement efficiency, E_D, is production of oil that remains in the part of the reservoir already swept by the displacing fluid (decreasing residual oil saturation, S_{or}), e.g. reducing capillary force by injection of surfactant.

To increase the volumetric displacement efficiency, E_{vol}, the aim is to produce oil that remains in the reservoir not swept by the displacing fluid, e.g. trapping mechanism and increasing the displacing fluid viscosity by the use of polymers.

This chapter will emphasis on the mobility ratio, residual oil saturation and capillary number which is relevant topics in this thesis and also important topics in understanding different EOR techniques.

3.1 Mobility

Mobility is a measure of how easily a phase, e.g. water, oil or gas, flows through a porous medium in multiphase flow [57, 63]. The mobility, λ_j, for a single fluid is defined as the ratio of the effective permeability of the fluid, k_{ej}, to the viscosity of the fluid, μ_j:

$$\lambda_j = \frac{k_{ej}}{\mu_j} = \frac{k_{rj}}{\mu_j} \cdot K \qquad \textbf{Equation 3.4}$$

where k_{rj} is the relative permeability of the fluid and K is the absolute permeability of the porous media.

More importantly is the concept of effective mobility ratio for waterfloods, which is defined as the mobility ratio between the displacing, λ_w, and displaced fluid, λ_o:

$$M = \frac{\lambda_w}{\lambda_o} = \frac{k_{rw}}{k_{ro}} \cdot \frac{\mu_o}{\mu_w} \qquad \textbf{Equation 3.5}$$

Mobility ratio is often given in terms of critical end point mobility [63]:

$$M^0 = \frac{k_{rw,or}}{k_{ro,iw}} \cdot \frac{\mu_o}{\mu_w} \qquad \textbf{Equation 3.6}$$

where $k_{rw,or}$ is the end point relative permeability of water at residual oil saturation, S_{or}, and $k_{ro,iw}$ is the end point relative permeability of oil at initial water saturation, S_{iw}.

The mobility ratio has significantly effect on the stability of the displacement, and also the recovery factor, see Figure 3.2. The favourable condition for stable displacement is low M^0 ($M^0 \leq 1$) which gives a delayed WBT and a smaller tail production of oil. A high M^0 ($M^0 > 1$) is unfavourable because it gives an unstable displacement which means early WBT and long tail production. Fingering can occur, which means that bypassing of a resident fluid by a displacing agent in a homogeneous, non-uniform medium [57].

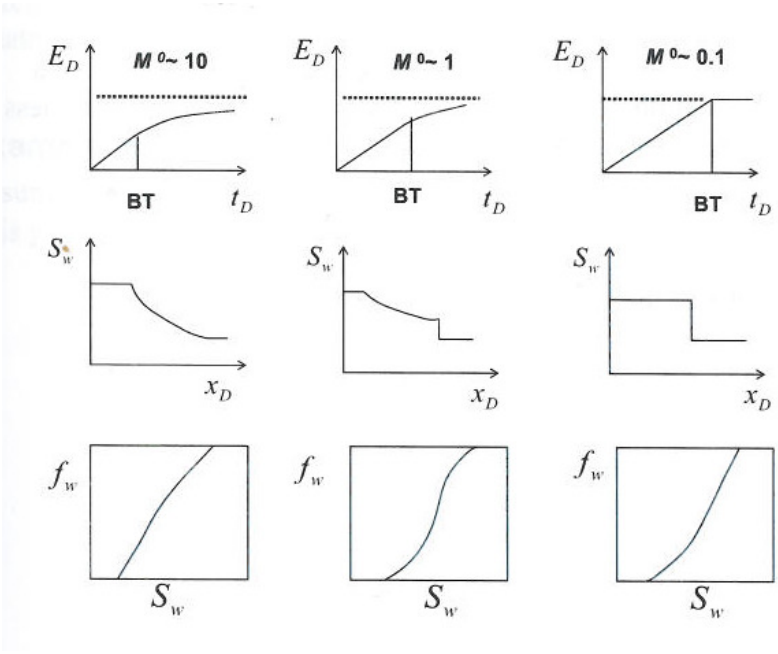

Figure 3.2 Schematic illustration of the effect of mobility ratio on displacement efficiency [63]

The mobility ratio between oil and water can be made more favourable by i) increasing the viscosity of water (e.g. adding polymers to the injection water), ii) decreasing the viscosity of oil (e.g. thermal EOR) or iii) decreasing the end point permeability of water (e.g. adding polymers to the injection water).

3.2 Residual oil saturation

The main target of EOR is the oil remaining trapped after primary and secondary recovery. The oil is trapped due to capillary forces between oil and water and the mechanism for residual phase saturation may be illustrated through two different simplified REV (Representative Elementary Volume) scale models, the pore doublet model and the snap-of model.

The pore doublet model describes the trapping phenomena through oil trapped by bypassing water in a doublet pore, e.g. Figure 3.3(b). This model assumes well-developed Poiseuille flow in each pore and that the presence of interface does not affect the flow [57]. The small-radius pore will be flooded first leaving some trapped oil in the large-radius pore.

The snap-off model describes the trapping of oil into globules that are localized in the middle of the pore bodies of the flow, e.g. Figure 3.3(e). The mechanism of trapping is due to capillary forces and is dependent on the size of the pore throats, IFT and wettability. If the capillary force between oil and water is higher than the viscous force acting on the oil, the oil will be trapped (neglecting the

gravitational force). This can be better understood when looking at the definition of capillary force (Equation 2.7).

In the reality the residual oil trapped in a porous medium is described by using a combination of the models. This was done by Chatzis et al. [65] and can be illustrated in Figure 3.3. The most common experimental observations of trapping in porous media is a relationship between residual non-wetting or wetting phase saturation and a local capillary number [57]. This will be discussed further in the next section.

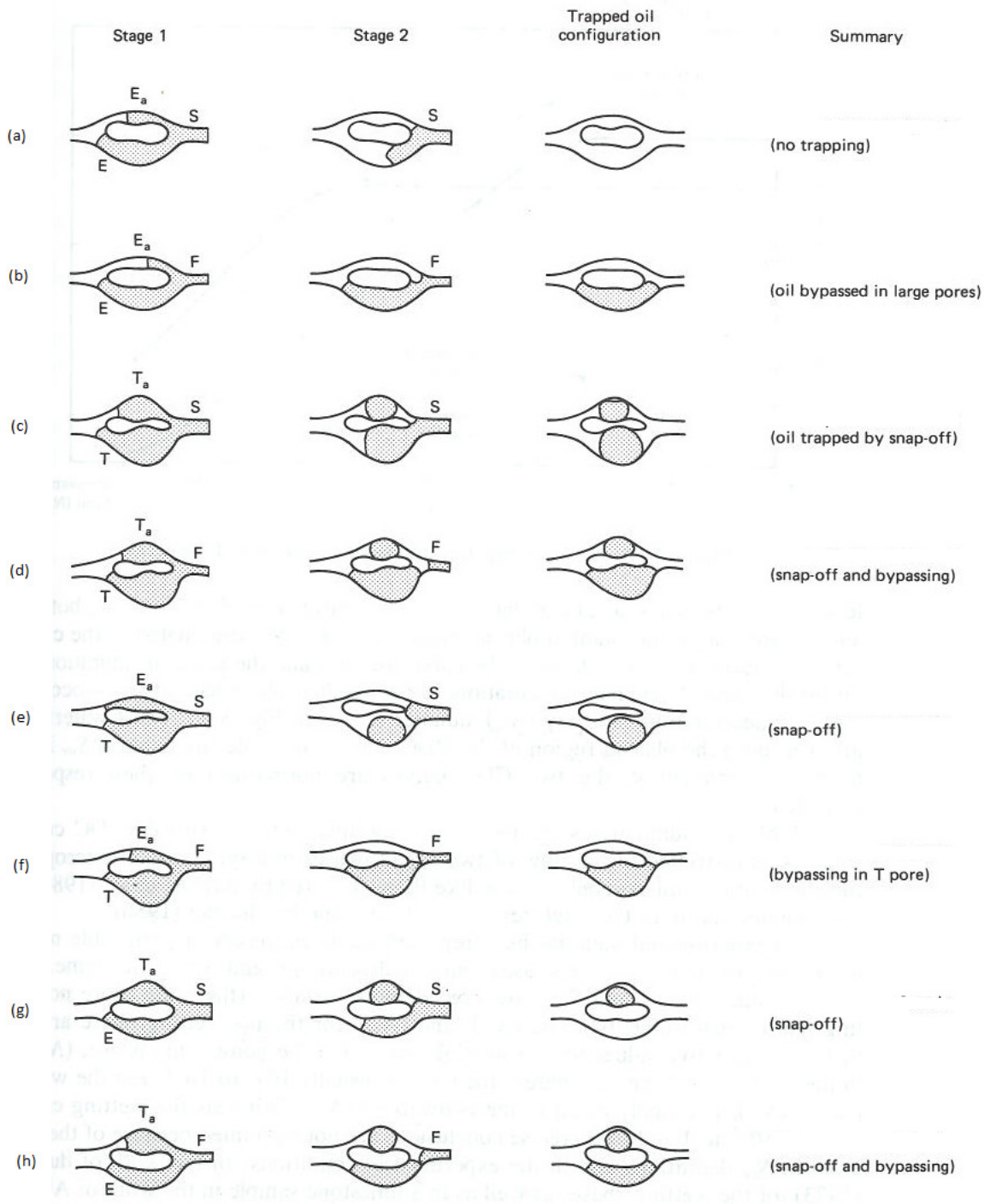

Figure 3.3 **Sketches of low capillary number trapping mechanisms and configuration of residual oil in pore doublets [65]**

3.3 Capillary number and CDC

The capillary number, N_{vc}, is a dimensionless number that expresses the ratio of the viscous force to the capillary force acting on the oil. N_{vc} is defined differently and one often used definition for the water displacing oil case is [57, 62-64]:

$$N_{vc} = \frac{\text{Viscous force}}{\text{Capillary force}} = \frac{u_w \cdot \mu_w}{\sigma_{o,w}} \qquad \textbf{Equation 3.7}$$

where u_w is the Darcy velocity of water (displacing fluid), μ_w is the viscosity of water and $\sigma_{o,w}$ is the IFT between oil and water. For a conventional synthetic sea water flood, N_{vc} is typically in the magnitude of 10^{-6}.

The capillary number as a function of residual saturation is often used and this relationship is called the capillary desaturation curve (CDC), schematically shown in Figure 2.1. The CDC is influenced by the wettability (Figure 3.4) and the pore size distribution (PSD), see Figure 3.5, of the porous medium. Reservoir rocks with a narrow PSD will give a higher oil recovery (the lowest residual oil saturation) with regard to increased capillary number.

It is worth noticing the general shape of the CDC. At low N_{vc} the CDC is relatively constant (plateau region) up to a given critical capillary number, $(N_{vc})_c$. A knee in the curve occurs and the residual saturation starts declining, see Figure 3.4.

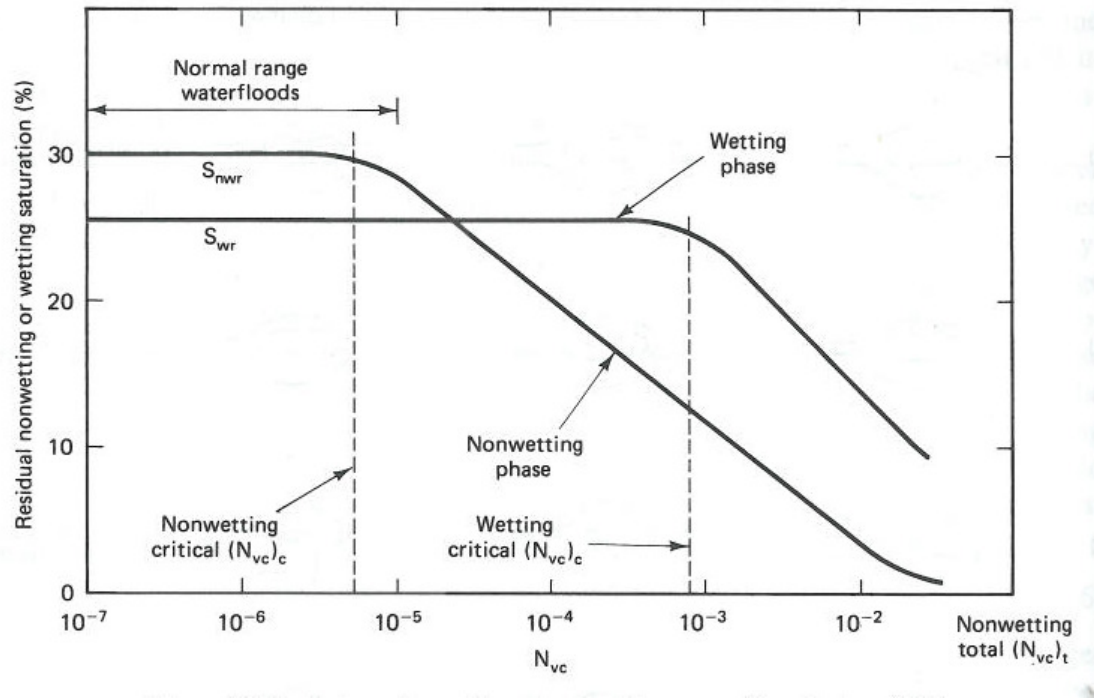

Figure 3.4 Schematic CDC for wetting and non-wetting phase [66]

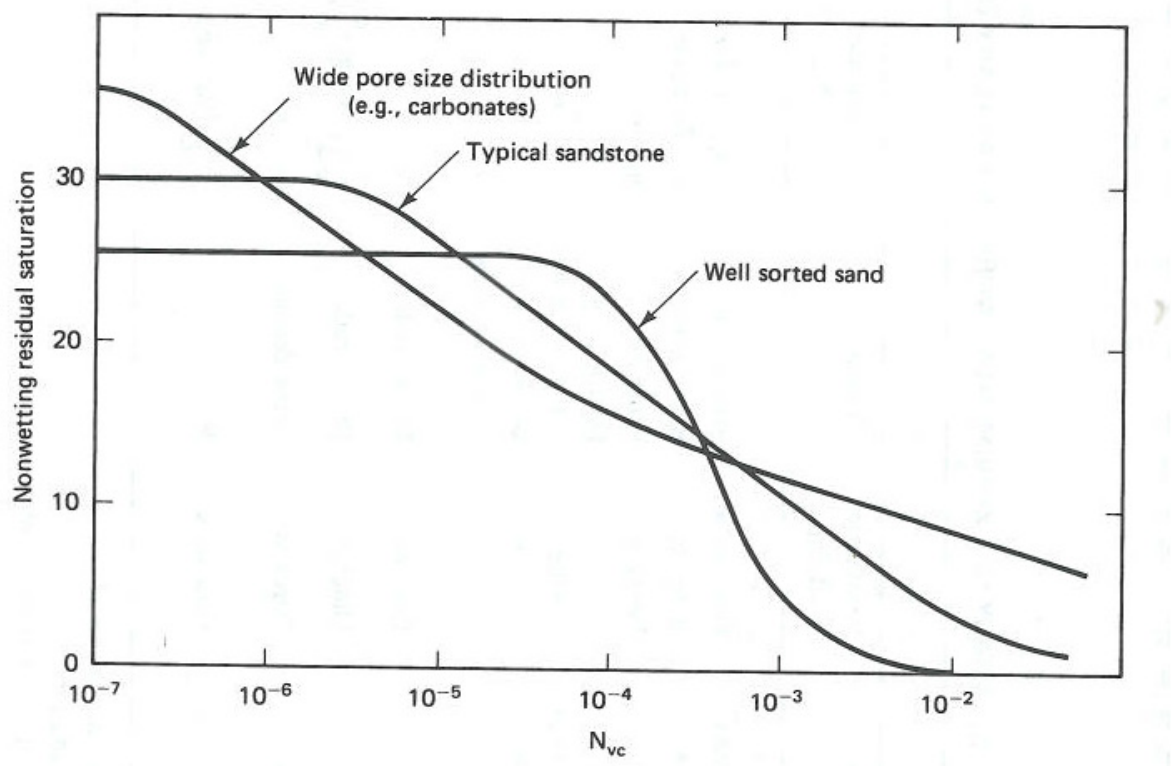

Figure 3.5 Schematic effect of PSD on the CDC [66]

The main target of EOR is to reduce the residual oil saturation, and this can be done by lowering the capillary number to the system. The capillary number can be reduced by changing the three parameters in Equation 3.7, hence:

1. Increase the velocity of the water
2. Increase the viscosity of the water (e.g. adding polymer to the water)
3. Decrease IFT between oil and water (e.g. adding surfactants to the water)

The x-axis in the CDC is logarithmic and thus, a large change in the capillary number is required to significantly change the S_{or}. This can be achieved by adding surfactant to the injection water, which may reduce the IFT by several orders of magnitude (factor of about 10^3 to 10^4).

4 Low Salinity waterflooding

Several criteria have been suggested in the literature to be necessary conditions for an increase in oil recovery by the low salinity effect (LSE):

- Presence of connate water is required [4]
- Significant clay fraction in the rock [4]
- Polar components presence in the oil phase [4, 40]
- Crude oil exposure to create mixed-wet [4, 11]
- Presence of divalent ions in the formation brine [4, 40]

The necessary conditions listed above are not always sufficient to guarantee LSE, indicating the complexity of crude oil/brine/rock (COBR) interactions. As previously mentioned, the necessary conditions listed above are not always sufficient, which indicates the complexity of COBR.

4.1 Proposed mechanisms for Low salinity effects

Numerous LS mechanisms have been proposed in the literature. No mechanism has been widely accepted as the yet prevailing mechanism because of the complex COBR interactions involved in the LSW process. The LSE is probably a result of several different mechanisms contributing together. Some of the suggested and most accepted mechanisms for LSW in sandstone are explained further in this section.

4.1.1 Wettability alteration

Wettability alteration is one of the most accepted and frequently suggested cause of increased recovery by LSW [11]. Wettability alteration is strongly dependent on the stability of the water film that exists between the mineral surface and the oil phase. The stability of the water film by the interfaces between oil/water and water/rock is determined by the disjoining pressure [67]. Disjoining pressure results from intermolecular or interionic forces, namely van der Waals, electrostatic and hydration forces. Electrostatic and hydration forces give rise to repulsive disjoining pressure, which promote water-wetness, by stabilizing the water film. The stability depends on brine pH and salinity, crude oil composition and mineral composition. Increasing salinity decreases the electrostatic repulsion, which in theory will result in a less stable film [67]. However, adhesion test performed by Buckley et al. [55] showed less adhesion at higher salinities. They argued that when salinity increases, the short range forces (hydration forces) must become more repulsive and stabilize the water film.

Numerous of studies have reported that wettability alteration is observed during LSW [4, 7, 9, 21, 28, 68]. In 1997, Tang and Morrow [7] investigate the salinity influence of the connate and invading brines on the wettability and oil recovery. Their study was based on spontaneous imbibition and

waterflooding using Berea sandstone using Dagang crude oil and synthetic RB with concentration of 24168 ppm. The oil recovery was highly sensitive to the salinity of the connate water and less sensitive to the injection brine. The highest reduction in residual oil saturation (S_{or}) was observed by diluting the connate water by 0.01 (17.6% difference in S_{or} compared with waterfloods utilizing RB connate water). Only a marginal reduction in S_{or} was observed by reducing the invading brine using RB connate water. Based on their spontaneous imbibition observations, they concluded that water-wetness and oil recovery increases with a decrease in salinity (Figure 4.1).

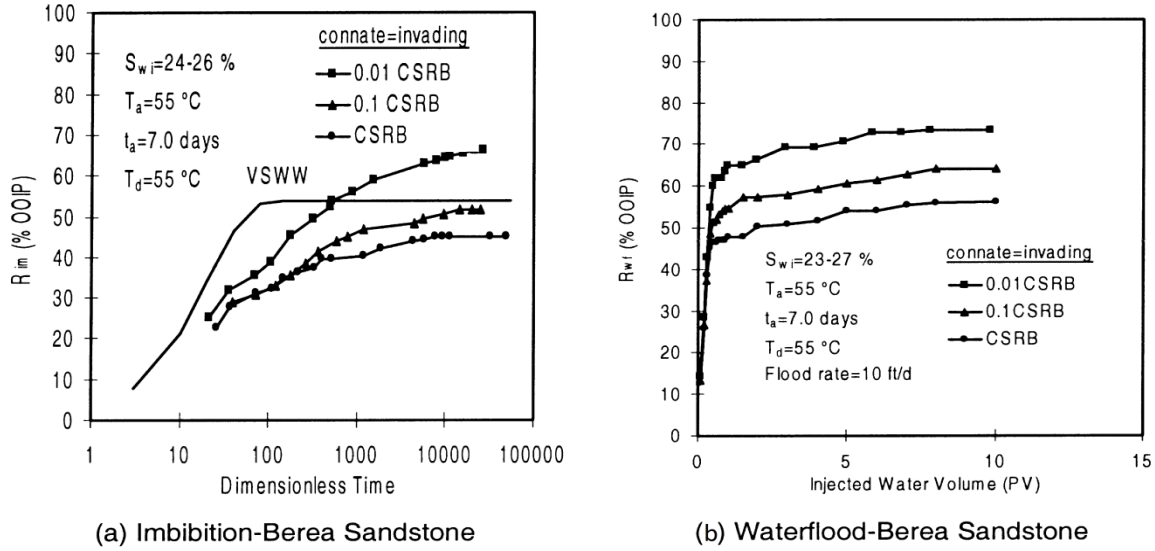

(a) Imbibition-Berea Sandstone (b) Waterflood-Berea Sandstone

Figure 4.1 **The impact of brine concentration on a) imbibition and b) waterflood on oil recovery in Berea core sample [4]**

Sandengen et al. [69], however, observed a change in wettability from water-wet to more oil-wet during LSW. Their result was based on relative permeability and capillary pressure data derived from both secondary and tertiary LSW.

Filoco and Sharma [40] reported the salinity of the connate brine to be the primary factor controlling the wettability, and thus the oil recovery. The oil recovery increased significantly with decreasing salinity of the connate brine, while the salinity of the displacing brine had no significant influence on the oil recovery. Their results were based on 104 Berea sandstone core plugs (2.5 cm both in diameter and length), using three different crude oils and salinity from 0.3% NaCl to 20% NaCl. The mechanism behind the increased oil recovery due to salinity was suggested as a result of wettability alteration from water-wet to mixed-wet state.

However, it is important to keep in mind that wettability indications are not straight forward. Supporting observations are increase in rate, waterflood characteristics and spontaneous imbibition. The indications are not necessarily a good wettability indicator.

4.1.2 Fines migration

Studies of the influence of brine composition in oil recovery were performed by Tang and Morrow [4] in 1999. They pointed out the importance of initial water presence, the use of crude oil (not refined oil) and clay present in the core material to achieve a favourable LSW. In addition to Berea sandstone, the LSW were conducted on Bentheimer sandstone (low clay content). The S_{or} in Bentheimer sandstone was reduced by only 4% by LSW. In contrast, the S_{or} in Berea was reduced by as much as 12%. An additional experiment was conducted in Berea after fines had been stabilized by firing and acidizing. Recovery of crude oil from this sandstone was essentially independent of salinity. Based on this, they proposed that the mechanism behind LSW was due to migration of fines. To explain the mechanism of fines migration the DLVO (Deryaguin, Landau, Verwey and Overbeek) theory of colloids was applied. When the salinity of the injection brine is reduced, the electrical double layer in the aqueous phase between particles is expanded and the tendency for stripping of fines is increased. Fines migration may lead to an increased oil recovery due to (1) wettability alteration or (2) diversion of flow.

In the first case it is assumed that the clay particles are mixed–wet. When the clay particles are mobilized, the system will become more water-wet, thus leading to an increase in oil recovery. This is in accordance with earlier research, also see section 2.5 (Wettability alteration), which indicates an optimum wettability at weakly water-wet conditions. It was also suggested that by detachment of clay particles, the surface would mobilize previously detained oil attached to these clay particles, contributing to a further increase in oil recovery.

The second case was based on observations of a permeability reduction during LSW after a HSW. It was suggested that clay particles blocked some of the flow channels, which lead to a diversion of the flow into new and unswept zones. This may give rise to a reduction in the residual oil. Thus, increase the oil recovery.

Even though Tang and Morrow [4] showed migration of fines during their LSW experiments, Lager et al. [17] argued that they had carried out numerous experiments on LSW in which no fines migration or permeability reduction had been observed.

4.1.3 pH variation

In numerous laboratory studies with LSW [17, 21], an increase in the pH of the effluent is observed. This rise in pH could be, in most cases, due to two coetaneous reactions, carbonate dissolution and cation exchange. The carbonate dissolution reactions are represented by:

$$CaCO_3 \Leftrightarrow Ca^{2+} + CO_3^{2-} \qquad \textbf{Equation 4.1}$$

$$CO_3^{2-} + H_2O \Leftrightarrow HCO_3^- + OH^- \qquad \textbf{Equation 4.2}$$

Carbonate dissolution is relatively slow and strongly dependent of the clay fraction. Cation exchange, on the other side, has a much faster reaction and occurs between clay minerals and the injected brine. In this process, H^+ from the liquid phase is substituted with cations adsorbed on the mineral surface, which leads to a decrease in H^+ concentration in the liquid phase. In 2010, Austad et al. [70] explained the mechanism behind LSW to be substitution of divalent cations like Ca^{2+} in the clay with H^+ from the brine, improving the water-wetness of the rock and an increase in pH is observed.

Due to the increase in pH (above 9), McGuire et al. [21] proposed that LSW behaves similar to alkaline flooding which could generate in situ surfactants. LSW would thus result in a reduction in IFT between the oil and the brine and also a wettability alteration may occur.

However, contradictory evidence weakens the trust in this mechanism causing the LSE. A necessary condition for alkaline flooding to generate enough surfactants is to have a crude oil with high acid number [71]. This condition is not a necessary condition for LSE. Positive response to LSW was observed with crude oil containing low acid number [6-8, 40]. In other cases, particularly when the pH is initially low, little change in pH is observed and the pH level normally associated with caustic flooding (wettability change and decreasing IFT) is not reach [72]. Increase oil recovery with LSW is also observed where no change in pH has been registered [73].

4.1.4 Multicomponent ionic exchange (MIE)

The multicomponent ionic exchange (MIE) simply means an ionic exchange involving more than one cation, i.e. Na^+, Ca^{2+}, Mg^{2+}. This mechanism between the mineral surface and the invading brine was first proposed by Lager et al., 2006 [17]. The theory is based on polar component in the oil phase being adsorbed to the clay mineral surface by ion binding with ions from the water phase. During LSW it is proposed that the double layer will expand and the polar oil components bonded to the divalent cations can be exchanged, e.g.:

$$\mathrm{Clay-Ca} + 2\mathrm{Na}^+ \Leftrightarrow \mathrm{Clay-Na_2} + \mathrm{Ca}^{2+} \qquad \textbf{Equation 4.3}$$

In different coreflood experiments conducted at BP and Heriot Watt University [17] they observed an decrease in Mg^{2+} and Ca^{2+} concentration of the effluent during LSW. The concentration dropped lower than the concentration of the invading brine, showing that the divalent ions were adsorbed by the rock material. These observations were the background for MIE mechanism being responsible for the increased oil recovery during LSW. Based on the extended DLVO theory by Amarson and Keil [74] and Sposito [75], Lager et al. proposed four cation exchange mechanisms possible occurring during a LSW; cation exchange, ligand bonding, cation bridging and water bridging (see Table 4.1 for further explanation and Figure 4.2 for illustration). During LSW, MIE will take place and remove organic polar compounds and organic-metallic complexes from the mineral surface and replace them with cations.

The mechanism of MIE could explain some of the unexpected results previously observed during LSW. It tells why LSW has no effect on mineral oil as no polar compounds are present to interact with the clay minerals. It also illustrates why there is no direct correlation between the acid number of the oil and oil recovery, since other components of the oil may be of importance.

Table 4.1 Adsorption mechanism of polar component on clay mineral [75]

Mechanism	Organic functional group involved	Explanation
Cation exchange	Amino, ring NH, heterocyclic N (aromatic ring)	Occurs when molecules containing quaternized nitrogen or heterocyclic ring replace exchangeable metal cations initially bound to clay mineral.
Cation bridging	Carboxylate, amines, carbonyl, alcoholic OH	Weak adsorption mechanism between polar functional group and exchangeable cations on the clay surface
Water bridging	Amino, Carboxylate, carbonyl, alcoholic OH	Occurs if exchangeable cation is strongly solvated (e.g. Mg^{2+}). Involves water molecules solvating the exchangeable cation and the polar functional group of the oil.
Ligand exchange	Carboxylate	Direct bond formation between multivalent cation and a carboxylate group. Stronger bond than cation bridging and cation exchange, and lead to detachment of organic-metallic complexes from mineral surface.

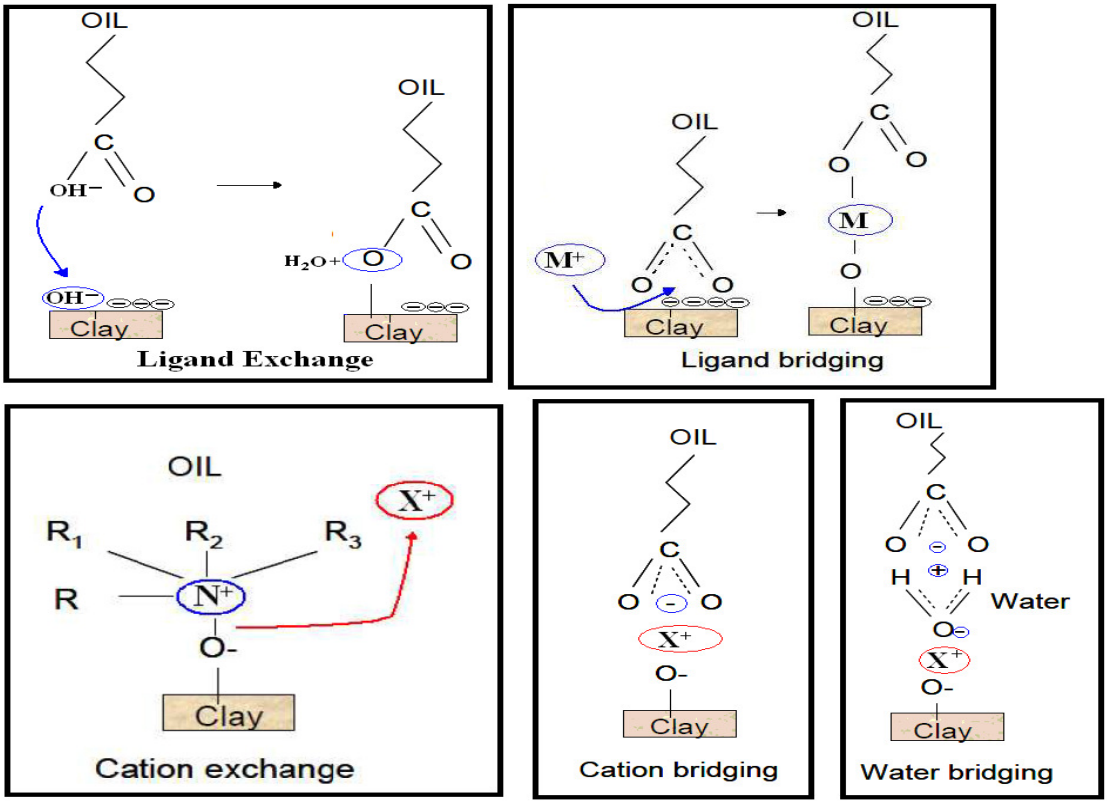

Figure 4.2 **MIE mechanism - Representation of the diverse adhesion mechanism occurring between clay surface and crude oil. Redrawn from [76]**

4.1.5 Double layer expansion

In 2009, Ligthelm et al. [68] proposed the LS mechanism to be the expansion of the electrical double layers that surround the clay and oil particles and increase in the level of zeta potential. It was suggested that a decrease in the ionic strength by lowering the salinity in the brine would increase the electrostatic repulsion between the clay particle and the oil, see Figure 4.3. Once the repulsive forces exceed the binding forces via the multivalent cation bridges, the oil particles may be adsorbed from the clay surfaces, which will lead to a change in wetting phase towards increased water-wetness.

If the electrolyte concentration is reduced further, the electrostatic forces within the clay minerals will start to exceed binding forces, which may lead to formation damage.

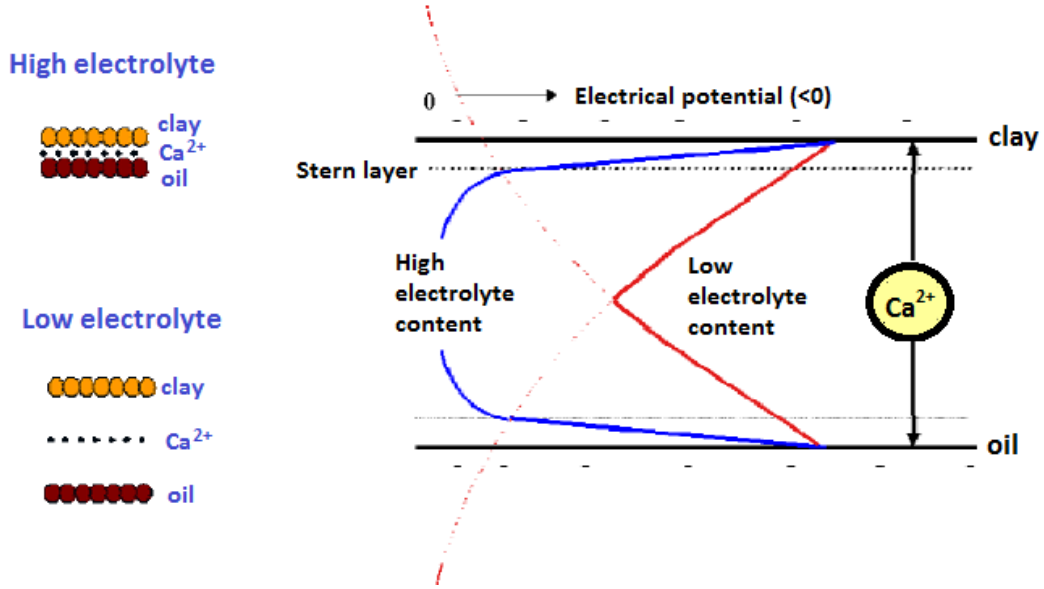

Figure 4.3 **Carton of bonding between clay surface and the oil in a highly saline and low saline brine environment. The Ca^{2+} ion represent the multivalent cations in the brine that act as bridge between clay and oil particles. Redrawn from [68]**

4.2 Summary of field tests

In 2004, Webb et al. [22] provided the first field evidence of reduction in residual oil saturation by LSW. A log-inject-log test was performed to determine the residual oil saturation, S_{or}, after waterfloods with different salinities in a clastic sandstone reservoir. Three different brines were tested; low (3000 ppm), intermediate (70000 ppm) and high (220000 ppm) salinity. The results were in line with previous laboratory tests from other fields showing a reduction of 25-50% in residual oil saturation when LSW was used.

The Endicott field, located in the North Slope of Alaska was selected as the first BP operated tertiary reduced-salinity EOR pilot. An extensive research programme was put together, consisting of different scientists like Webb, McGuire, Lager and Seccombe in order to analyse the LSW from the Endicott field. Several core measurements, including numerous single well chemical tracer tests (SWCTT) and simulation studies from the Endicott field were presented in 2008 [15]. SWCTT showed an increase in LSW recovery from 8-19% and determined that a 40% slug by pore volume was fully effective [15, 21]. Evidence of increased oil recovery due to LSW at reservoir scale was also shown on Endicott field [14, 16], see Figure 4.4. A clear drop in water cut was observed, and tertiary LSW is expected to drop residual oil saturation from 41% to 28% at the end of the production [14].

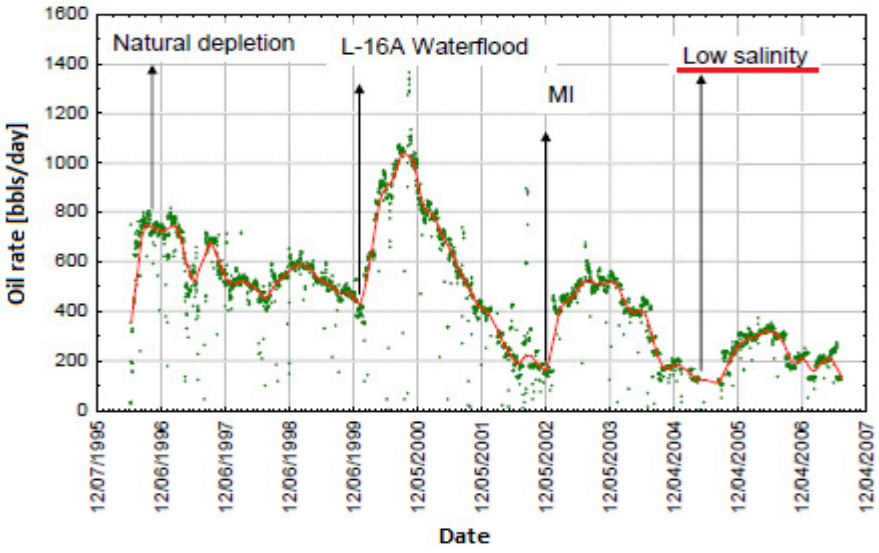

Figure 4.4 The effect of LS injection on oil rate into an Alaskan reservoir [16]

Shell has also reported results from field trials [77, 78]. An unintended LSW into a Middle East oil field (Omar field in Syria) led to production of an oil bank. A change in wettability from oil-wet to a more water-wet system was observed leading to an associated incremental recovery of 10-15% OOIP. Another reported field trial in Syria also lead by Shell [78] is the Sijan field. The tertiary LSW appears to be still immature and the breakthrough of LS water has not yet occurred (2011).

Another interesting field trial has been carried out by Statoil at the Snorre field, located in the North Sea area [39]. The potential for increased oil recovery by LSW at Snorre has been investigated through both laboratory measurements and a field test. Results indicate that the potential of LSE is low. One suggested reason is believed to be that the wetting conditions in the Snorre field are naturally close to optimal (neutral-wet to weakly water-wet) so that sea water injection already is efficient.

During 2011, the Saudi Aramco finalized the design of several single well chemical tracer tests to demonstrate the potential of increased oil recovery by tuning the sea water in upper Jurassic carbonate reservoir. They successfully completed two field trials, first-ever field trials in carbonate reservoirs, with an 0.07 reduction in the residual oil saturation beyond conventional sea water flooding [33].

There are some concerns implementing LSW on field basis. One of the concern regarding LSW is detrimental rock/fluid interactions, causing reduction in permeability and therefore reducing injectivity into a reservoir [13]. Another possible challenge is the economic issue concerning injection of LS brine when there is an absence of fresh water. This may be solved by construction of desalination facilities.

5 Surfactant

Surfactant is a chemical that reduce the IFT between two immiscible fluids, e.g. oil and water. The main target of surfactant flooding is to decrease the capillary trapped S_{or} after a waterflood. This will increase the microscopic displacement efficiency, E_D, which will lead to an increase of the recovery factor, E_R. Another effect of the surfactant is that it may alter the wettability of the rock [66], which can lead to higher oil recovery. The use of surfactants (surface-active chemicals) in order to improve oil recovery dates back to the late 1920's and early 1930's [64]. However, serious attention to surfactant flooding did not start until the 1960's.

The efficiency of the surfactant depends on several factors, such as the character of the surfactant, temperature and the salinity of the brine, which will be further discussed in this chapter.

Another important issue concerning the surfactant injection is the economical aspect of the process. In order to increase oil recovery, the injected surfactants need to achieve a low enough IFT such that residual oil is mobilized. In addition, high surfactant retention may contribute to large chemical cost and reduce the effect of the surfactant. The retention will not further be take in to account, but it is important to keep in mind that a balance between the IFT, oil recovery and surfactant loss must be considered, evaluating the economical aspect of surfactant injection.

5.1 Properties and characteristics

The specific dual structure of the surfactant, having a well-defined hydrophilic (head) and a lyophilic (tale) component, is responsible for their tendency to concentrate at interfaces. This will lead to a reduction of IFT and reduce the capillary forces between to immiscible fluids. The lyophilic component is most often a long chain hydrocarbon radical, from 8 to 18 carbon atoms, straight or branched, saturated or not, possibly associated with naphthenic or aromatic structures [62].

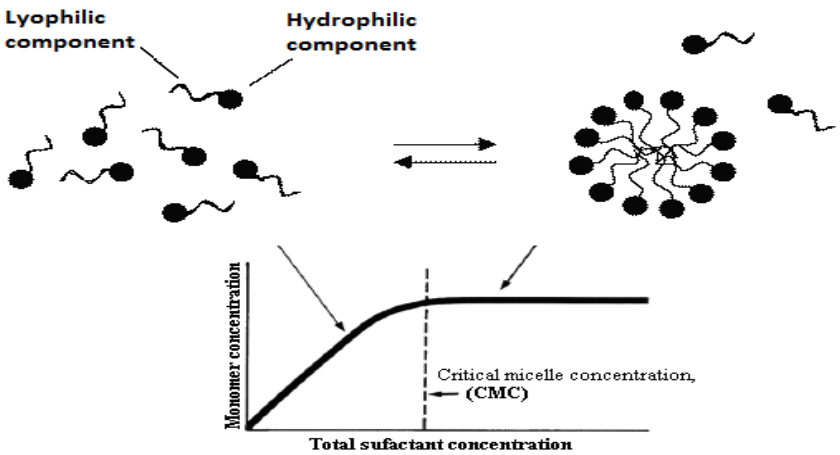

Figure 5.1 Left: Surfactant monomers Right: Surfactant micelle

Surfactants are classified into four groups, depending on their hydrophilic component;

- Anionic (negatively charged). The most commonly surfactants used in EOR, because of their low retention, relative low cost and availability. The surfactant used in this thesis is of this type (sulphate surfactant).
- Cationic (positively charged). Not normally used in EOR because they extensively adsorb onto anionic mineral surfaces.
- Non-ionic. Limited water solubility by temperature. They are highly salt-tolerant. Mainly used as co-surfactants.
- Zwitterionic. Containing two charged head groups of different signs. Not normally used in EOR because of their high cost and high retention.

When an anionic surfactant (monomer) is dissolved in water, molecules of the surfactant start to dissociate into a cation (e.g. Na^+) and an anionic monomer [1]. If the surfactant concentration is further increased, the monomers start to aggregate themselves into micelles in the bulk phase with the hydrophilic part oriented outward, see Figure 5.1. This critical concentration is called critical micelle concentration, CMC, and is normally in the range of 10^{-4} to 10^{-5} M [57]. Further increase in the surfactant concentration after CMC will only lead to an increase in the micelle concentration and not in that of monomers.

When an aqueous surfactant phase is in contact with an oleic phase the surfactant, due to its dual nature, will accumulate in the interface as an oriented monolayer, the hydrophilic part in the aqueous phase and the lyophilic part in the oleic phase. This process leads to the alteration of the solubility of the surfactant in the bulk phases which might affect the system and also affect the IFT of the system.

The most common structure of the micelles is spherical micelles, but other structures may occur, were some are shown in Figure 5.2. The structure of the surfactant aggregate is dependent on three parameters [79]; the volume of the hydrocarbon chain in a given geometrical structure, V_{HC}, the effective/critical length of the hydrocarbon length, l_C, and the effective strength of the polarity of the head, a_H. These parameters are all summarized in the “packing parameter”, P, which are defined as:

$$P = \frac{V_{HC}}{a_H \cdot l_C} \qquad \textbf{Equation 5.1}$$

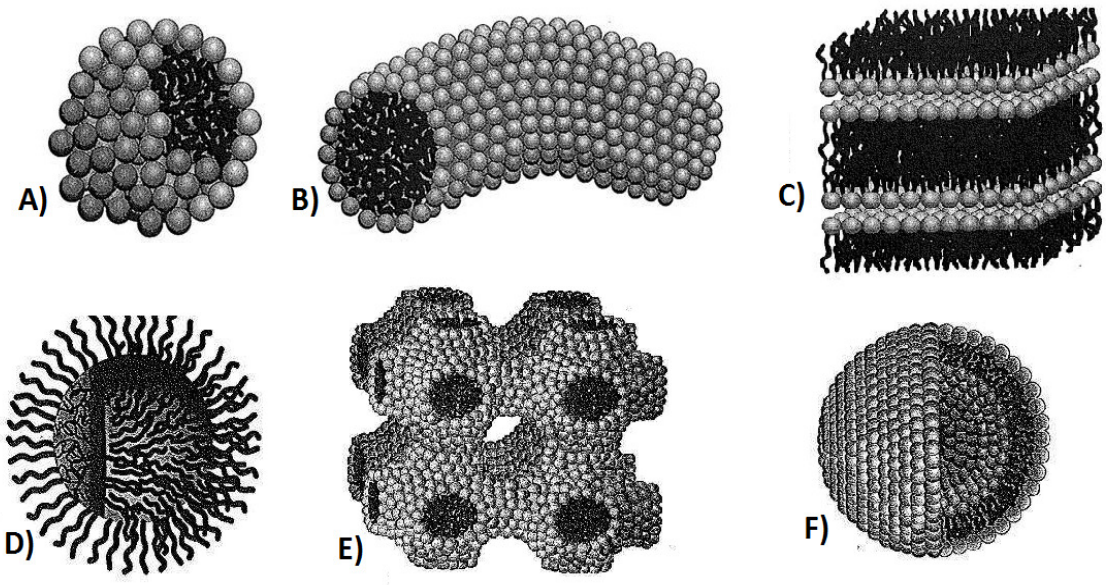

Figure 5.2 **Different ionic surfactant structures: A) Spherical micelles B) cylindrical micelles C) planar bilayers D) inverted micelles E) bi-continuous structures and F) vesicles. Redrawn from [18].**

5.2 Surfactant-Brine-Oil Phase behaviour

As previously mentioned, the salinity of the brine is one important factor affecting the surfactant-brine-oil phase behaviour. Depending on the salinity of the brine, three different types of phase systems can form, which was introduced by Winsor in 1954 [80] and was later adapted to surfactant flooding [81, 82]. It is assumed constant pressure and temperature.

The term "microemulsion" can be defined as a homogeneous phase containing surfactant, brine and oil apparently in thermodynamic equilibrium with one or more other phases [82]. Emulsion (a heterogeneous system consisting of at least one immiscible liquid dispersed in another in the form of small droplets usually with a diameter of <0.1 mm [83]) is, in contrast to microemulsion, not thermodynamic stable, and will not be further discussed in this section.

5.2.1 Type II (-) System:

At low brine salinity a typical surfactant will have a good solubility in the aqueous phase and poor solubility in the oleic phase. The overall SOB composition near the interface will split into two phases: an excess oil phase and a microemulsion phase containing mainly water, some surfactant and small amount of oil solubilized inside micelles causing them to swollen [1]. This low brine salinity system is called type II (-)because only two phases can form near the oil-brine boundary and the tie-lines in the two-phase region have negative slopes, see Figure 5.3.

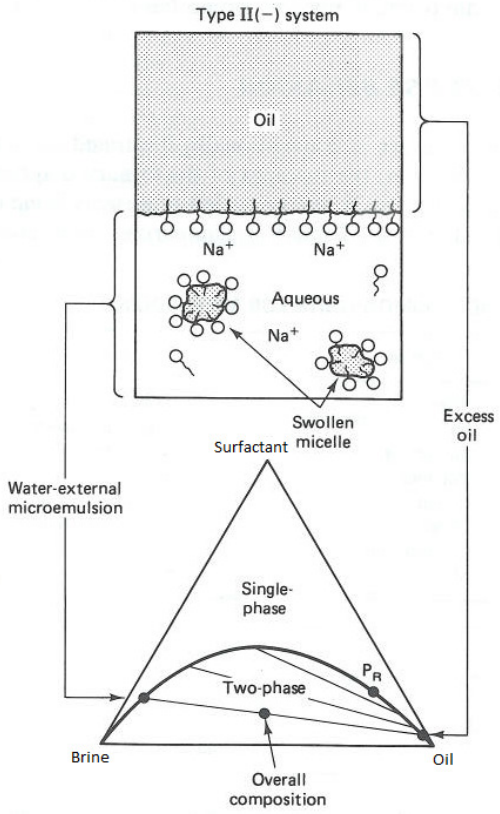

Figure 5.3 Schematic representation of type II(-) system [66]

5.2.2 Type II (+) System:

At high brine salinity a typical surfactant will have a good solubility in the oleic phase and drastically reduction of solubility in the aqueous phase, due to electrostatic force in the brine. The overall SOB composition near the interface will split into two phases: an excess water phase and a microemulsion phase containing swollen micelles of surfactant with some solubilized brine [1]. Similar to the type II(-) system, this high brine salinity system is called type II(+) because only two phases can form near the oil-brine boundary and the tie-lines in the two-phase region have positive slopes, see Figure 5.4.

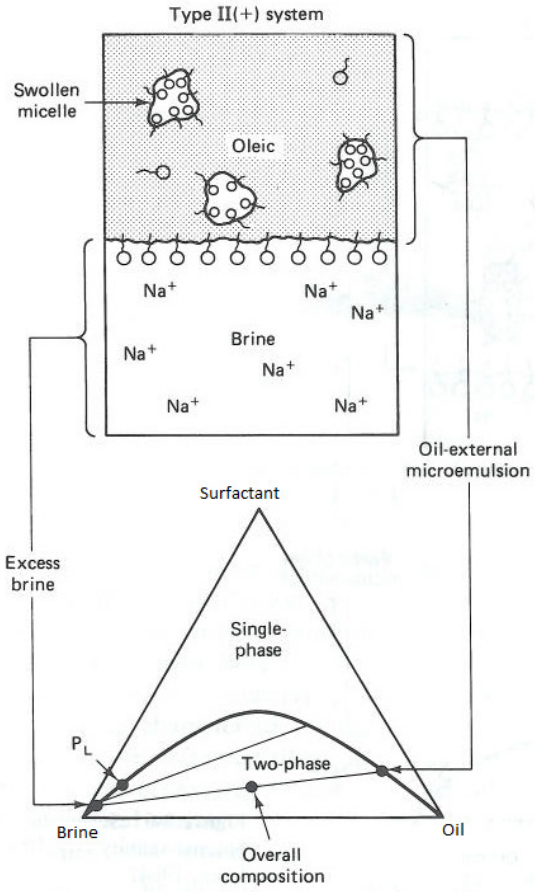

Figure 5.4 Schematic representation of type II(+) system [66]

5.2.3 Type III System:

At intermediate brine salinities a region of three phases can form; excess oil, excess brine and a microemulsion phase, whose composition is presented by the invariant point, see Figure 5.5. This system has to IFTs, one between the excess brine and the microemulsion and another between the excess oil and the microemulsion [1].

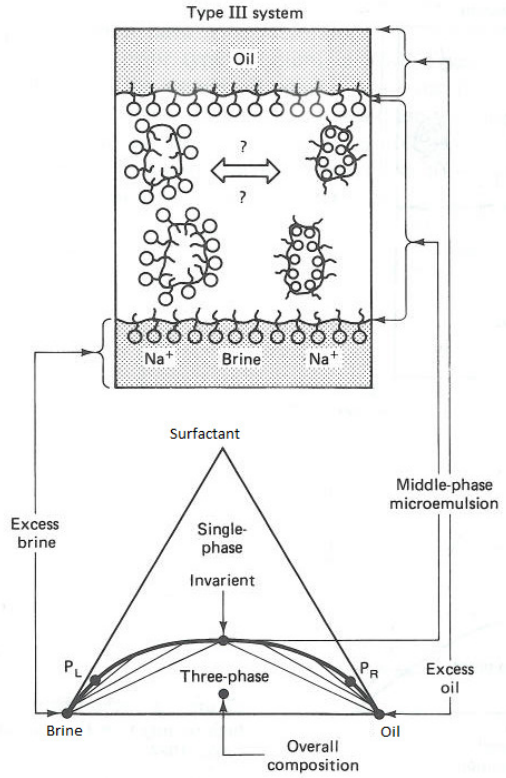

Figure 5.5 Schematic representation of type III system [66]

It has been observed in previous experiments, that the type III system has the lowest IFTs, and is therefore favourable with regard to increased oil recovery, thus this phase environment is the most attractive by surfactant flooding [57], see Figure 5.6.

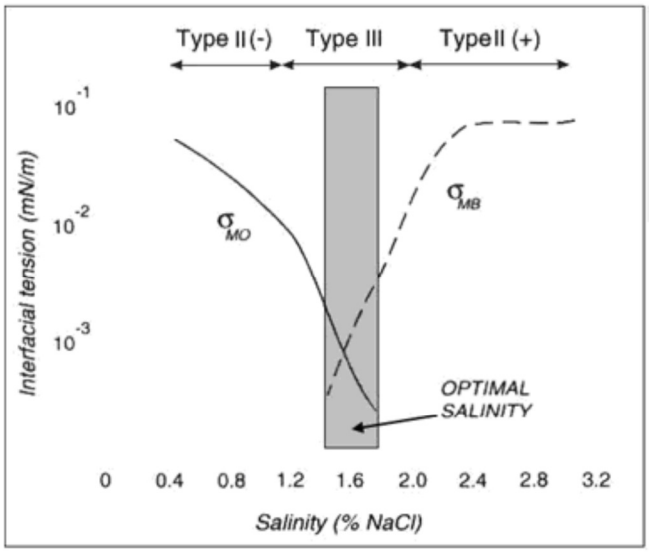

Figure 5.6 IFT as function of salinity (% NaCl)

5.3 Hydrolysis

A well-known problem related to the sulfate surfactants is their thermal instability with regards to hydrolysis, which may occur within the reservoir conditions and interfere with the performance of the surfactant [84]. Alkoxy sulfate surfactants (which is used in this study) are found to have poor hydrolytic stability at elevated temperatures (>65°C) [84]. The hydrolysis rate is dependent on several factors such as pH, brine and temperature. The chemical reaction that takes place during a hydrolysis of sulfate surfactant is:

$$\begin{aligned} &R-(PO)_x-C-O-SO_3^-(aq)+H_2O(aq) \\ &\qquad \rightarrow R-(PO)_x-C-OH(aq)+H_2SO_4(aq) \end{aligned}$$

Equation 5.2

As can be seen from the chemical reaction, the formation of sulphuric acid (H_2SO_4) will take place during a hydrolysis of surfactant. This will give rise to a decrease in the pH of the effluent.

Optimal stability of the alkoxy sulfate surfactants occurs when the pH of the solution is maintained in the range of 10-11 or the temperature is below 65°C [85]. If neither of the two criteria is fulfilled, alkali can be used to stabilize the alkoxy sulfate surfactants or more drastically the surfactant can be replaced.

6 Experimental equipment and procedures

There are different methods in determining different reservoir rock/fluid properties, such as core analysis, well logging techniques and well testing. The core analysis is important to the reservoir evaluation and in predicting the reservoir production performance as well as decisions on implementing EOR actions. However, this methodology has its limitations regarding full size reservoir analysis. It is only a small part of the formation that is investigated, which is not favourable for predicting productions in heterogeneous reservoirs.

This experiment was conducted on 4 Bentheimer sandstone core samples (B1, B2, B3, and B4). The core samples were first injected with synthetic sea water (SSW). After reaching residual oil saturation, S_{or}, low salinity (LS) brine (1/10 of salt content in SSW) was injected into the core samples. Finally, low salinity surfactant (LS-S) brine was injected, all until irreducible oil saturation was achieved. The experiments on sample B1 and B2 were conducted at a temperature of 90°C, while sample B3 and B4 were analysed at room temperature (23°C).

In addition to the main experiment different fluid analysis were performed, including density, viscosity and IFT measurement of the fluids injected. Further the pH of the effluent was measurement. The different fluid analyses are explained in more detail in chapter 6.3.

6.1 Chemicals, fluids and core material

To gain a better understanding of the mechanisms behind this experiment it is important to obtain information of the core material and the fluids involved. This matter will be further investigated in this section.

6.1.1 Bentheimer sandstone

The rock utilized in this master thesis is outcrop Bentheimer sandstone obtained from a quarry in Nordhern in the north of Germany. The permeability of this sandstone is in the Darcy magnitude and the porosity is measured to be close to 24% (Table 7.5).

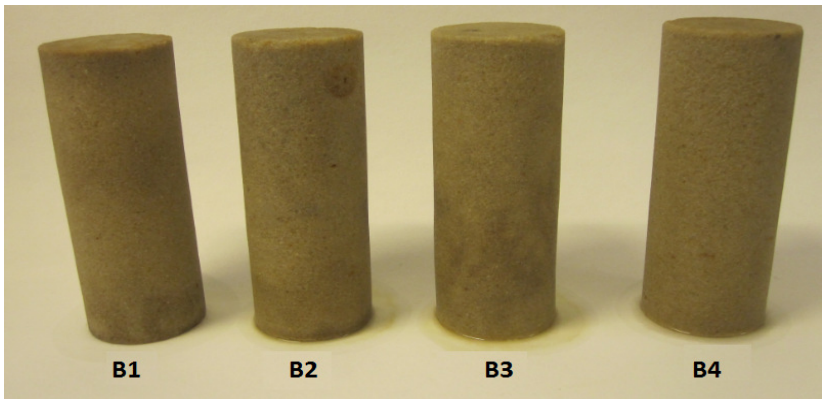

Figure 6.1 **Bentheimer core samples, photo taken after experiments**

A small sample (1cm x 1cm) from the same batch of Bentheimer sandstone used in this thesis was sent to Weatherford Laboratories in Stavanger for analysis. Two different analyses were performed, a mineralogy analysis based on the standard X-ray diffraction, XRD, [86] and pore size distribution, PSD, [87] based on standard mercury injection. The results from the XRD are displayed in Table 6.1 and Figure 6.2. The results from the PSD are graphed in Figure 6.3.

Table 6.1 **Mineral composition of Bentheimer sandstone obtained from XRD**

Mineral	Molecular formula	Contents [±0.1%]
Illite/Smectite	-	TR
Illite+Mica	$(K,H_3O)(Al,Mg,Fe)_2(Si,Al)_4O_{10}[(OH)_2,(H_2O)]$	3.2
Kaolinite	$Al_2Si_2O_5(OH)_4$	0.0
Chlorite	ClO_2^-	0.0
Quartz	SiO2	90.6
K Feldspar	$KAlSi_3O_8$	4.6
Plagioclase	$NaAlSi_3O_8 – CaAl_2Si_2O_8$	0.0
Calcite	$CaCO_3$	0.6
Dolomite	$CaMg(CO_3)_2$	0.0
Siderite	$FeCO_3$	1.0
Pyrite	FeS_2	TR

TR = Trace amounts

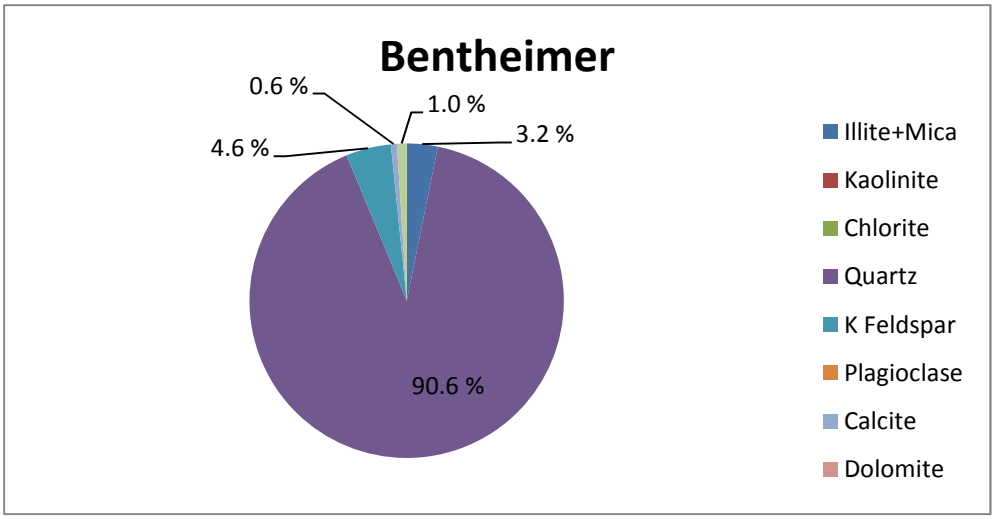

Figure 6.2 Mineralogy of Bentheimer

The PSD of the Bentheimer sample, as presented in Figure 6.3, indicates that the pore size is more homogeneous, as suggested by the narrow distribution. The peak in the distribution gives an average pore throat radius of 11.9 µm.

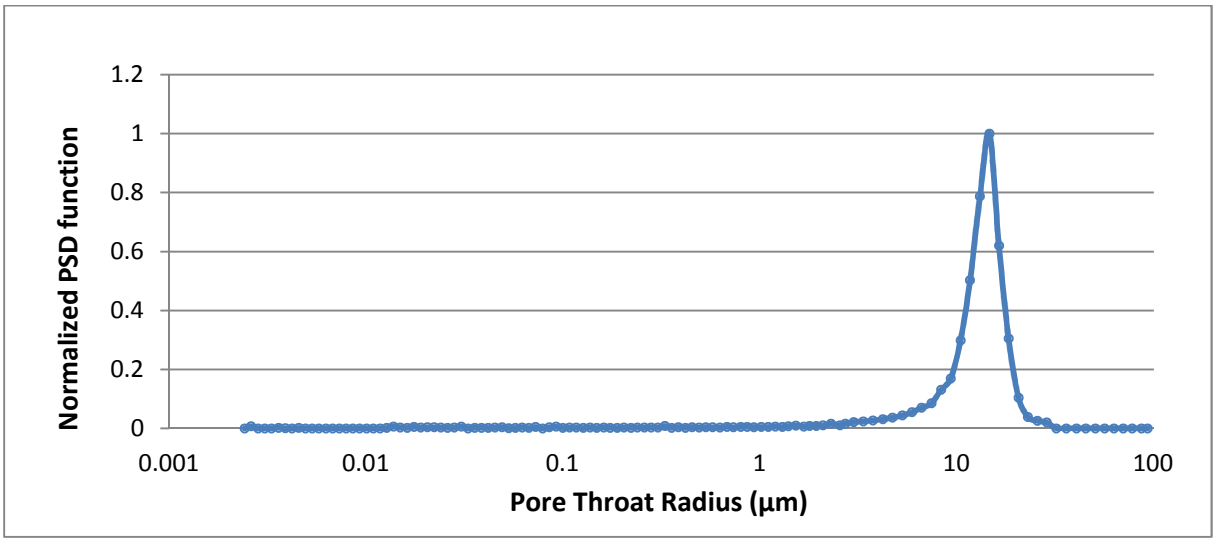

Figure 6.3 PSD of Bentheimer sandstone based on standard mercury injection

The sample which was sent to Weatherford Laboratories for analysis was small (one cubic centimetre) and may not necessarily be representative for the rock batch.

6.1.2 Synthetic Sea Water (SSW)

SSW is used for establishing connate (initial) water and injected as a primary waterflood of the four core samples. The composition and ionic strength of the SSW used in this thesis is typical to the composition of the North Sea water, where poisonous chemicals like Barium and Strontium is eliminated but the same ionic strength is accomplished. The composition of the brine is listed in Table 6.2. The SSW was put on stir for approximately a day before it was filtered using a 0,45μm vacuum filter from PALL Corporation, this in order to remove unwanted particles from the brine. The amount of Total Dissolved Solid (TDS) in the SSW is 42656 ppm.

Table 6.2 SSW composition, in total 5kg

Salt	Mass [g]	Concentration of salt [ppm]	Ionic strength	Manufacturer
NaCl	124.45	24890	0.884	Sigma-Aldrich
$CaCl_2 \cdot 2H_2O$	8.63	1726	0.073	Sigma-Aldrich
$MgCl_2 \cdot 6H_2O$	55.62	11124	0.341	Sigma-Aldrich
$NaHCO_3$	0.96	192	0.005	Fluka Chemika
Na_2SO_4	20.28	4056	0.178	Sigma-Aldrich
KCl	3.34	668	0.019	Fluka Chemika
H_2O (Distilled water)	4786.72	0	0.000	-
Total	**5000.00**	**42656**	**0.749**	**-**

6.1.3 Low Salinity water (LS)

The low salinity water was prepared by diluting filtered sea water by a factor of 10 (10 wt% SSW and 90 wt% distilled water). The amount of TDS in LS is 4266 ppm. The LS was used as an injection fluid after SSW flooding and also in combination with surfactants.

6.1.4 Oils

Marcol152 from ExxonMobil is a viscous mineral oil (viscosity approx. 50 mPa·s at 25°C) and was therefore used to get the lowest S_{wi} possible before ageing. This may be favourable in order to obtain a more sufficient wettability alteration [28].

Before injection of crude oil, n-Decane manufactured by Merck Schuchardt, was used to measure the effective permeability before ageing. From experience, n-Decane provides a more favourable stable differential pressure, and was therefore selected for permeability measurements.

The crude oil used in this study is North Sea oil produced from two different wells at the same field. The crude oil conducted in B1 and B4 contained a significant amount of gas, which is unfavourable for the ageing experiment. The oil was therefore put to stir for two days to minimize the effect of the gas.

Crude oil from the same North Sea field is analysed by Bøe [88]. Both acid number (AN) and base number (BN) were analysed as well as crude oil composition (SARA analysis), Table 6.3 and Table 6.4.

Table 6.3 Acid and base number of the crude oil [88]

Acid number [mg KOH/g oil]	Base number [mg KOH/g oil]
2.84 ±0.01	0.95 ±0.01

Table 6.4 Crude oil composition (SARA analysis) [88]

Saturated [wt%]	Aromatic [wt%]	NSO [wt%]	Asphaltenes [wt%]
55.0	38.0	6.2	0.7

The viscosity of the crude oils was in the range of 70 cP. Compared to SSW which has a viscosity of only 1cP, the mobility ratio becomes incredibly unfavourable. To achieve a more favourable mobility ratio thus a more effective displacement situation, the crude oil was diluted by addition of Xylene to lower the viscosity. The diluted crude oil utilized in experiments conducted in core sample B1 and B4, is denoted Dilute Crude oil 1 (DC1). The diluted crude oil utilized in experiments conducted in core sample B2 and B3, is denoted Dilute Crude oil 2 (DC2).

6.1.5 Surfactant

The preparation of the surfactant solution was done by mixing 0.5 wt% of surfactant in LS water. The surfactant used is S-13D, an isotridecyl alcohol 13PO sulphate surfactant (83.50% active matter) supplied by Stepan Company (illustration can be seen in Figure 6.4). No co-surfactant or co-solvent was added to the system.

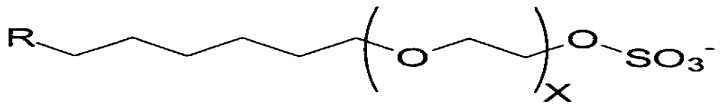

Figure 6.4 **Alcohol alkoxy sulfate surfactant**

6.2 Procedures

In this section the different methods and procedures utilized are described in more detail. The main experimental setup used during flooding experiments is schematically shown in Figure 6.5.

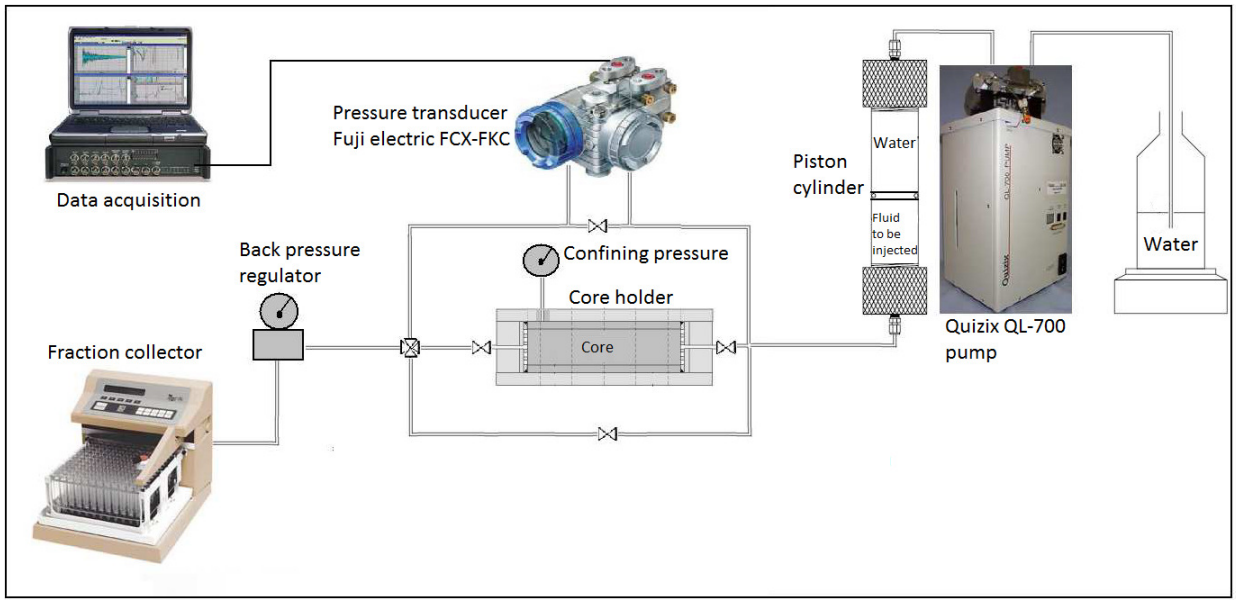

Figure 6.5 **Experimental setup [76]**

6.2.1 Core preparations

All four core samples used in this study were carefully cut to desired lengths (≈ 10 cm) and with a diameter of approximately 3.8 cm. The cores were then dried in an oven at 70°C for approximately 2 days. The core was then weighed, the volume was measured, and then it was placed in a Hassler core holder (see section 6.3.5). The dead volume of the core holder and tubes was measured before inserting the core samples. After the cores were placed in the core holder a confining pressure of 20-30 bar (always 10 bar greater than the injection pressure) was applied outside the sleeve to prevent fluids from bypassing the core during experiments. The confining pressure was achieved by placing a fluid outside the sleeve at high pressure (20-30 bar). When the injection fluid was either brine or

surfactant solution, distilled water was used as sleeve fluid. The sleeve fluid was changed to Marcol152 when oil was injected in to the core sample, to problems in case of any leakage through the sleeve.

6.2.2 Porosity measurements

The porosity of a core can be measured by a range of laboratory techniques. To calculate the porosity, it is necessary to determine at least two of the three basic parameters (V_p, V_b or V_m) in Equation 2.1.

In this master thesis, the measurement of V_p and V_b has been conducted to calculate the porosity.

Measurement of pore volume,V_p:
V_p was found by the principle of material balance. The core sample was placed in a Hassler sleeve inside a core holder and then the core was vacuumed to a pressure of less than 0.3 mbar. The inlet of the core holder was then connected to a pump, and water was injected to the core until it reached a pressure of 5 bars. The pump was then set to constant pressure delivery until the volume was constant. The water injected, $V_{w,\,injected}$, is then equal to the pore volume, V_p:

$$V_p = V_{w,injected} \qquad \textbf{Equation 6.1}$$

The measured pore volume is consistently lower than the actual pore volume due to incomplete saturation.

Measurement of bulk volume, Vb:
The bulk volume, V_b, was found by measuring the diameter, d, and the length, l, of the core with a calliper. The bulk volume (volume of cylinder) was then calculated by the equation:

$$V_b = \frac{1}{4} \cdot \pi \cdot d^2 \cdot l \qquad \textbf{Equation 6.2}$$

The length and the diameter of the cores were measured four times and the average of the values was used for further porosity calculation.

6.2.3 Permeability measurements

The absolute permeability is measured based on Darcy's law (Equation 2.2). The experimental setup for measuring the permeability is the same as in Figure 6.5 except the fraction collector was replaced by a glass bottle. By knowing the viscosity of the fluid injected, the length and diameter of the core, the permeability can be estimated by measuring the differential pressure at different flow rates. By plotting rate as a linear function of differential pressure, slope is then used to calculate the permeability, as shown in Figure 6.6.

The fluid used for absolute permeability measurements was SSW.

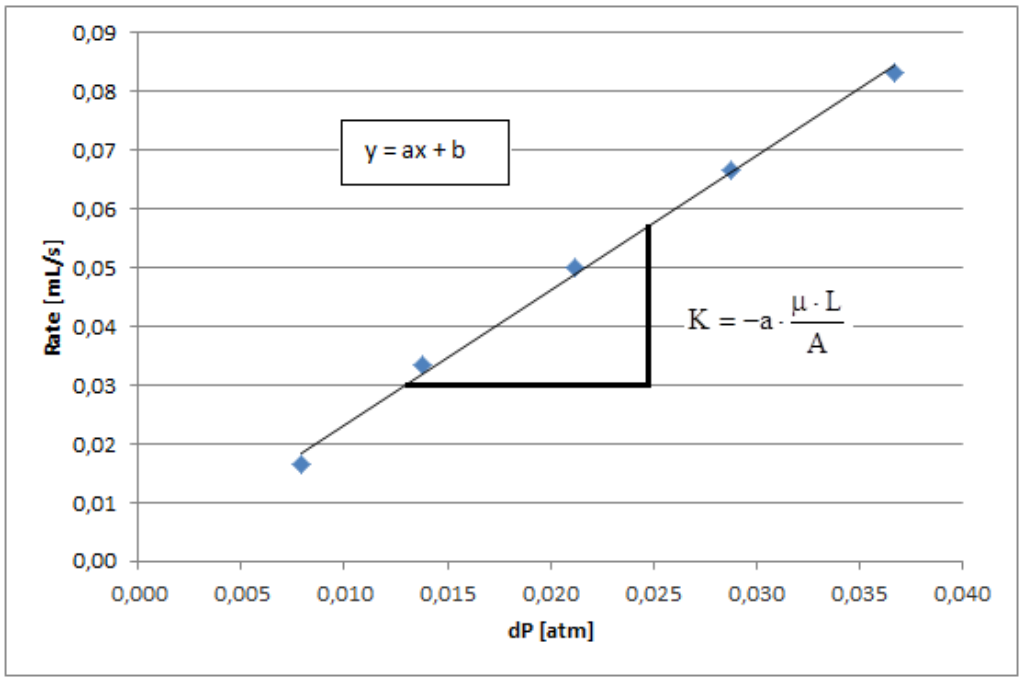

Figure 6.6 Illustration of how to calculate the permeability

When applying this method only two reference points are necessary to plot a linear relationship, however, in this study all the permeability measurements was conducted with five points to minimize the uncertainty.

The end point effective permeability was measured with the same procedure as abovementioned.

6.2.4 Drainage

The drainage of the core samples carried out in three steps. First Marcol152 (high viscosity oil) was injected into the core samples at different rates from 0.1mL/min to 1.0mL/min (minimize end effects) and the produced water was measured in a graduated flask. At initial water saturation n-Decane (selected on the basis of giving stable differential pressure) was injected similar to Marcol152 and the effective permeability at S_{wi} was measured. Similarly the core samples were flooded with crude oil using a 0.5 µm inline filter to avoid injection of larger particles.

6.2.5 Aging (wettability alteration)

After the core samples were flooded thoroughly with crude oil they were put in a heat cabin at 110°C for two weeks in order to change the wettability from strongly water-wet. The high temperature was set to enhance the reaction between crude oil components and the core material. During the two

weeks of aging, the core samples were flooded with 1 PV of “fresh” crude oil in both directions (inlet and outlet) using inlet filter as previously. This was conducted three times during the wettability alteration in order to accelerate the aging procedure.

When subjecting the core samples to high temperatures the volume of the fluids inside the core holder will expand and possible damage to the core may occur. To control the confining pressure, a vertical 20 bar cylinder filled with Marcol-152 (also used as sleeve fluid) at the bottom and nitrogen gas at the top was connected to the sleeve. To control the pressure inside the core at any time during high temperature, at least one of the valves (inlet or outlet) was open (to avoid closed system).

After two weeks the crude oil was displaced with diluted crude oil (40 wt% Xylene, 60 wt% crude oil) to obtain a better mobility ratio to water. Diluted crude oil was injected at different rates all until differential pressure was stable. The effective oil permeability was then measured.

Figure 6.7 **Core samples inside the heat cabin, cylinder to the right controls the confining pressure**

6.2.6 Synthetic sea water flooding (SSW)

The diluted crude oil was displaced with SSW with a concentration of 42656 ppm (TDS), see Table 6.2. The experimental setup is according to Figure 6.5, except the oil production was registered in an Amott cell (Figure 6.8) instead of the fraction collector.

The SSW was injected at different increasing rates (0.1-1.0mL/min), to eliminate capillary end effect. In each flow rate, water was injected until no oil was produced and the pressure was stabilized. The differential pressure across the core samples was continuously, automatically recorded during the

flooding experiments. At the end of the displacement experiment, the effective SSW permeability was measured.

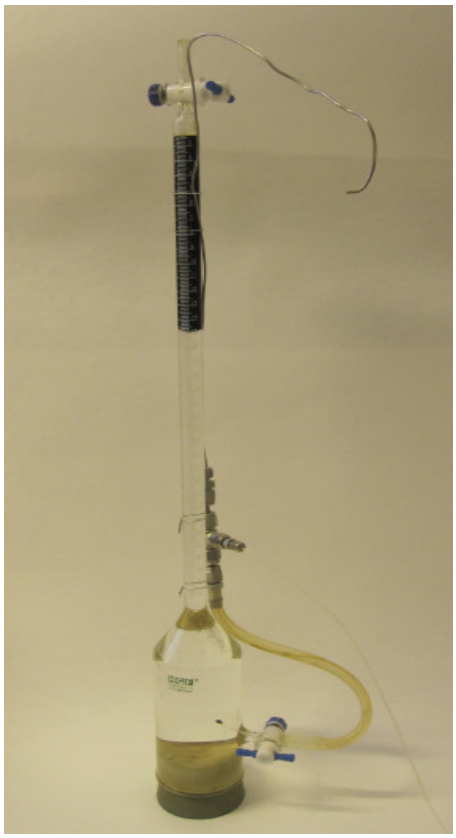

Figure 6.8 Oil production readings in Amott cell

6.2.7 Low salinity (LSW) and low salinity surfactant (LS-S) waterflooding

The low salinity waterflooding (LSW) was initiated at residual oil saturation ($S_{or,SSW}$) established by SSW injection. The low salinity surfactant (LS-S) waterflooding was initiated at residual oil saturation ($S_{or,LS}$) established by LS. The experimental setup for the LS flooding and LS-S flooding is according to Figure 6.5. The procedure is similar to SSW displacement, except the effluent was collected in test tubes instead of the Amott cell. The volume of effluent collected in each tube depended on the rate of injection, see Table 6.5. The reason for collecting the effluent in tubes was to be able to analyse the pH of the effluent with regards to production time. The pH was systematically measured in all the tubes.

During LS-S flooding the effluent was sometimes consisting of a three phase production (water, oil and emulsions) and the volume of oil in the tubes was therefore hard to estimate. To overcome this challenge, salt (NaCl) was added to the test tubes to remove the emulsion phase.

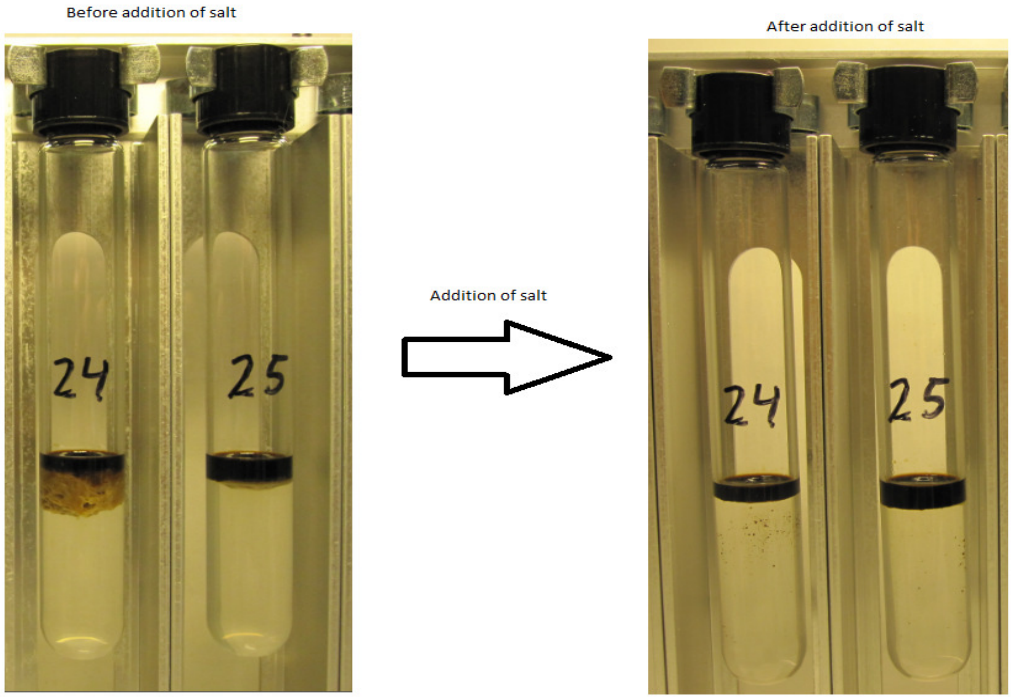

Figure 6.9 **Removing emulsion by adding salt to the system**

6.2.8 Volume estimations when using Fraction collector

One challenge when using the fraction collector is estimating the volume of oil in the test tubes. This was solved by using a set of reference test tubes with known volume, see Figure 6.10. They were made by first adding the same surfactant solution used in this thesis to the tubes and then adding known volume of oil by using a pipette. Then the volume of produced volume was estimated by comparing with the test tubes.

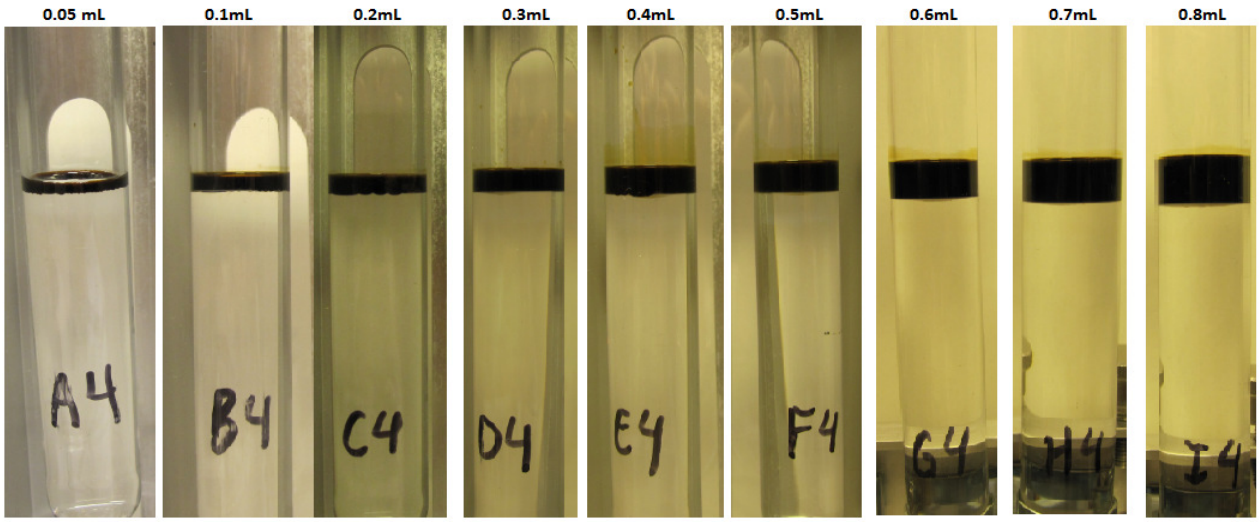

Figure 6.10 **Reference test tubes**

6.2.9 S_{or} estimation by Mohr's titration after LS-S

The residual oil saturation after LS-S flooding, $S_{or,LS\text{-}S}$, is calculated by the use of mass balance throughout the experiment. This method will lead to some source of error and it can be hard to keep track of these errors. To obtain another estimation of the $S_{or,LS\text{-}S}$, Mohr's method was applied [89].

At least 10 PV of LS was injected to the core samples at a rate of 1.0mL/min to displace the surfactant solution. Then a $NaNO_3$ solution with the same ionic strength as the LS water was injected. The same ionic strength was used to avoid any possible oil production. The amount of $NaNO_3$ injected was accurately recorded (approximately 5PV), the effluent was collected in a closed flask and then the mass of the fluid was measured.

The concentration of chloride ions in the effluent, $[Cl^-]_{eff}$, is determined by the principle of Mohr's titration. The solution was divided into several volumes which were titrated against 0.01M $AgNO_3$ (indicator: 5 wt% Potassium chromate and 1 wt% Potassium dichromate). The $S_{or,LS\text{-}S}$ is then calculated by the equation:

$$S_{or,LS-S} = 1 - S_w = 1 - \frac{V_{effl} \cdot \frac{[Cl^-]_{eff}}{[Cl^-]_{LS}} - V_{dead}}{V_p}$$

Equation 6.3

where V_{eff} is the volume of effluent, $[Cl^-]_{eff}$ is the concentration of chloride ions in the effluent from titation, $[Cl^-]_{LS}$ is the concentration of chloride ions in the LS water, V_{dead} is the dead volume of the core holder and V_p is the pore volume of the core sample.

When deciding the amount of $NaNO_3$ to inject into the core samples, the following two considerations had to be taken into account.

1) There should be injected enough $NaNO_3$ so that the LS water was displaced

2) The more $NaNO_3$ that was injected the smaller got the concentration of the chloride ions in the effluent and hence the error increased.

A balance between 1) and 2) was made and approximately 5 PV (135mL) of $NaNO_3$ was injected.

6.3 Experimental apparatus and equipment

In this section all the apparatus used for fluid analysis is described in detail with emphasis on setting, principle, procedure and uncertainties in the apparatus. At the end of this section other equipment used to perform the main experiments in this master thesis is briefly discussed.

6.3.1 Rheometer

Viscosity measurements were performed by a Modular Compact Rheometer, Physica MCR 300, from Anton Paar (Figure 6.11). The instrumental error is set to be ±2.5% (from Physica Instruction Manual). The rheometer is equipped with two sets of geometry, double gap geometry (DG-26.7) and cone plate geometry (CP-75). The type of geometry utilized depends on the estimated viscosity of the solution. For viscosities above 10 cP (crude oil) the CP-75 geometry was applied and viscosities less than 10cP (diluted crude oil, n-Decane, brine solutions and surfactant solutions) the DG-26.7 geometry was used. When measuring viscosity with temperature higher than room temperature, the measurements were conducted on the CP-75 geometry due to more stable results.

At 90°C viscosities observed were not reproducible, and thus the viscosities at different temperatures (40, 50, 60, 70°C) were measured. The viscosity at 90°C was found by extrapolation.

The temperature during the measurements was controlled by a Peltier water circulating apparatus (±0.1°C).

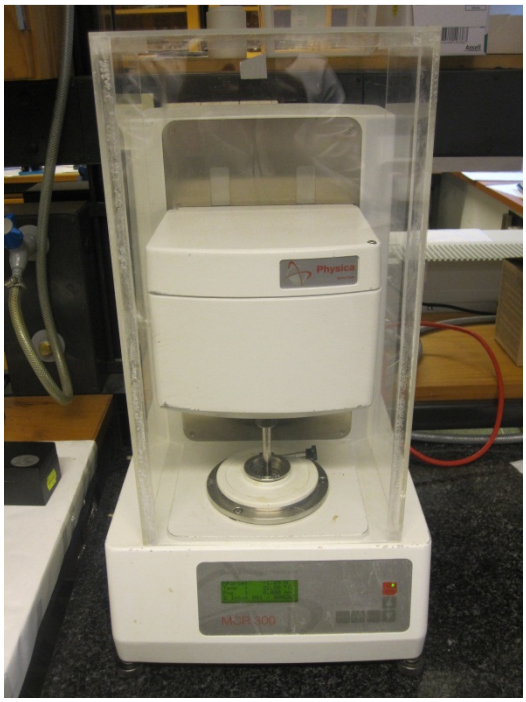

Figure 6.11 Physica MCR 300 from Anton Paar

Both geometries consist of a measuring bob, which is rotated by the instrument motor and a lower plate/cylindrical cup which stands still. When a rotational speed is applied to the measuring bob, the measuring bob requires a certain amount of torque for this speed. The measurement pre-set is the rotational speed (shear rate, $\dot{\gamma}$) and the measurement result is the torque (shear stress, τ), see Figure 6.12. Then the viscosity, μ, is calculated easily by rearranging Equation 2.11:

$$\mu = \frac{\tau}{\dot{\gamma}}$$ **Equation 6.4**

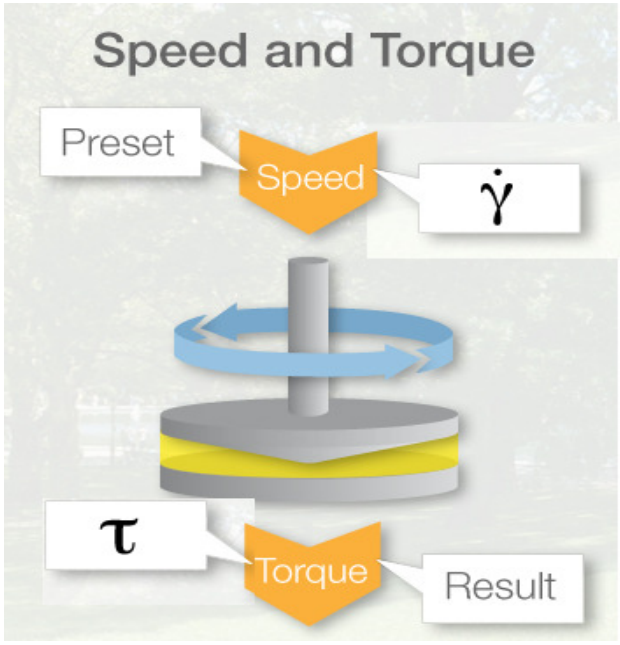

Figure 6.12 Principle behind the rheometer (Cone-plate illustration)

Measuring the viscosity at room temperature (23°C) the shear rate was set to increase during 30 logarithmic intervals (45 seconds each) from 10-1000 s^{-1}, and then similarly decreasing from 1000-10s^{-1}. Since the fluids are Newtonian fluids the viscosity is theoretically independent of shear rate. When measuring the viscosity as a function of shear rate, the function is not constant at low shear rates (to low shear stress to measure accurately) and high shear rates (turbulent flow). The chosen viscosity was therefore taken at 200s^{-1} (Figure 6.13).

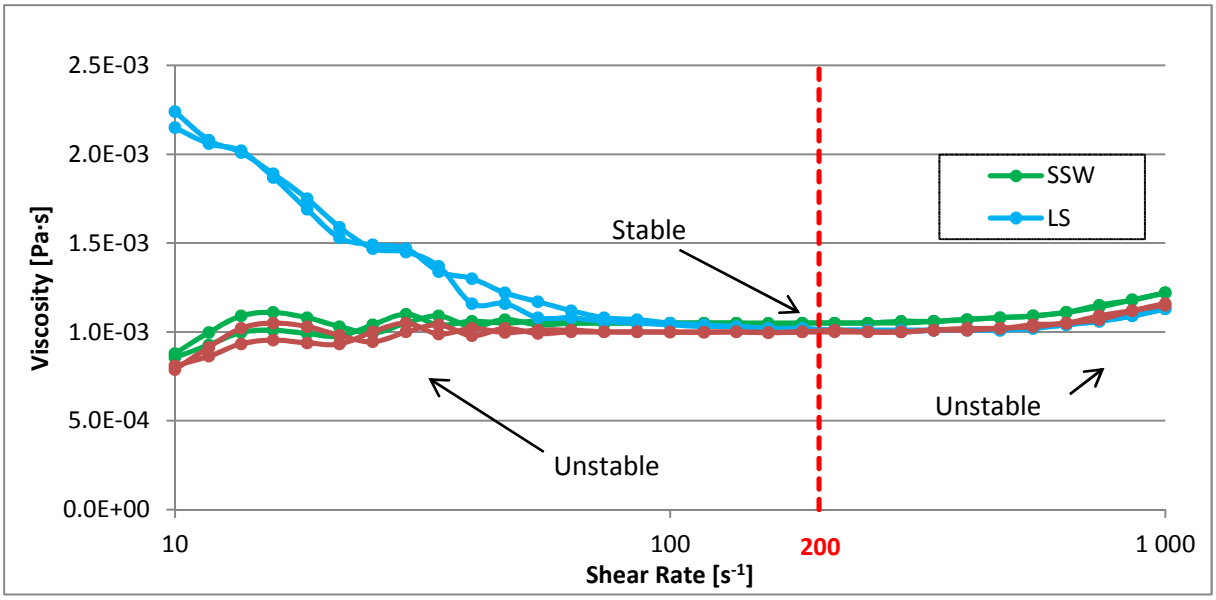

Figure 6.13 **Viscosity profile (at T = 23°C). The viscosity is constant at a shear rate of 200 s^{-1}**

To get the viscosities at 90°C, the shear rate was set at constant rate (200s^{-1}) with increasing temperature at time intervals of 5 minutes. Viscosity at each temperature was then found based on the average of the stable viscosities, see Figure 6.14. Then the viscosities were plotted against temperature and an exponential approach was made based on studies by El-Dessouky et al. [90].

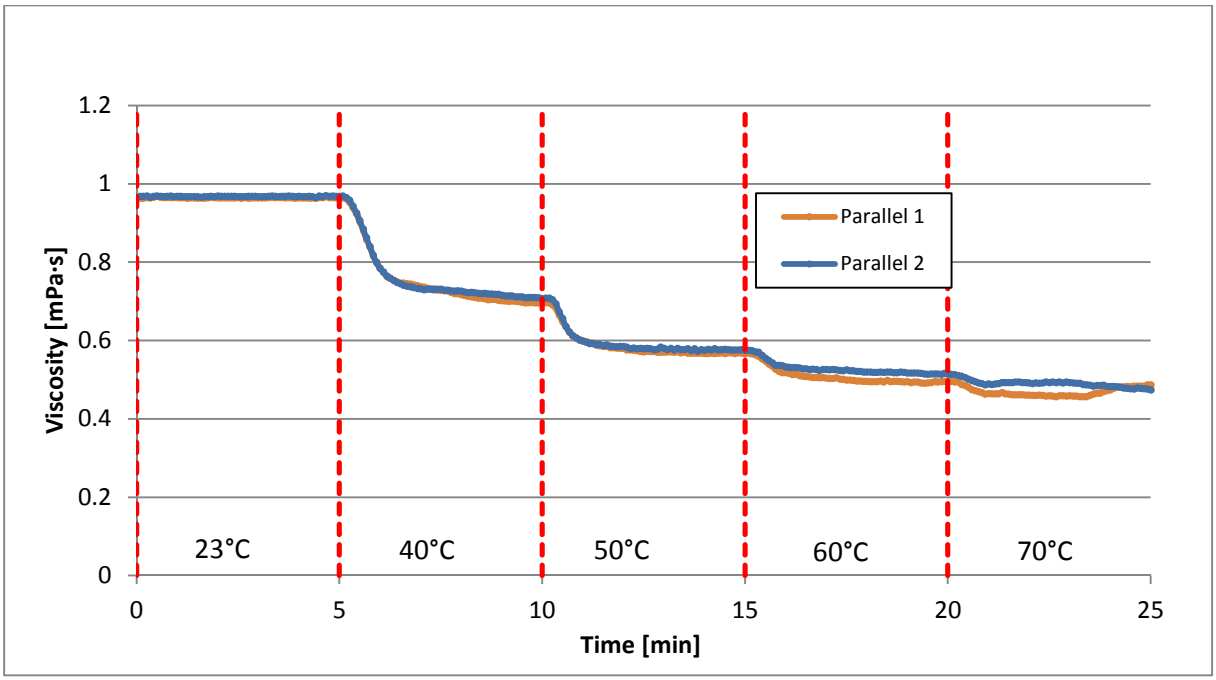

Figure 6.14 **Viscosity profile with increasing temperature (LS)**

6.3.2 Densitometer

The fluid densities were measured using a DMA 60 processing unit and a DMA 602 HT density measuring cell made of glass. The apparatus are produced by Anton Paar, see Figure 6.15. There is a high temperature range for this setup (-180 to +150°C), and the maximum instrumental error is set to be $\pm 10^{-4}$ g/cm^3. The temperature is controlled by a water bath connected to the densitometer. Measurements of densities with this apparatus are based on the law of harmonic oscillations.

The densities were measured for six different fluids (crude oil, two different diluted crude oils, LS, SSW and LS-S) at different temperatures (23, 40, 50, 60, 70°C). The density values measured were needed as input values when measuring the IFT using the spinning drop instrument.

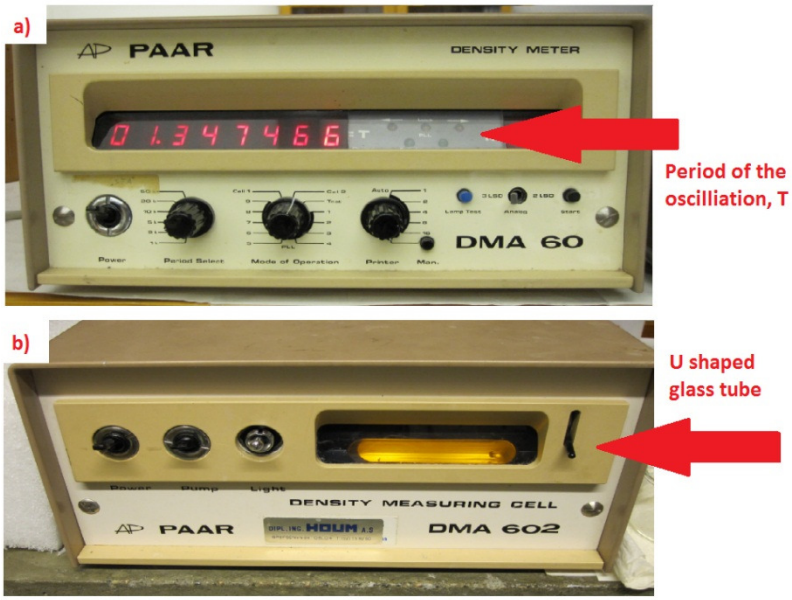

Figure 6.15 **Densitometer: a) DMA 60 processing unit, b) DMA 602 HT density measuring cell**

The sample is introduced into a U shaped sample tube (1mL) which is electromagnetically excited to vibrate at its natural frequency. From the frequency change caused by a specific sample inside the sample tube the density of the sample can be determined with high precision.

The density of a fluid, ρ, can be expressed as a function of its period, T:

$$\rho = \frac{1}{A} \cdot (T^2 - T_{water}{}^2) - \rho_{water} \qquad \textbf{Equation 6.5}$$

where A is an apparatus constant, T_{water} and ρ_{water} is reference values (hence water).

To estimate the apparatus constant, A, the periods of water and air (T_{air} and T_{water}) was measured and also the pressure, temperature and the air humidity was needed to calculate the air density.

The apparatus constant A is calculated by the equation:

$$A = \frac{T_{air}^{\ 2} - T_{water}^{\ 2}}{\rho_{air} - \rho_{water}} \qquad \textbf{Equation 6.6}$$

where T_{air} and T_{water} are measurements of air and water periods respectively, ρ_{water} is the literature density of water [91] and ρ_{air} is calculated from the equation above:

$$\rho_{air} = 0{,}46464 \cdot \frac{P - 0{,}08987 \cdot F}{T} \cdot 10^{-3} \qquad \textbf{Equation 6.7}$$

where P is the pressure in mmHg, F is the relative humidity in % and T is the temperature in Kelvin. The apparatus constant, A, needs to be calculated for each temperature used in this experiment.

The sample is filled into the U shaped tube by injection with a 3 mL syringe. Before each measurement the tube was thoroughly cleaned and then the sample was injected. A light behind the tube made it possible to inject the sample and avoid air bubbles in the system. After 8 minutes of waiting time, the periodic number was noted when only the sixth decimal was changing.

For the aqueous samples the test tubes were cleaned with distilled water, acetone and then air dried. If the sample was crude oil or diluted crude oil the test tubes were cleaned in the sequence; toluene, acetone, distilled water and then air dried.

For each fluid density measured, three parallels were carried out and an average of the values was calculated.

6.3.3 Spinning drop tensiometer

IFT measurements were performed with computer controlled Spinning Drop Tensiometer SITE100 from Krüss GmbH, see Figure 6.16. This apparatus can only measure the IFT in the range 10^{-6}-10 mN/m. Due to the low upper limit the tensiometer is unable to measure the IFT on the majority of the oil/brine system without surfactants. The spinning Drop Tensiometer is connected to a camera and controlled by the Krüss DSA2 software which is used for image acquisition, analysis evaluation.

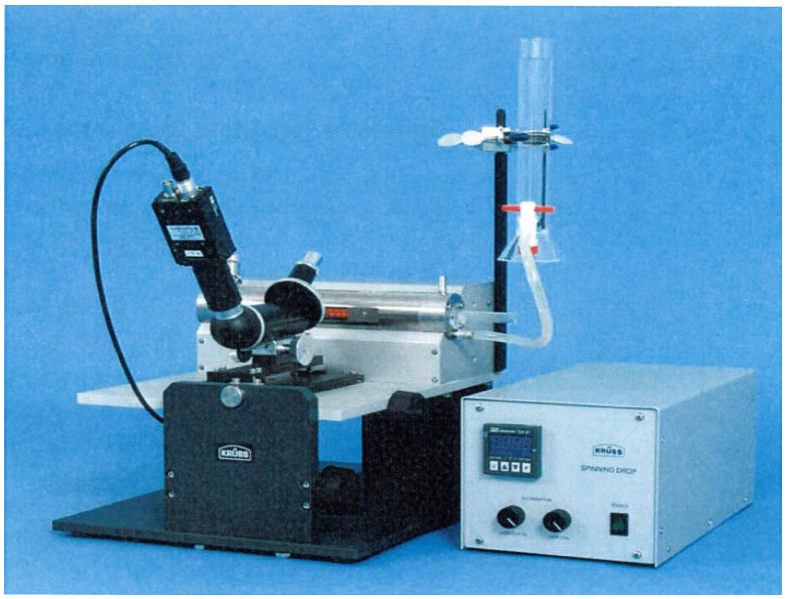

Figure 6.16 Spinning Drop Tensiometer SITE100 from Krüss GmbH

Several methods may be applied when measuring IFT, such as the Spinning drop method, Capillary rise method, Wilhelmy Plate method, Ring method and Pendant drop method. The spinning drop method has been developed to measure very low IFT. This is favourable when measuring IFT on surfactant systems (low IFT).

The method of spinning drop is based on the principle of balance between centrifugal forces and IFT. In this method a light drop phase is situated in a horizontal, rotating, cylindrical glass tube containing a heavier bulk phase. The less dense fluid will then form a drop, which elongates along the axis of rotation. The shape of the drop will be dependent on the velocity of the rotation, ω. If ω is very small the drop will be almost spherical (due to IFT) and under the influence of gravitational force. On the other hand, if ω is sufficiently high, the drop will stretch out and become cylindrical. When the drop length is at least 4 times greater than the drop radius, r, the following approximate expression holds:

$$\sigma = \frac{1}{4} \cdot r^3 \cdot \omega^2 \cdot (\rho_H - \rho_L) \qquad \textbf{Equation 6.8}$$

To be able to use the spinning drop method, the density of the light phase, ρ_L, and the density of heavier phase, ρ_H, must be known.

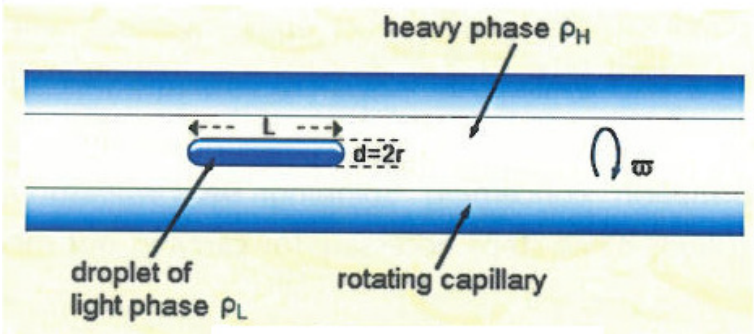

Figure 6.17 Illustration of the principle behind the spinning drop method

The IFT was measured between the surfactant solution used in this thesis (heavier phase) and diluted crude oil at different temperatures (23.0°C, 40.0°C and 60.0°C) to be able to extrapolate to 90°C.

Before starting the measurements, the apparatus was calibrated with a 0.668mm wide needle when only the heavy phase was present. To avoid air bubbles in the heavy phase, the rotation velocity was set to 5000 RPM until no air bubbles were seen on the screen.

A drop of crude oil was injected and the IFT was measured continuously (30 seconds interval) at 4 different rotation velocities for each of the temperatures.

6.3.4 pH meter

Measurements of pH were performed with the Waterproof Handheld H160 pH meter produced by Hach Company. The pH meter also measures the temperature of the solution. This pH meter gives an accuracy of ±0.01pH.

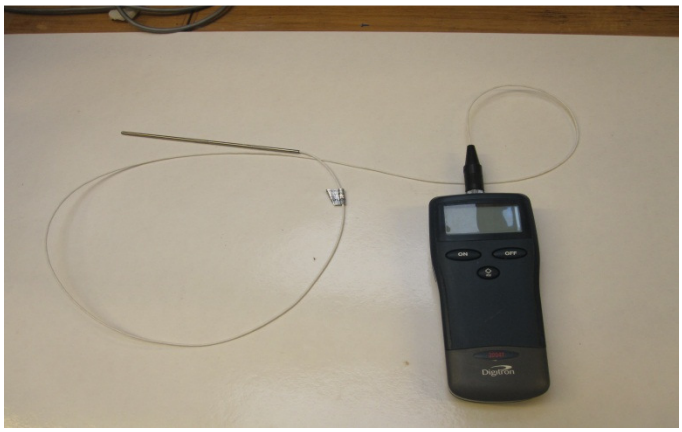

Figure 6.18 Hach Handheld H160 pH meter

An electrochemical cell for pH measurements consists of three parts [92]:

1. An indicating electrode whose potential is directly proportional to pH
2. A reference electrode whose potential is independent of pH
3. The aqueous sample to be measured.

If all three parts are in contact with each other, a potential can be measured between the indicating electrode and the reference electrode, which depends on the pH of the sample and its temperature. Because of the complexity of a pH measurement, the combination of indicating and reference electrode must be calibrated in advance, to compensate for slight changes over time. The relation between measured potential E (mV), reference potential E^0, pH and temperature (K) is given by the Nernst equation:

$$E(T) = E^0(T) - \frac{R \cdot T}{F} \cdot pH \qquad \textbf{Equation 6.9}$$

where R is the molar gas constant ($8.3144 Jmol^{-1}K^{-1}$), T is the temperature(Kelvin) and F is the Faraday constant ($96485 Cmol^{-1}$). When temperature is known, the pH can be calculated from Equation 6.9. The pH of the solution was given directly on the pH meter and no pH calculation was needed in this thesis.

A two-point calibration was conducted on the pH meter before starting the measurements (pH=4 and pH=7). The probe was placed in the solution, stirred and after a few seconds the pH and the temperature appeared on the screen on the pH meter. The probe was gently washed with soap and distilled water between each of the measurements, to reduce measuring errors.

6.3.5 Other experimental equipment

Other experimental equipment utilized includes:

- The core samples were mounted into Hassler Core holders, Figure 6.19 a). The core samples were held in a rubber sleeve inside the Hassler core holder thus forcing the flow to be uniaxial.
- A Quizix (QL-700) pump from Chandler Engineering Company L.L.C , Figure 6.19 b), was used combined with a windows-based software program that allows complete and automated control of the pump system.
- The pressure drop across the cores during the experiments where measured by Fuji electric FCX-FKC differential pressure transmitter (maximum 5bar), Figure 6.19 c). Voltage signals were transferred to computer and the data processing was carried out in a LabView program.
- A Foxy Jr. fraction collector (capacity of 100 - twelve mL test tubes) was used to collect fluid samples during the experiments, Figure 6.19 d). The time setting of the collector was depending on the rate and is summarized in Table 6.5.

- Swagelok 1/8 stainless steel valves, Figure 6.19 f), fittings and perfluoroalkoxy tubing were used in all the experiments.
- Vacuum ejector from Edwards (model RV3) was used to evacuate air from the core samples before porosity measurements, Figure 6.19 e). The core samples were evacuated down to a pressure of less than 300 mTorr which was measured by Granville-Phillips 275 Mini-Convetron.
- Back pressure regulator (BPR) was used to prevent development of air bubbles in the system at any time, Figure 6.19 g). This was set to 5.0 bar during the experiments at room temperature and 10 bar in the experiments carried out at 90°C.

Table 6.5 Time setting of fraction collector

Rate [mL/min]	Fraction time [min]	Volume [mL]
0.1	120	12.0
0.3	30	9.0
1.0	10	10.0

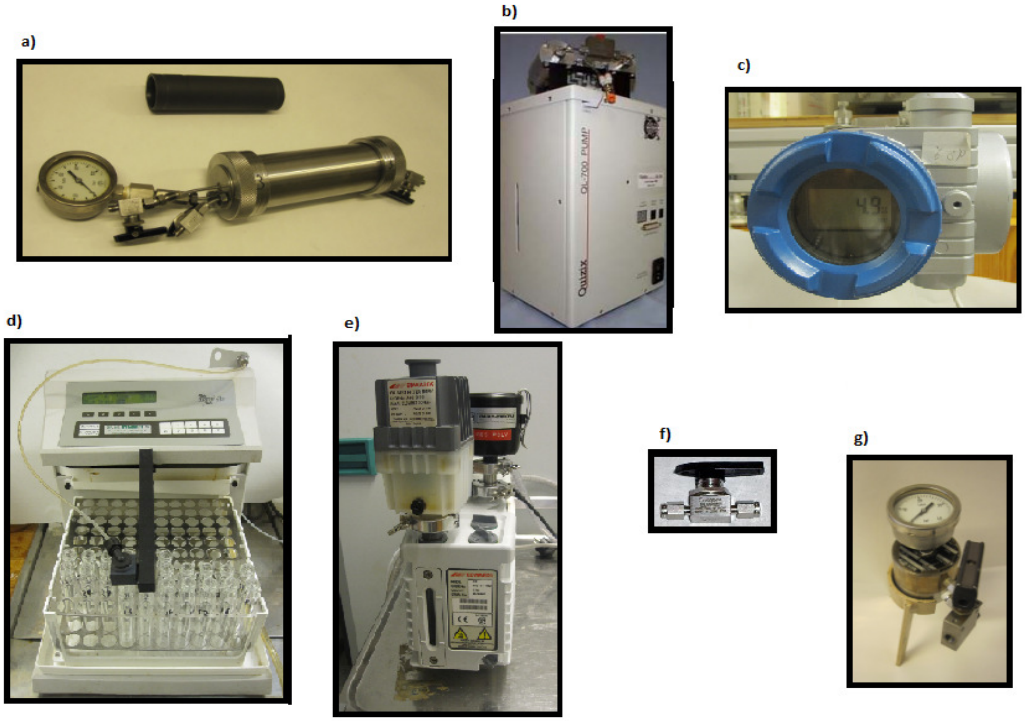

Figure 6.19 Different experimental equipment a) Hassler core holder and sleeve on top, b) Quizix pump (QL-700) c) Fuji electric FCX-FKC differential pressure transmitter d) Foxy Jr. fraction collector e) Vacuum ejector from Edwards f) Swagelok valve g) Back pressure regulator

7 Main results and discussion

The main objective of this study was to investigate the impact of LS injection and a combination of LS with surfactant flooding on oil recovery using four aged Bentheimer cores at two different temperatures (23°C and 90°C).

The core flooding experiments were conducted using two different diluted crude oils, hereafter denoted DC1 and DC2 (Diluted Crude oil 1 and 2, respectively). DC1 were used in coreflood experiments concerning B1 and B4 (parallel 1), and DC2 were used in coreflood experiments concerning B2 and B3 (parallel 2).

Another difference in the coreflood experiments are the temperature. Experiments on B1 and B2 were conducted at 90°C and B3 and B4 were conducted at 23°C, see Table 7.1.

Table 7.1 List of the diluted crude oil used on the different core samples as well as the temperature during the core flood experiments

Parallel	Core ID	Diluted crude oil	Temperature [°C, ±0.5]
1	**B1**	DC1	90.0
	B4	DC1	23.0
2	**B2**	DC2	90.0
	B3	DC2	23.0

The procedure of the flooding experiments was carried out in the same manner on each of the core samples. The main flooding experiments can be divided into three steps:

1. First injection of SSW down to S_{or} was achieved in order to investigate the effect of LS injection in tertiary mode. The SSW was injected with different rates to reduce capillary end effects.
2. Low salinity (LS) injection was carried out in order to consider the potential of LSE in aged Bentheimer. The LS was also injected at different rates to reduce capillary end effects.
3. Combined low salinity and surfactant injection (LS-S) was performed in order to investigate the impact of reduced capillary force in a low salinity environment. The LS-S was also injected at different rates to reduce capillary end effects.

7.1 Fluid and rock properties

Knowledge of fluid and rock properties is of fundamental importance in reservoir engineering. This knowledge may help obtain a better insight to the experiments, as well as gaining a better understanding of the concept behind waterflooding.

7.1.1 Density results

The fluid densities of the LS-S solution and the two diluted crude oils, listed in Table 7.2, shows, as expected [60], a decreasing behaviour as the temperature is increasing. The densities of DC1 are slightly smaller than DC2, which indicates that DC1 contains lighter components. The density results are further used as inputs in the IFT measurements.

Table 7.2 Fluid densities, ρ, of LS-S solution and two different diluted crude oils (DC1, DC2)

T [°C]	ρ_{LS-S} [g/mL]	ρ_{DC1} [g/mL]	ρ_{DC2} [g/mL]
23.0	1.0002 ±0.0001	0.8980 ±0.0002	0.9143 ±0.0002
40.0	0.9946 ±0.0001	0.8844 ±0.0004	0.8855 ±0.0004
60.0	0.9854 ±0.0001	0.869 ±0.001	0.870 ±0.001

7.1.1 Interfacial tension results

IFT was measured between the two different diluted crude oils (DC1 and DC2) and the surfactant solution (0.5 wt%), later denoted $\sigma_{LS-S,DC1}$ and $\sigma_{LS-S,DC2}$. This was carried out at different temperatures. As can be seen in Table 7.3, the $\sigma_{LS-S,DC1}$ is significantly lower than the $\sigma_{LS-S,DC2}$, which in turn contributes to a lower capillary force between the two fluids. There are a considerably increase in the IFT as the temperature increases for both of the system.

Table 7.3 IFT, σ, between LS-S and DC1, and LS-S and DC2 at different temperatures

T [°C]	$\sigma_{LS-S,DC1}$ [mN/m]	$\sigma_{LS-S,DC2}$ [mN/m]
23.0	0.116 ±0.006	0.146 ±0.006
40.0	0.76 ±0.01	0.78 ±0.01
60.0	1.21 ±0.02	1.46 ±0.02
90.0	1.7* ±0.1	2.4* ±0.1

* Calculated by a logarithmic extrapolation of the other values

7.1.1 Viscosity results

The viscosities of the various fluids at different temperatures are listed in Table 7.4. As shown in the table, the viscosities of the diluted crude oils differs, where the DC1 are slightly more viscous than DC2. For the aqueous solutions, the viscosities increase with decreasing temperature as expected. By comparing LS and SSW, the viscosities decrease with increasing salinity in the water.

Table 7.4 Viscosities of the diluted crude oils (DC1 and DC2) and the aqueous solutions (SSW, LS and LS-S) at different temperatures, and n-Decane at room temperature

T [°C]	μ_{DC1} [mPa·s]	μ_{DC2} [mPa·s]	μ_{SSW} [mPa·s]	μ_{LS} [mPa·s]	μ_{LS-S} [mPa·s]	$\mu_{n\text{-Decane}}$ [mPa·s]
23.0	4.3 ±0.1	4.3 ±0.1	1.01 ±0.03	0.95 ±0.03	0.97 ±0.03	0.84 ±0.03
40.0	3.0 ±0.1	3.0 ±0.1	0.71 ±0.03	0.66 ±0.03	0.71 ±0.03	-
50.0	2.7 ±0.1	2.6 ±0.1	0.65 ±0.03	0.55 ±0.03	0.57 ±0.03	-
60.0	2.5 ±0.2	2.4 ±0.2	0.54 ±0.04	0.48 ±0.04	0.51 ±0.04	-
70.0	0.4 ±0.2	2.3 ±0.2	0.47 ±0.04	0.47 ±0.04	0.47 ±0.04	-
90.0	2.4* ±0.3	2.3* ±0.3	0.33* ±0.05	0.33* ±0.05	0.31* ±0.05	-

* Calculated by extrapolation of the other values

7.1.1 Rock properties

Before starting the main experiments, it is important to choose core samples with similar physical properties. In order to achieve this, a total of eleven core samples were investigated, whereas four were selected for further experiments, see Table 7.5.

Table 7.5 Physical properties of the core samples

Core ID	Length [cm]	Diameter [cm]	Bulk volume [cm^3]	Pore Volume [cm^3]	Porosity [%]	Absolute Permeability [D]	S_{wi}	OOIP [%]
B1	9.92 ±0.01	3.775 ±0.005	111.0 ±0.2	27.1 ±0.2	24.4 ±0.2	2.04 ±0.06	0.15 ±0.03	23.1 ±0.1
B2	9.93 ±0.01	3.775 ±0.005	111.2 ±0.2	26.6 ±0.2	23.9 ±0.2	2.09 ±0.05	0.14 ±0.03	22.8 ±0.1
B3	9.92 ±0.01	3.776 ±0.005	111.1 ±0.2	26.7 ±0.2	24.1 ±0.2	1.41 ±0.03	0.16 ±0.03	22.5 ±0.1
B4	9.95 ±0.01	3.779 ±0.005	111.6 ±0.2	26.8 ±0.2	24.0 ±0.2	1.23 ±0.05	0.13 ±0.03	23.3 ±0.1

It can be seen in Table 7.5 that the volume and porosity of the four core samples are comparable. The absolute permeability on the other hand differs from one another. Two of the core samples, B1 and B2, have permeability in 2 D range, and also B3 and B4 have a similar permeability range (1.2 D - 1.4 D). Based on these values, waterflooding experiments on B1 and B2 was conducted at a temperature of 90°C and B3 and B4 was conducted in room temperature (23°C).

Variations in porosity and permeability seem to have little influence on initial water saturation, S_{wi}, and OOIP in the core. However, it is worth noticing the low S_{wi} in B4, which in turn give rise to a more favourable initial condition prior to wettability alteration. The degree of wettability alteration may increase by decreasing S_{wi} as was illustrated by Jadhunandan [28].

7.2 Production profiles

Summary of important results from different stages in the flooding sequence of the core samples are listed in Table 7.7 to Table 7.10. Figure 7.1 to Figure 7.4 display pressure drop profile and oil recoveries as function of volume injected.

The different colours in the oil recovery profile illustrate variation in the injection rate (Figure 7.1 to Figure 7.4). The red dotted line distinguishes the different flooding steps. The grey curve represents the pressure distribution. Although the pressure was measured continuously during the experiments, the pressure was not always recorded, which resulted in a lack of pressure data. During the LS-S core flood experiments, the pressure was highly unstable, which may indicate the formation of emulsion. In addition, in all four cases, the pressure build-up became extremely high (exceeded the limit of the pressure transducer).

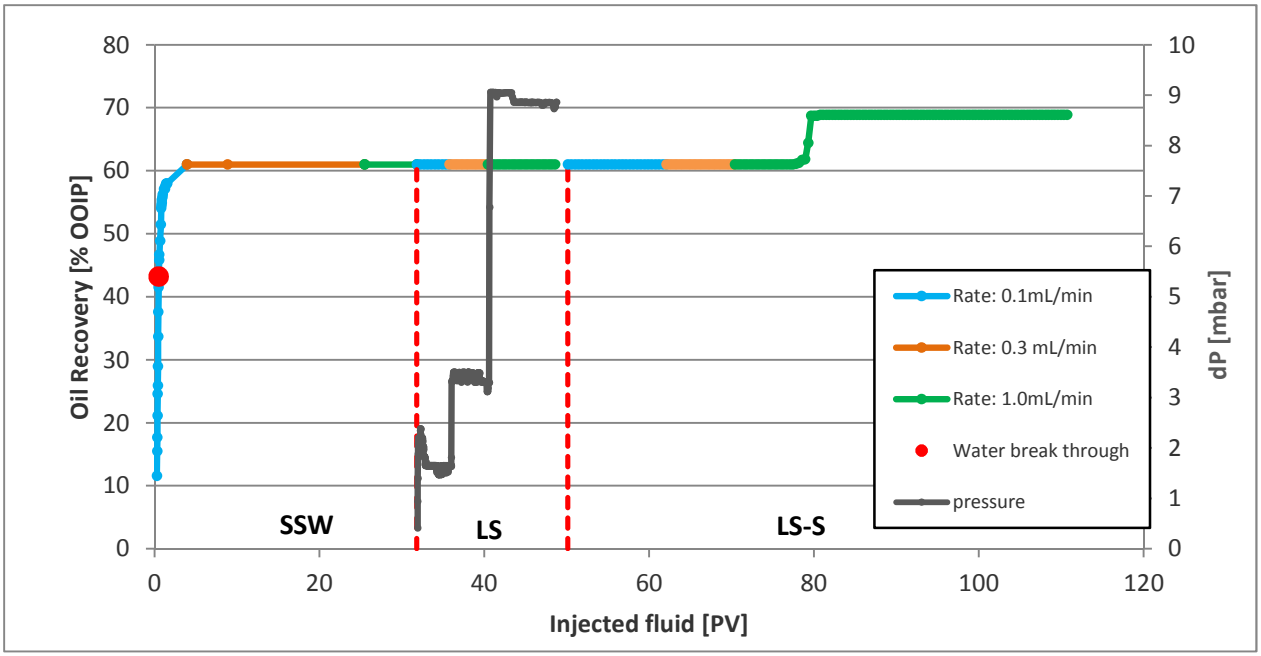

Figure 7.1 **Oil recovery curve obtained from coreflood experiment on Bentheimer core B1. The grey curve represents the pressure distribution, the curve with different colours (correspond to different rates) represent the amount of oil produced in terms of OOIP through the three steps.**

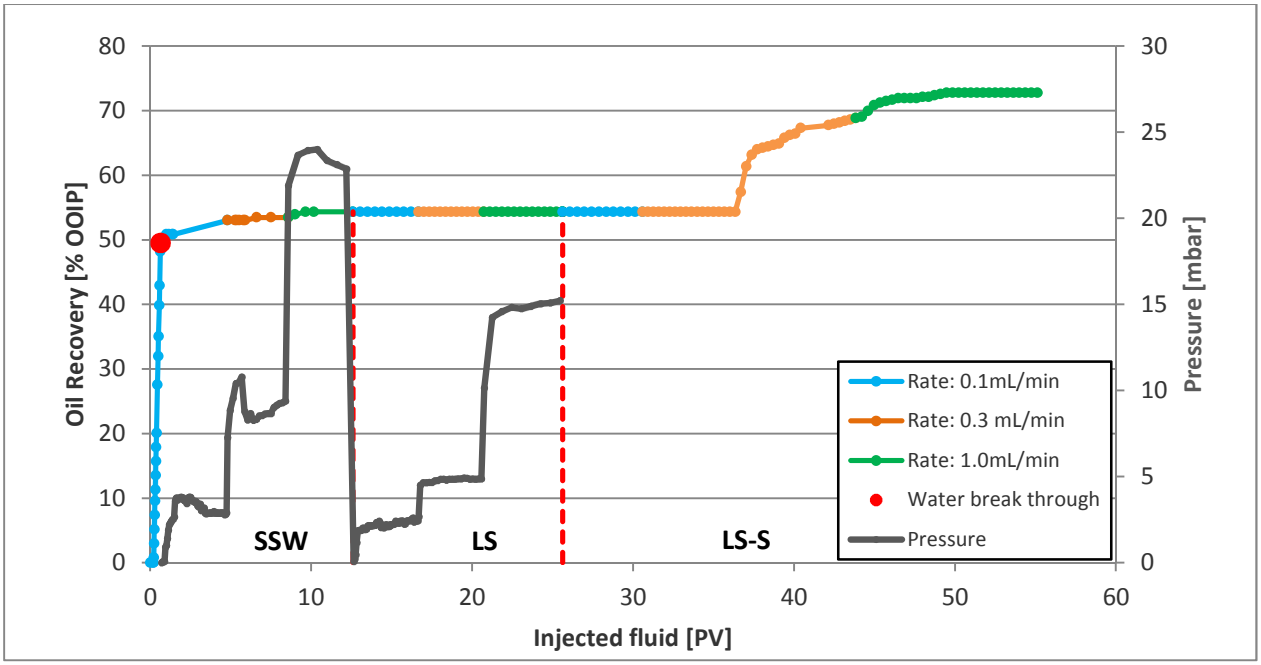

Figure 7.2 **Oil recovery curve obtained from coreflood experiment on Bentheimer core B2. The grey curve represents the pressure distribution, the curve with different colours (correspond to different rates) represent the amount of oil produced in terms of OOIP through the three steps.**

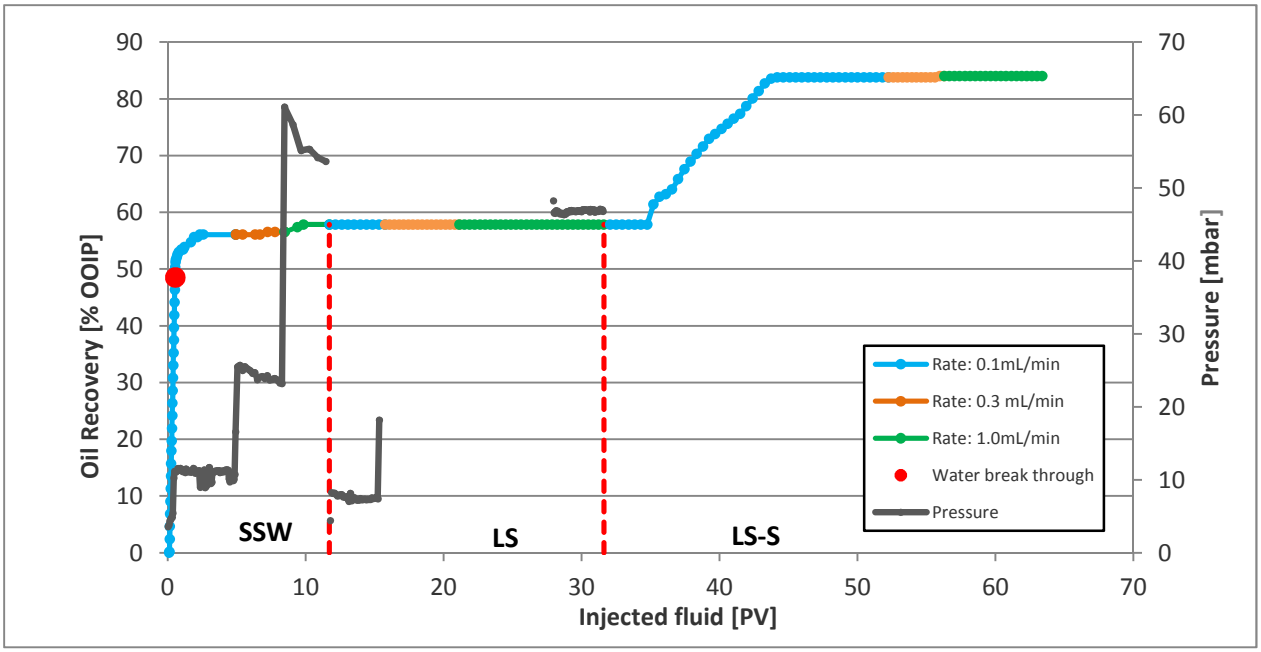

Figure 7.3 **Oil recovery curve obtained from coreflood experiment on Bentheimer core B3. The grey curve represents the pressure distribution, the curve with different colours (correspond to different rates) represent the amount of oil produced in terms of OOIP through the three steps.**

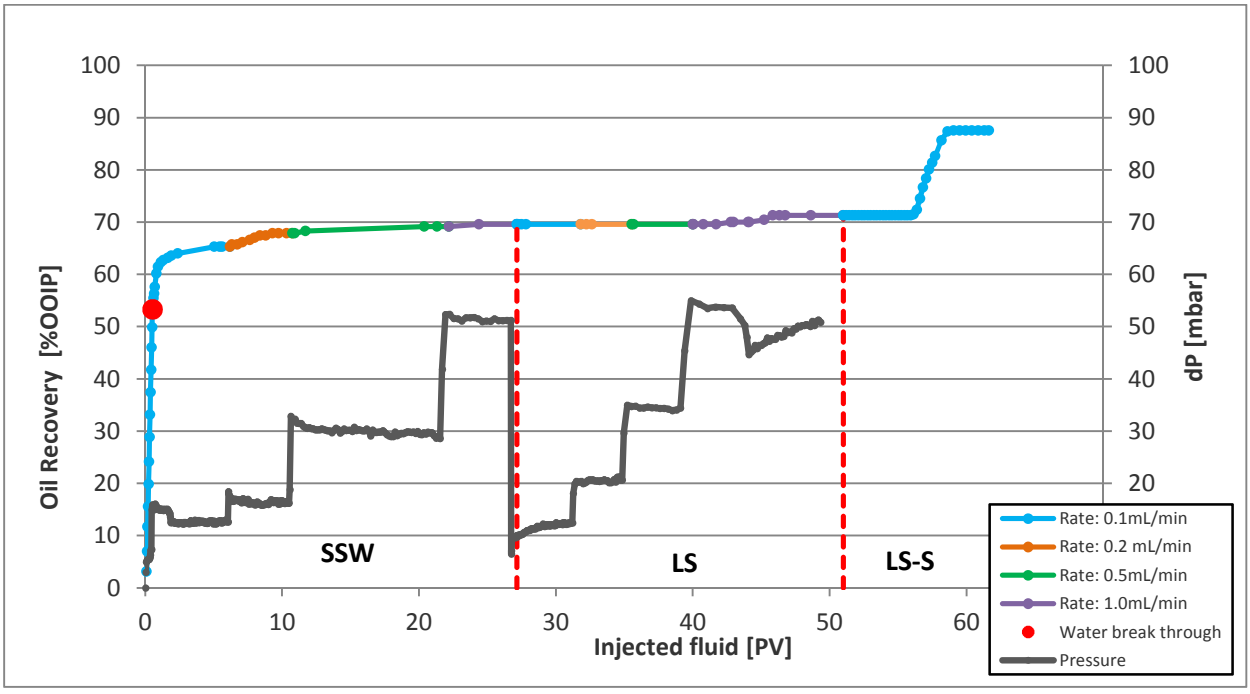

Figure 7.4 **Oil recovery curve obtained from coreflood experiment on Bentheimer core B4. The grey curve represents the pressure distribution, the curve with different colours (correspond to different rates) represent the amount of oil produced in terms of OOIP through the three steps. During LS at a rate of 1.0 mL/min, there was a 12 hour stop in the injection before the injection continued.**

7.3 Synthetic Sea Water (SSW) flooding

Before starting the LS and LS-S experiments, all the core samples were flooded with SSW to establish S_{or}. The SSW injection was carried out at different increasing rates (from 0.1-1.0 mL/min) all until the oil production stopped and the differential pressure was stable. The purpose of the SSW injection is to establish a conventional waterflood in which LS potential will be investigated in a tertiary mode. Some of the experimental parameters of the SSW injection are listed in Table 7.6.

Table 7.6 Experimental results (SSW)

Core ID	WBT [% OOIP]	SSW Recovery [% OOIP]	$S_{or.SSW}$	k_{rw} ($S_{or,SSW}$)
B1	43.23 ±0.05	61.00 ±0.05	0.333 ±0.002	0.23 ±0.03
B2	49.50 ±0.05	54.33 ±0.05	0.391 ±0.002	0.12 ±0.02
B3	49.50 ±0.05	57.85 ±0.05	0.355 ±0.002	0.209 ±0.008
B4	53.30 ±0.05	69.58 ±0.05	0.265 ±0.002	0.25 ±0.01

7.3.1 Observations

During the aging process, the core samples were subjected to crude oil at 110°C for two weeks. This was carried out in order to alter the wettability of the strongly water wet outcrop core samples. To test whether the aging process has resulted in a decrease of the core samples water wetness, the study of the waterflood characteristics such as production profiles, WBT and the endpoint permeability to water is needed [20]. These characteristics may only serve as an indication of the wettability state.

A waterflood in a strongly water wet system is recognized with modest additional oil recovery after breakthrough (narrow two phase production). In addition, the WBT occurs much earlier in an oil-wet systems [93]. This is also illustrated in Figure 2.6. A substantial two phase production period can be observed for both B1 and B4 which implies a less water-wet system (Figure 7.5). B2 and B3 have a minor two phase production, which may signal a smaller change in the wettability.

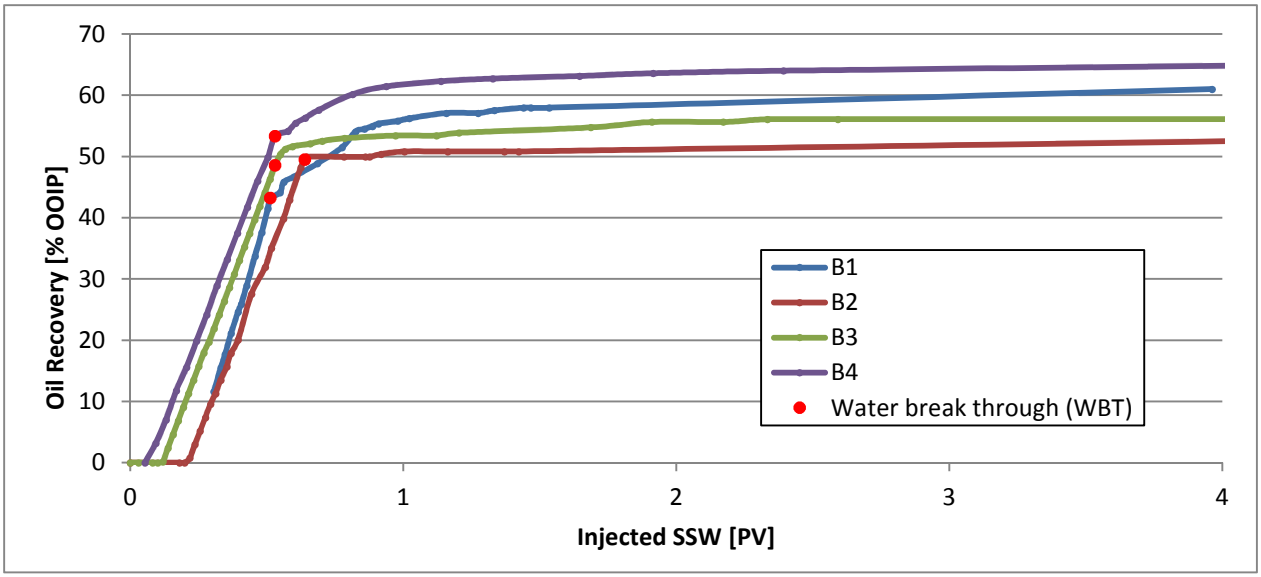

Figure 7.5 **Oil production curve for the first 4 PV of SSW injection**

A comparison of the relative permeability to oil at initial water saturation, k_{ro}, before and after aging, may also give an indication of the wetting alteration. The k_{ro} of the cores are expected to decrease as the wettability alters from strongly water-wet [42] . As can be seen in Table 7.7, this is not the case for the four core samples, which have an increase in the k_{ro} before and after aging. This may indicate a poor wettability alteration of the core sample. This method however, is not favourable to detect small changes in the wettability (e.g. between strongly and moderate water-wet) [44].

Table 7.7 **Absolute permeability (K), and end point relative permeability of oil, k_{ro} (S_{wi}) before and after aging in the four core samples (B1-B4)**

Core ID	Absolute Permeability [D]	k_{ro} (S_{wi}) before aging	k_{ro} (S_{wi}) after aging
B1	2.04 ±0.06	1.02 ±0.05	1.30 ±0.04
B2	2.09 ±0.05	1.11 ±0.05	1.15 ±0.03
B3	1.41 ±0.03	0.99 ±0.04	1.28 ±0.03
B4	1.23 ±0.05	0.72 ±0.04	1.54 ±0.06

As can be seen in Figure 2.5 in section 2.4 (Rock Wettability), the S_{or} is declining as the wettability is changing towards neutral-wet. The low S_{or} value for B4 (Table 7.6Table 7.8 may also suggest a greater wettability alteration compared to B1-B3.

7.4 Low salinity (LS) waterflooding

After SSW injection, the LS brine was injected utilizing the rate sequence and temperatures in accordance with SSW flooding. The LS procedure was similar for all the cores. It was of interest to explore the potential of LS in Bentheimer sandstone after a conventional SSW injection (tertiary mode) and also the temperature influence on the recovery.

7.4.1 Oil recovery from LS

The important experimental parameters from LS injection are listed in Table 7.8. There was no response to LS in three of the four core samples (B1, B2 and B3). One of the core samples however, showed a positive response to injection of LS. There was no response by injection of LS at lower rates, though at 1 mL/min an incremental recovery of 1.71% OOIP was observed, resulting in a residual oil saturation, $S_{or,LS}$, of 0.250.

Table 7.8 Experimental results (LS)

Core ID	LS Incremental Recovery [% OOIP]	Total Recovery after LS [% OOIP]	$S_{or.LS}$	$\Delta S_{or.LS}$ ($S_{or,SSW}$ - $S_{or,LS}$)	k_{rw} ($S_{or,LS}$)
B1	0.00 ±0.05	61.00 ±0.05	0.333 ±0.002	0.000 ±0.003	0.29 ±0.05
B2	0.00 ±0.05	54.33 ±0.05	0.391 ±0.002	0.000 ±0.003	0.18 ±0.03
B3	0.00 ±0.05	57.85 ±0.05	0.355 ±0.002	0.000 ±0.003	0.235 ±0.006
B4	1.71 0.05	71.29 0.05	0.250 ±0.002	0.015 ±0.003	0.24 ±0.01

7.4.2 Observations

The pressure profile during the experiments conducted on core samples B2 and B3 during LS shows a minor reduction in pressure compared to the SSW injection at the same rate (see Figure 7.2 and Figure 7.3). However, as can be seen from Figure 7.4, a slight increase in the pressure during LS compared to SSW at the same rate was observed for B4. The increase in pressure may contribute to the increase in oil recovery.

A change in the end point relative permeability before and after LS injection may indicate a change in the wettability of the core sample. Figure 7.6 shows the change in the end point relative permeability of water, k_{rw}, before and after LS injection for each of the core samples. For B1, B2 and B3 k_{rw} increases during LS injection. This change in k_{rw} may be explained by relocation of the residual oil

trapped in the core samples, although it most likely implies a change in wettability towards more oil-wet. The same change in wettability was made by Sandengen et al. [69] in their work with reservoir cores and fluids. They explained the wettability alteration due to ionic exchange, however in their research this leads to an increase in the oil recovery.

Due to the decrease in S_{or} in B4 one would expect the relative permeability to water to increase (see Figure 2.9). However, k_{rw} decreases during LS injection for B4. This decrease in k_{rw} could be explained by swelling of clay, fines migration or a change in wettability towards more water-wet (see Figure 2.9).

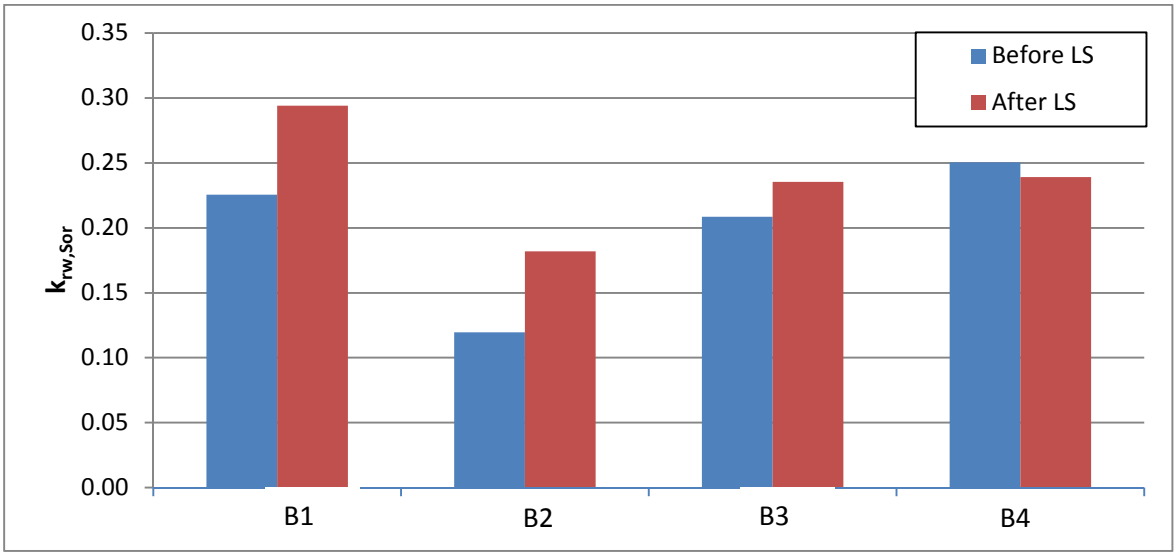

Figure 7.6 Comparison of the k_{rw} (S_{or}) before and after LS injection for the four core samples (B1-B4)

If swelling of clay is significant, it will influence the pressure profile. The pressure build up across the core will most likely be notable and increase monotonically [20]. As can be seen from Figure 7.4, the differential pressure during LS is stabilizing at each rate and not increasing. This implies that it is most likely not clay swelling being responsible for the decrease in k_{rw} of B4. In addition, the clay content in the Bentheimer sandstones seems to be marginal, see Table 6.1.

Migration of fines and subsequent blocking of the pore can reduce the endpoint relative permeability to water [94]. If fines migration is responsible for the reduction in k_{rw} of B4, this may be observed as fluctuation and increase in the pressure profile. As mention, the pressure profile is stabilizing at each rate and not alternating during LS injection in B4, fines migration is most likely not responsible for the decrease in k_{rw}. No fine production was observed in any of the experiments.

It appears that a change in wettability towards more water-wet is the most reasonable mechanism behind the decrease in k_{rw} in B4. A change in wettability towards more water-wet was also observed by e.g. Tang and Morrow [4].

The temperature seems to have insignificant impact on the oil recovery in both SSW injection and LSW. This can be illustrated by the oil recovery of B1 and B2 (90°C) compared with B3 and B4 (23°C) in Table 7.8.

The pH of the effluent was measured during the LS injection conducted in core samples B1, B2 and B3 (Figure 7.7). No significant variation in the pH of the effluent was observed. The pH of the effluent from core sample B4 was unfortunately not measured during LS injection. However, the pH value of the effluent after LS injection (start of LS-S injection, see Figure 7.8) was measured to approximately 8. This indicates that the pH of the effluent may also be stable during LS injection in core sample B4.

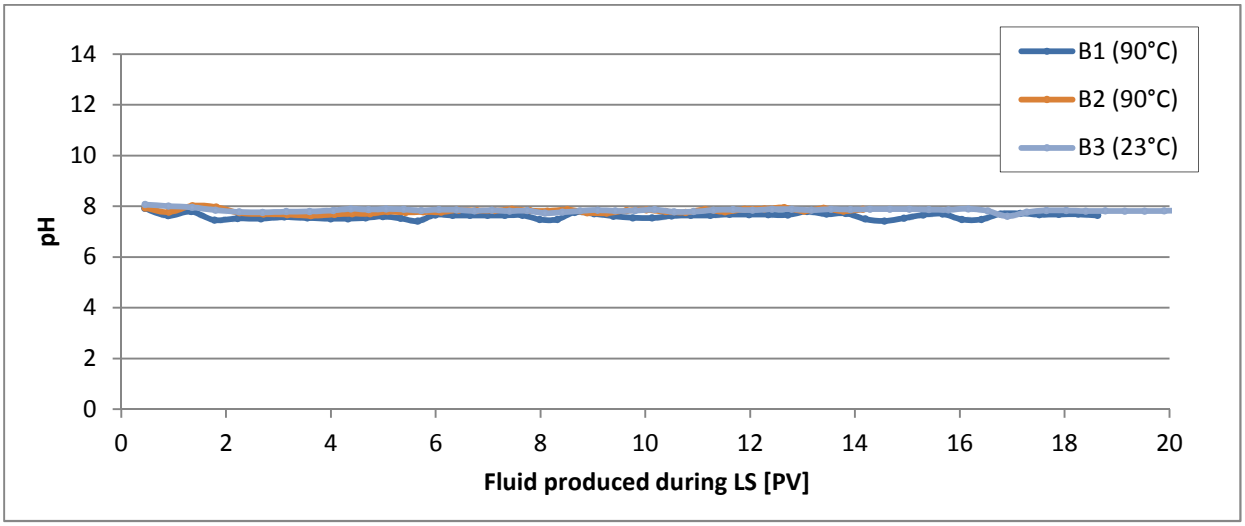

Figure 7.7 **Comparison of effluent pH during LS flooding in B1-B3 (the pH of B4 was not measured during LS injection). The pH is given as a function of fluid produced during LS injection.**

The change in pH is associated with the clay fraction in the rock material. The lack of pH variation may give an indication that the amount of clay content in the Bentheimer sandstone is not enough to change the pH. Previous studies has also characterized the Bentheimer sandstone to contain less clay than e.g. Berea sandstone [4, 25].

As identified by Tang and Morrow [4] one necessary condition for LSE is the presence of a significant amount of clay in the rock material. The XRD measurements conducted on a small Bentheimer sample (see Table 6.1 and Figure 6.2) may also imply the lack of clay content (Illite+Mica, Kaolinite and Chlorite) in the Bentheimer sandstone.

Another important consideration for LSE is the exposure to crude oil in order to change the initial wettability condition. The change in wettability during the aging process may not be as sufficient for all the core samples. E.g. the core sample B4 seems to have had a greater change in wettability compared to B2 and B3 (see Figure 7.5). This may explain why LS had a positive effect in core sample B4 and not in B1-B3. In other words, the aging process may have a great influence on the LSE.

7.5 Low salinity surfactant (LS-S) flooding

Following LS brine injection, the core samples were continuously flooded with LS-S brine. The LS-S procedure was similar for all the cores. It was of interest to explore the surfactant ability to remobilise and produce remaining oil left behind after SSW and LS injection and also the temperature influence on the recovery.

7.5.1 Residual saturation after LS-S

The residual oil saturation after LS-S, $S_{or,LS\text{-}S}$, was encountered by two separate methods; (1) calculated by mass balance during the experiments and (2) calculated by the principle of Mohr's titration, see Table 7.9. By using the principle of Mohr's titration gave rise to a high uncertainty. Thus, the $S_{or,LS\text{-}S}$ calculated by the mass balance will be further used.

Table 7.9 Residual saturation after LS-S by both mass balance and Mohr's titration

Core ID	$S_{or.LS\text{-}S}$ (by mass balance)	$S_{or.LS\text{-}S}$ (by Mohr's titration)
B1	0.266 ±0.002	0.12 ±0.06
B2	0.233 ±0.002	0.4 ±0.2
B3	0.135 ±0.002	0.2 ±0.1
B4	0.095 ±0.002	0.18 ±0.09

7.5.2 Oil recovery

Important experimental parameters from the core samples conducted after LS-S injection are given in Table 7.10. Continuous injection of LS-S gave rise to a high recovery of oil. When comparing the difference in recovery of the four core samples it is important to be aware of the difference in the experiments:

- *Temperature.* Coreflood experiments on B1 and B2 were conducted at a temperature of 90°C, while the coreflood experiments on B3 and B4 were conducted at a temperature of 23°C.
- *Crude oils.* Coreflood experiments on B1 and B4 were conducted with a slightly more viscous crude oil then the one used in B2 and B3. This will have an impact on the mobility ratio, M^0, between the oil and the brine.

Table 7.10 Experimental results (LS-S)

Core ID	LS-S Incremental Recovery [% OOIP]	Total Recovery after LS-S [% OOIP]	$S_{or.LS-S}$	$\Delta S_{or.LS-S}$ ($S_{or,LS}$ - $S_{or,LS-S}$)	k_{rw} ($S_{or,LS-S}$)
B1	7.87 ±0.05	68.87 ±0.05	0.266 ±0.002	0.067 ±0.003	0.25 ±0.04
B2	18.44 ±0.05	72.78 ±0.05	0.233 ±0.002	0.158 ±0.003	0.09 ±0.01
B3	26.18 ±0.05	84.03 ±0.05	0.135 ±0.002	0.220 ±0.003	0.124 ±0.003
B4	17.78 0.05	89.07 0.05	0.095 ±0.002	0.155 ±0.003	0.046 ±0.002

7.5.3 Observations

During the LS-S injection, formation of emulsion was observed in all the four core samples, hence Figure 6.9 (before addition of salt). A reduction in endpoint relative permeability is observed from LS to LS-S. This is most likely because of the formation of emulsion which may clog the pores which in turn reduces the endpoint relative permeability.

Overall comparison of the recoveries reveals that B3 and B4 have a higher total recovery then B1 and B2. This temperature impact on the system reveals that the system becomes less effective with high temperatures. This may be explained by the observations made when measuring the pH of the effluent during LS-S injection.

The pH of the effluents from B3 and B4 are relatively stable during the injection of LS-S (flooding conducted at 23°C). On the other hand, the pH of the effluents from B1 and B2 are decreasing significantly during the injection of LS-S (flooding conducted at 23°C), see Figure 7.8. The acidic environment is most likely caused by hydrolysis of the surfactant at elevated temperature (see section 5.3). Even though the surfactant system was only exposed to the high temperature (90°C) for short period of time (at most ten hours), this was sufficient to destabilize the surfactant. This may explain why the recovery decreases with high temperatures.

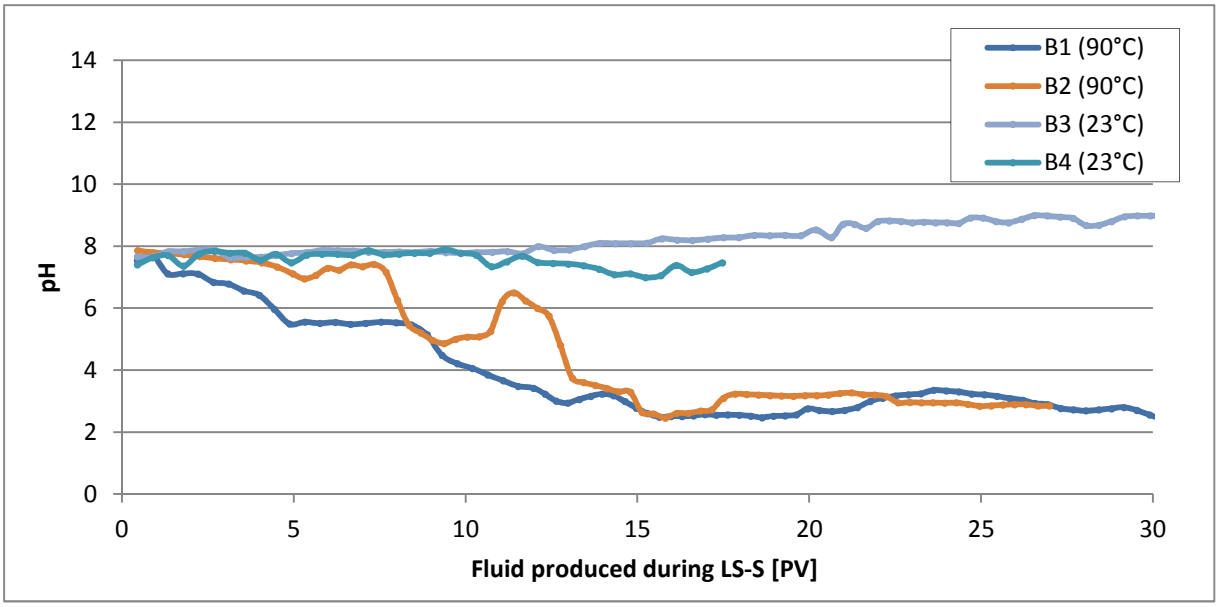

Figure 7.8 **Comparison of effluent pH during LS-S flooding in B1-B4. The pH is given as a function of fluid produced during LS-S injection.**

The impact of the crude oil may explain the difference in $\Delta S_{or,LS\text{-}S}$ in the two parallels (B1/B2 and B3/B4). As mentioned above, B1 and B4 were conducted using a slightly more viscous crude oil then the one used in B2 and B3. This difference will affect the mobility to oil, the less viscous crude oil will contribute to higher oil mobility, hence have a positive impact on the mobility ratio, M^0.

The mobility ratios shown in Table 7.11 demonstrate that M^0 is consistently much lower for B2 compared to B1. This may be the cause of the higher recovery and also higher $\Delta S_{or,LS\text{-}S}$ for B2. For B3/B4 parallel it is slightly different. The M^0 is consistently lower for B4 then B3. This is due to the low mobility to water in B4, caused by the low k_{rw}. However the lower viscosity of the oil will contribute to a more favourable M^0 in B3. Another contributing aspect of the recovery is the capillary number which will be further discussed in the next section.

Table 7.11 **Mobility ratios, M^0, during SSW, LS, and LS-S flooding**

Core ID	M^0_{SSW}	M^0_{LS}	$M^0_{LS\text{-}S}$
B1	1.3 ±0.3	1.6 ±0.3	1.5 ±0.3
B2	0.7 ±0.1	1.1 ±0.2	0.6 ±0.1
B3	0.7 ±0.1	0.8 ±0.1	0.41 ±0.07
B4	0.7 ±0.1	0.7 ±0.1	0.13 ±0.02

7.5.4 Capillary Desaturation Curve

The capillary number, N_{vc}, represents the ratio of the viscous force to the capillary force acting on S_{or} and a CDC express S_{or} as a function of N_{vc}. The N_{vc} during LS and LS-S are listed in Table 7.12 together with their residual oil saturation of the four core samples.

Maldal et al. [95] studied CDC for different Bentheimer sandstones and found that when changing wettability from strongly water-wet to mixed-wet condition resulted in a significant decrease of remaining oil for low capillary numbers. This is illustrated as the black curves in Figure 7.9. Another interesting observation by Maldal et al., was that changing the temperature, pressure and fluid system did not alter the CDC.

Table 7.12 **Residual oil saturation, S_{or}, and capillary number, N_c, during LS and LS-S injection on B1, B2, B3 and B4. The capillary number calculated for the LS injection was based on an 25 mN/m IFT between the diluted crude oil and the LS brine.**

Core ID	$S_{or,LS}$	N_{vc} (LS)	$S_{or,LS-S}$	N_{vc} (LS-S)
B1	0.333 ±0.002	$2.0 \cdot 10^{-7}$ $\pm 0.3 \cdot 10^{-7}$	0.266 ±0.002	$2.7 \cdot 10^{-6}$ $\pm 0.5 \cdot 10^{-6}$
B2	0.391 ±0.002	$2.0 \cdot 10^{-7}$ $\pm 0.3 \cdot 10^{-7}$	0.233 ±0.002	$1.9 \cdot 10^{-6}$ $\pm 0.3 \cdot 10^{-6}$
B3	0.355 ±0.002	$5.67 \cdot 10^{-7}$ $\pm 0.3 \cdot 10^{-7}$	0.135 ±0.002	$9.8 \cdot 10^{-5}$ $\pm 0.4 \cdot 10^{-5}$
B4	0.250 ±0.002	$5.67 \cdot 10^{-7}$ $\pm 0.3 \cdot 10^{-7}$	0.095 ±0.002	$4.0 \cdot 10^{-5}$ $\pm 0.2 \cdot 10^{-5}$

By comparing the N_{vc} (LS-S) of the two parallels, N_{vc} is higher for B2 compared to B1 and similar higher for B3 compared to B4.This is due to the different IFT of the crude oil used. By looking at Table 7.3 the IFT is slightly lower for DC1 (diluted crude oil utilized in B1 and B4) compared to DC2 (diluted crude oil utilized in B2 and B3).

The shape of CDC is strongly dependent on the wettability of the core material, hence illustrated by Maldal et al. [95] in Figure 7.9. The CDC of the four core samples are illustrated as the coloured curves in Figure 7.9. These curves would seem to suggest that the core samples have wettability state in between the strongly water-wet and neutral-wet conditions. However the location of the CDC for B4 may be associated with a less water-wet state than for B1-B3, which supports the idea that the wettability state of B4 differs from the other core samples.

Even though there was no oil production in B1-B3 and marginal oil production in B4, oil may be redistributed due to changes in the COBR interactions taking place during LS injection. When the capillary forces are reduced during a LS-S injection, this redistribution could give rise to a higher oil recovery than by surfactant injection alone. This may be illustrated by the steep change in S_{or} by injection of LS-S compared to the black curves in Figure 7.9.

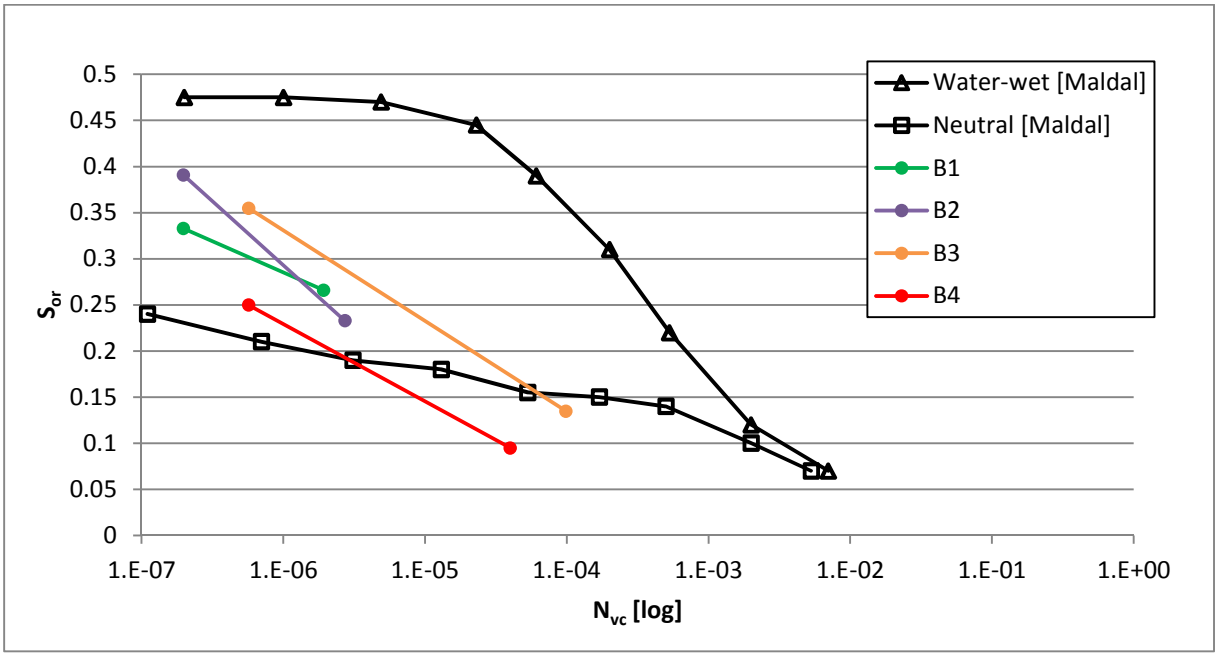

Figure 7.9 **CDC for Bentheimer sandstone. The two black curves from Maldal [95] illustrates the wettability impact on the CDC. The curves in colours represent B1-B4.**

8 Conclusion

The potential for enhanced oil recovery by combined low salinity and low salinity surfactant flooding in four Bentheimer sandstones have been investigated through laboratory measurements. Results indicate that the potential of enhanced oil recovery by injection of low salinity (LS) brine is marginal (incremental recoveries of less than 2% OOIP), whereas low salinity surfactant (LS-S) injection gave significant increase in the oil recovery (incremental recoveries of 8-26% OOIP).

The lack of oil production during LS injection in this study is believed to be related to insufficient wettability alteration prior to the waterflood and/or poor amount of clay present in Bentheimer. No change in pH of the effluent was observed during LS injection.

The temperature has little effect on the oil recovery during LS injection, however, during LS-S injection, both the pH and oil recovery decreased at elevated temperature. This implies a destabilization of the surfactant at higher temperature (hydrolysis).

Despite the insignificant response to low salinity brine, oil may however be redistributed due to changes in crude oil/rock/brine interactions taking place during low salinity injection. By reducing the capillary forces by injection of surfactant, this redistribution may give rise to an increase in the oil recovery beyond the oil recovery by surfactant flooding alone.

9 Further work

Despite growing interest in low salinity waterflooding, there are still many aspects of the underlying mechanisms that need further investigation. Here are some actions to implement in order to gain a better insight of the low salinity and low salinity surfactant mechanisms:

- A comprehensive wettability study. Initial wettability and wettability alteration during low salinity waterflooding are two major factors influencing the recovery by low salinity injection. The wettability state of the core material can be measured quantitative (e.g. by Amott method [30] or USBM method [96]) or a measurement of the wettability from fractional and mixed-wettability core samples with the nuclear magnetic relaxation (NMR) method [97].
- Obtain a picture of the saturation distribution in the core sample by using in-situ x-ray measurements. This is of importance in order to locate the residual oil saturation and the source of the oil produced.
- To optimize the low salinity surfactant recovery it is of importance to examine the surfactant phase behaviour and temperature dependence prior to the waterflooding.
- Extensive effluent analysis, such as ion and fines analysis should be carried out in order to obtain a better understanding of the mechanisms behind the low salinity and low salinity surfactant process.
- In addition, a comparison between surfactant in low salinity solution and surfactant in synthetic sea water, in both secondary and tertiary mode, will provide a greater understanding.

10 References

1. Zolotuchin, A.B. and J.-R. Ursin. (2000). "*Introduction to petroleum reservoir engineering*". Høyskoleforl. Kristiansand. 407
2. Tang, G.Q. (1998). "*Brine composition and waterflood recovery for selected crude oil/brine/rock systems*". University of Wyoming. 22597-PA
3. Tang, G. and N. Morrow. (1996) "*Effect of temperature, salinity and oil composition on wetting behavior and oil recovery by waterflooding*". in *SPE annual technical conference*. Denver CO.
4. Tang, G.Q. and N.R. Morrow. (1999). "*Influence of brine composition and fines migration on crude oil/brine/rock interactions and oil recovery".* Journal of Petroleum science and Engineering. 24. 99-111
5. Tang, G. and N.R. Morrow. (2002). "*Injection of dilute brine and crude oil/brine/rock interactions".* Geophysical monograph. 129. 171-179
6. Morrow, N.R., et al. (1998). "*Prospects of improved oil recovery related to wettability and brine composition".* Journal of Petroleum science and Engineering. 20. 267-276
7. Tang, G. and N. Morrow. (1997). "*Salinity, temperature, oil composition, and oil recovery by waterflooding".* SPE Reservoir Engineering. 12. 269-276
8. Zhang, Y. and N. Morrow. (2006) "*Comparison of Secondary and Tertiary Recovery With Change in Injection Brine Composition for Crude-Oil/Sandstone Combinations*".
9. Yildiz, H.O. and N.R. Morrow. (1996). "*Effect of brine composition on recovery of Moutray crude oil by waterflooding".* Journal of Petroleum science and Engineering. 14. 159-168
10. Zhou, X., et al. (1995). "*The effect of crude-oil aging time and temperature on the rate of water imbibition and long-term recovery by imbibition".* SPE Formation Evaluation. 10. 259-266
11. Morrow, N. and J. Buckley. (2011). "*Improved Oil Recovery by Low-Salinity Waterflooding".* Journal of Petroleum Technology. 63. 106-112
12. Zhang, Y., X. Xie, and N. Morrow. (2007). "*Waterflood performance by injection of brine with different salinity for reservoir cores".* Society of Petroleum Engineers. 109849-MS.
13. Webb, K., A. Lager, and C. Black. (2008) "*Comparison of high/low salinity water/oil relative permeability*". in *the International Symposium of the Society of Core Analysts*. Abu Dhabi: BP Exploration.
14. James C. Seccombe, S., Arnaud Lager, SPE, Kevin Webb, SPE, Gary Jerauld, SPE, and Esther Fueg, SPE, BP. (2010). "*Demonstration of Low-Salinity EOR at Interwell Scale, Endicott Field, Alaska".* SPE129692.
15. James C. Seccombe, S., Arnaud Lager, SPE, Kevin Webb, SPE, Gary Jerauld, SPE, and Esther Fueg, SPE, BP. (2008). "*Improving Wateflood Recovery: LoSalTM EOR Field Evaluation".* SPE113480.
16. Lager, A., et al. (2008) "*LoSal enhanced oil recovery: Evidence of enhanced oil recovery at the reservoir scale*". in *SPE/DOE Symposium on Improved Oil Recovery*. Tulsa, Oklahoma, USA: Society of Petroleum Engineers.
17. Lager, A., et al. (2006). "*Low Salinity Oil Recovery-An Experimental Investigation1".* Petrophysics. 2008-v49n1a2. 49.
18. Alagic, E. (2010). "*Combination of low salinity water flooding with surfactant injection: a new hybrid EOR process*". PhD Dissertation. University of Bergen. Department of Chemistry
19. Alagic, E. and A. Skauge. (2010). "*Combined Low Salinity Brine Injection and Surfactant Flooding in Mixed−Wet Sandstone Cores".* Energy & Fuels. 10.1021/ef1000908. 24. 3551-3559
20. Edin Alagic, K.S., Arne Skauge, Jonas Solbakken. (2011). "*Effect of crude oil aging on low salinity and low salinity surfactant flooding".* Journal of Petroleum science and Engineering.

21. McGuire, P., et al. (2005) "*Low Salinity Oil Recovery: An Exciting New EOR Opportunity for Alaska? s North Slope*".SPE Western Regional Meeting. California. 93903-MS
22. Webb, K., C. Black, and H. Al-Ajeel. (2004) "*Low Salinity Oil Recovery-Log-Inject-Log*". in *SPE/DOE Symposium on Improved Oil Recovery*. Tulsa, Oklahoma: Society of Petroleum Engineers.
23. Webb, K., C. Black, and I. Edmonds. (2005) "*Low salinity oil recovery-the role of reservoir condition corefloods*". in *European Association of Geoscientists and Engi neers, presented at 13th European Symposium on Improved Oil Recovery.*
24. Spildo, K., A. Johannessen, and A. Skauge. (2012) "*Low Salinity Waterflood at Reduced Capillarity*". in *SPE Improved Oil Recovery Symposium*. Tulsa, Oklahoma, USA.
25. Skauge, B.S.S.a.A. (2012). "*Wettability and Oil Recovery by Low Salinity Injection".* SPE EOR Conference at Oil and Gas West Asia, 16-18 April 2012, Muscat, Oman.
26. Bernard, G. (1967) "*Effect of floodwater salinity on recovery of oil from cores containing clays*". in *SPE California Regional Meeting*. Los Angeles, California: Society of Petroleum Engineers.
27. Martin, J. (1959) "*The Effects of Clay on the Displacement of Heavy Oil by Water*". In SPE Venezuelan Annual Meeting. 1411-G
28. Jadhunandan, P.P., N.M.I.o. Mining, and T.D.o.P. Engineering. (1990). "*Effects of brine composition, crude oil, and aging conditions on wettability and oil recovery*". Department of Petroleum Engineering, New Mexico Institute of Mining & Technology.
29. Jadhunandan, P. and N. Morrow. (1995). "*Effect of wettability on waterflood recovery for crude-oil/brine/rock systems".* SPE Reservoir Engineering. 10. 40-46
30. Amott, E. (1959). "*Observations relating to the wettability of porous media".* Trans, AIME. 216. 156-162
31. RezaeiDoust, A., et al. (2009). "*Smart Water as Wettability Modifier in Carbonate and Sandstone: A Discussion of Similarities/Differences in the Chemical Mechanisms".* Energy & Fuels. 23. 4479-4485
32. Ali A. Yousef, S.A.-S., and Mohammed Al-Jawfi, Saudi Aramco. (2012). "*The Impact of the Injection Water Chemistry on Oil Recovery from Carbonate Reservoirs".* SPE EOR Conference at Oil and Gas West Asia, 16-18 April 2012, Muscat, Oman. SPE 154077.
33. Yousef, A., S. Al-Saleh, and M. Al-Jawfi. (2012) "*Improved/Enhanced Oil Recovery from Carbonate Reservoirs by Tuning Injection Water Salinity and Ionic Content*". SPE Improved Oil Recovery Symposium. Tulsa, Oklahoma, USA. 154076-MS
34. Yousef, A., et al. (2010) "*Laboratory investigation of novel oil recovery method for carbonate reservoirs*". Canadian Unconventional Resources and International Petroleum Conference. Calgary, Canada. 137634-MS
35. Yousef, A., et al. (2011). "*Laboratory Investigation of the Impact of Injection-Water Salinity and Ionic Content on Oil Recovery From Carbonate Reservoirs".* SPE Reservoir Evaluation & Engineering. 14. 578-593
36. Yousef, A., S. Al-Salehsalah, and M. Al-Jawfi. (2011) "*New Recovery Method for Carbonate Reservoirs through Tuning the Injection Water Salinity: Smart WaterFlooding*". SPE EUROPEC/EAGE Annual Conference and Exhibition. Vienna, Austria. 143550-MS
37. Yousef, A., S. Al-Saleh, and M. Al-Jawfi. (2011) "*Smart WaterFlooding for Carbonate Reservoirs: Salinity and Role of Ions*". SPE Middle East Oil and Gas Show and Conference. Manama, Bahrain. 141082-MS
38. Siyambalagoda Gamage, P. and G. Thyne. (2011) "*Comparison of Oil Recovery by Low Salinity Waterflooding in Secondary and Tertiary Recovery Modes*". SPE Annual Technical Conference and Exhibition. Denver, Colorado.147375-MS
39. Skrettingland, K., et al. (2011). "*Snorre Low-Salinity-Water Injection--Coreflooding Experiments and Single-Well Field Pilot".* SPE Reservoir Evaluation & Engineering. 14. 182-192

40. Filoco, P. and M. Sharma. (1998) "*Effect of Brine Salinity and Crude Oil Properties on Relative Permeabilities and Residual Saturations*". SPE Annual Technical Conference and Exhibition, New Orleans, Louisiana. 49320-MS
41. Friedman, F. (1986) "*Surfactant and Polymer Losses During Flow through Porous Media. Pres, at Soc. Pet. Eng*". SPE Reservoir Engineering. 11779-PA
42. Craig, F.F., E.S.o. Petroleum, and F.H.L.D. Memorial. (1971). "*The reservoir engineering aspects of waterflooding*". HL Doherty Memorial Fund of AIME.
43. Anderson, W. (1986). "*Wettability literature survey-part 1: rock/oil/brine interactions and the effects of core handling on wettability".* Journal of Petroleum Technology. 38. 1125-1144
44. Anderson, W. (1986). "*Wettability literature survey-part 2: Wettability measurement".* Journal of Petroleum Technology. 38. 1246-1262
45. Anderson, W.G. (1987). "*Wettability literature survey-part 4: Effects of wettability on capillary pressure".* Journal of Petroleum Technology. 39. 1283-1300
46. Skauge, A., et al. (2007). "*Theoretical and experimental evidence of different wettability classes".* Journal of Petroleum science and Engineering. 57. 321-333
47. Raza, S.H., L.E. Treiber, and D.L. Archer. (1968). "*Wettability of reservoir rocks and its evaluation".* Journal Name: Prod. Mon.; (United States); Journal Volume: 32:4. Medium: X; Size: Pages: 2-4, 6-7
48. Jerauld, G. and J. Rathmell. (1997). "*Wettability and relative permeability of prudhoe bay: a case study in mixed-wet reservoirs".* SPE Reservoir Engineering. 12. 58-65
49. Hamon, G. (2000) "*Field-wide variations of wettability*". SPE Annual Technical Conference and Exhibition. Dallas, Texas. 63144-MS
50. Rueslatten, H., et al. (1994) "*A combined use of cryo-SEM and NMR-spectroscopy for studying the distribution of oil and brine in sandstones*". SPE/DOE Improved Oil Recovery Symposium. Tulsa, Oklahoma. 27804-MS
51. Skauge, A. (2011). "*Selected Topics in Petroleum Engineering*". Lecture note in PTEK312. University of Bergen. Bergen
52. Skauge, A. and B. Ottesen. (2002) "*A summary of experimentally derived relative permeability and residual saturation on North Sea reservoir cores*". International symposium of the Society of Core Analysts. California. SCA202-12
53. Ashraf, A., et al. (2010) "*Laboratory investigation of low salinity waterflooding as secondary recovery process: effect of wettability*". SPE Oil and Gas India Conference and Exhibition. Mumbai, India. 129012-MS
54. Owens, W. and D.L. Archer. (1971). "*The effect of rock wettability on oil-water relative permeability relationships".* Journal of Petroleum Technology. 23. 873-878
55. Buckley, J., Y. Liu, and S. Monsterleet. (1998). "*Mechanisms of wetting alteration by crude oils".* SPE Journal. 3. 54-61
56. Graue, A. (2006). "*Experimental Resevoir Physics, PTEK214*". University of Bergen
57. Lake, L.W. (1989). "*Enhanced oil recovery*". Prentice Hall. University of Texas at Austin
58. Odeh, A.S. (1958). "*Effect of viscosity ratio on relative permeability*". AIME. 216, 346-53
59. Jan R. Lien, M.J.o.A.S. (2007). "*Introduksjon til petroleums- og prosessteknologi, PTEK100*". University of Bergen
60. Becke, A.D. (1992). "*Density-functional thermochemistry. I. The effect of the exchange-only gradient correction".* The Journal of Chemical Physics. 96. 2155
61. Torsæter, O. and M. Abtahi. (2003). "*Experimental reservoir engineering laboratory workbook*". Department of Petroleum Engineering and Applied Geophysics, Norwegian University of Science and Technology. [Trondheim].
62. Bavière, M. (1991). "*Basic concepts in enhanced oil recovery processes*". Published for the Society of Chemical Industry by Blackwell. Oxford.
63. Skauge, M.S.A. (2009). "*Reservoarteknikk II, PTEK213*". University of Bergen

64. Donaldson, E.C. and G.V. Chilingar. (1985). "*Enhanced Oil Recovery: Fundamentals and analysis*". Elsevier Science Ltd.
65. Chatzis, I., N. Morrow, and H. Lim. (1983). "*Magnitude and detailed structure of residual oil saturation".* Old SPE Journal. 23. 311-326
66. Lake, L. (1984) "*A Technical Survey of Micellar Polymer Flooding*". Presented at EOR, a symposium for the Independent Producer, Southern Methodis University, Dallas, Texas
67. Hirasaki, G. (1991). "*Wettability: fundamentals and surface forces".* SPE Formation Evaluation. 6. 217-226
68. Ligthelm, D., et al. (2009) "*Novel Waterflooding Strategy By Manipulation Of Injection Brine Composition*". EUROPEC/EAGE Conference and Exhibition. Amsterdam, Netherlands. 119835-MS
69. Sandengen, K. (2011). "*Experimental evidence of low salinity water flooding yielding a more oil-wet behaviour".* Paper presented at The International Symposium of the Society of Core Analysts held in Austin, Texas, USA 18-21 September, 2011.
70. Austad, T., A. Rezaeidoust, and T. Puntervold. (2010) "*Chemical mechanism of low salinity water flooding in sandstone reservoirs*". SPE Improved Oil Recovery Symposium. Tulsa, Oklahoma, USA. 129767-MS
71. Dezabala, E., et al. (1982). "*A chemical theory for linear alkaline flooding".* Old SPE Journal. 22. 245-258
72. Jerauld, G., et al. (2006) "*Modeling low-salinity waterflooding*". SPE Annual Technical Conference and Exhibition. San Antonio, Texas, USA. 102239-MS
73. Winoto, W., et al. (2012) "*Secondary and Tertiary Recovery of Crude Oil from Outcrop and Reservoir Rocks by Low Salinity Waterflooding*". SPE Improved Oil Recovery Symposium. Tulsa, Oklahoma, USA. 154209-MS
74. Arnarson, T.S. and R.G. Keil. (2000). "*Mechanisms of pore water organic matter adsorption to montmorillonite".* Marine Chemistry. 71. 309-320
75. Sposito, G. (1989). "*The chemistry of soils*". Oxford University Press, USA. 275
76. Solbakken, J.S. (2010). "*An experimental study of low salinity surfactant floodingin low permeability Berea Sandstone*". Master's Thesis. University of Bergen
77. Vledder, P., et al. (2010) "*Low Salinity Water Flooding: Proof Of Wettability Alteration On A Field Wide Scale*". SPE Improved Oil Recovery Symposium. Tulsa, Oklahoma, USA. 129564
78. Mahani, H., et al. (2011) "*Analysis of field responses to low-salinity waterflooding in secondary and tertiary mode in Syria*". SPE EUROPEC/EAGE Annual Conference and Exhibition. Vienna, Austria. 142960-MS
79. Pashley, R.M. and M.E. Karaman. (2004). "*Applied colloid and surface chemistry*". Wiley. Chichester.
80. Winsor, P.A. (1954). "*Solvent properties of amphiphilic compounds*". Butterworths Scientific Publications.
81. Healy, R., R. Reed, and D. Stenmark. (1976). "*Multiphase microemulsion systems".* Old SPE Journal. 16. 147-160
82. Nelson, R. and G. Pope. (1978). "*Phase relationships in chemical flooding".* Old SPE Journal. 18. 325-338
83. Myers, D. (2006). "*Surfactant science and technology*". Wiley. Hoboken, N.J.
84. Talley, L. (1988). "*Hydrolytic stability of alkylethoxy sulfates".* SPE Reservoir Engineering. 3. 235-242
85. Stephanie Adkins, S., Gayani Pinnawala Arachchilage, SPE, Sriram Solairaj, SPE, Jun Lu, SPE, Upali Weerasooriya, SPE, Gary Pope, SPE, The University of Texas at Austin. (2012). "*Development of Thermally and Chemically Stable Large-Hydrophobe Alkoxy Carboxylate Surfactants".* SPE Improved Oil Recovery Symposium, 14-18 April 2012, Tulsa, Oklahoma, USA.

86. Warren, B.E. (1969). "*X-Ray Diffraction".* Courier Dover Publications, USA.
87. Ritter, H. and L. Erich. (1948). "*Pore size distribution in porous materials".* Analytical Chemistry. 20. 665-670
88. Bøe, S.O. (1998). "*Syre/base eigenskaper til råolje og deira innverknad på fukting i vann-olje-kvarts system*".Master's Thesis. University of Bergen.
89. Vogel, A.I., G.H. Jeffery, and A. Israel. (1989). "*Vogel's textbook of quantitative chemical analysis*". Longman Scientific & Technical Harlow.
90. Hisham T. El-Dessouky, H.M.E. (2002). "*Fundamentals of Salt Water Desalination (Appendix A: Themodynamic Properties)*". Elsevier Science. 424
91. Weast, R.C. (1989). "*CRC Handbook of Chemistry and Physics*". 69th Edition. CRC Press. Florida. p. F-4
92. Bier, D.A. (2010). "*ELECTROCHEMISTRY, Theory and Practice*". Lab Product Application Manager. Hach Company. (Colorado, U.S.)
93. Anderson, W. (1987). "*Wettability literature survey-part 6: The effects of wettability on waterflooding".* Journal of Petroleum Technology. 39. 1605-1622
94. Khilar, K.C. and H.S. Fogler. (1987). "*Colloidally induced fines migration in porous media".* Rev. Chem. Eng. 4. 2
95. Maldal, T., Gilje, E., and Gulbrandsen, A.H. (1997). "*Correlation of Cap. Number Curves and Res. Oil Saturations for Reservoir and Model Sandstones,".* In Situ (1997) 21, No. 3, 239.
96. Donaldson, E. (1981). "*Oil-water-rock wettability measurement".* Am. Chem. Soc., Div. Pet. Chem., Prepr.;(United States). 26.
97. Brown R.I.S., F.I. (1959). "*Measurements of Fractional Wettability of Oilfield Rocks by the Nuclear Magnetic Relaxation Method".* Trans., AIME 207, 262-64.

Appendices

A.1 Density data

Table A. 1 **Measured fluid density data, ρ, and the average density together with the uncertainty, Δρ, of the low salinity surfactant solution (LS-S) and of the two different crude oils (DC1 and DC2) at various temperatures. Three parallels were performed for each fluid**

Temp (°C)	ρ_{LS-S} [g/mL]	$\Delta\rho_{LS-S}$ [g/mL]	ρ_{DC1} [g/mL]	$\Delta\rho_{DC1}$ [g/mL]	ρ_{DC2} [g/mL]	$\Delta\rho_{DC2}$ [g/mL]
23.0	1.0002	1.0002 ±0.0001*	0.8981	0.8980 ±0.0002*	0.9143	0.9143 ±0.0002*
	1.0002		0.8984		0.9145	
	1.0002		0.8983		0.9143	
40.0	0.9946	0.9946 ±0.0001*	0.8840	0.8844 ±0.0004*	0.8852	0.8855 ±0.0004*
	0.9946		0.8843		0.8856	
	0.9946		0.8848		0.8857	
60.0	0.9854	0.9854 ±0.0001*	0.869	0.869 ±0.001*	0.870	0.870 ±0.001*
	0.9854		0.869		0.870	
	0.9855		0.870		0.870	

* The uncertainty is estimated based on the variation in the measured densities

A.2 Interfacial tension data

Table A. 2 **Measured interfacial tension data, σ, and average interfacial tension together with the uncertainty, Δσ, between the low salinity surfactant solution (LS-S) and the two different crude oils (DC1 and DC2) at various temperatures. The σ was measured at four different rotation velocities for each temperature**

T [°C]	Rotation velocity (RPM)	$\sigma_{LS\text{-}S,DC1}$ [mN/m]	$\Delta\sigma_{LS\text{-}S,DC1}$ [mN/m]	$\sigma_{LS\text{-}S,DC2}$ [mN/m]	$\Delta\sigma_{LS\text{-}S,DC2}$ [mN/m]
23.0	3300	0.118	0.116 ±0.006	0.141	0.146 ±0.006
	3400	0.119		0.150	
	3500	0.118		0.155	
	2400	0.109		0.136	
40.0	6000	0.75	0.76 ±0.01	0.78	0.78 ±0.01
	6200	0.79		0.78	
	5800	0.77		0.76	
	6400	0.77		0.78	
60.0	6200	1.22	1.21 ±0.02	1.45	1.46 ±0.02
	6000	1.22		1.47	
	6400	1.19		1.46	
	5800	1.19		1.46	
90.0	-	1.7*	1.7 ±0.1	2.4*	2.4 ±0.1

* Estimated based on extrapolation, see Figure A. 1.

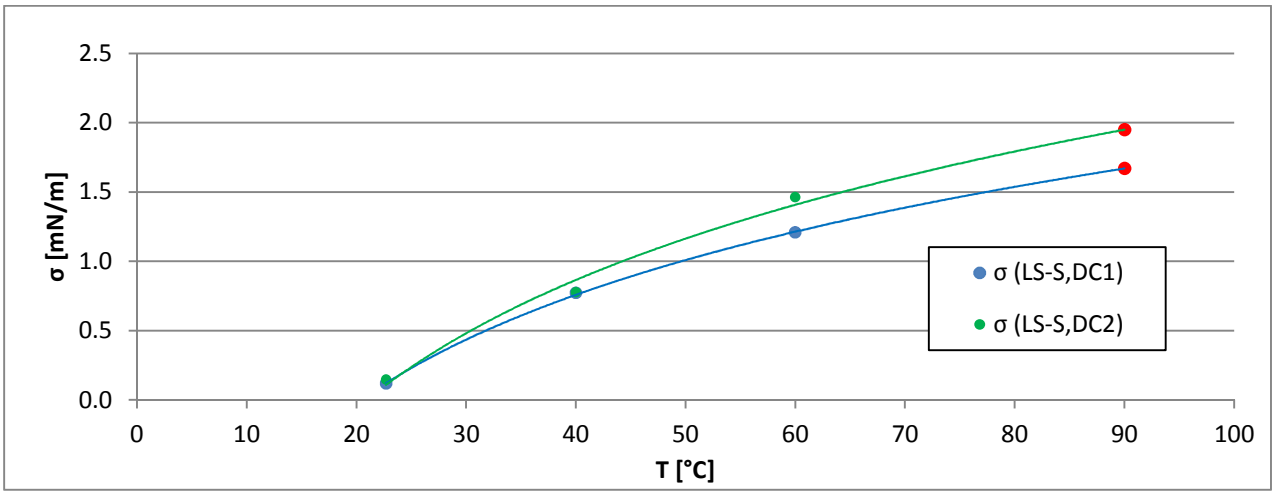

Figure A. 1 **The average interfacial tension (σ) at the different temperatures for both diluted crude oils (DC1 and DC2) are graphed as a function of temperature (T). Logarithmic extrapolation (gave the best curve fitting of the data points) of the function in order to estimate σ at T = 90°C**

A.3 Viscosity data

1) Viscosity of the diluted crude oils:

Table A. 3 **Measured viscosity data, μ, and average viscosity together with the uncertainty, Δμ, of the two different crude oils (DC1 and DC2) at various temperatures. Two parallels were performed for each diluted crude oil.**

T [°C]	μ_{DC1} [mPa·s]	$\Delta\mu_{DC1}$ [mPa·s]	μ_{DC2} [mPa·s]	$\Delta\mu_{DC2}$ [mPa·s]
22	4.3	4.3	4.2	4.3
	4.3	±0.1	4.3	±0.1
40	3.0	3.0	3.0	3.0
	3.0	±0.1	3.0	±0.1
50	2.7	2.7	2.5	2.6
	2.7	±0.1	2.6	±0.1
60	2.5	2.5	2.4	2.5
	2.5	±0.2	2.5	±0.2
70	2.4	2.4	2.2	2.3
	2.4	±0.2	2.4	±0.2
90	2.4*	2.4 ±0.3	2.3*	2.3 ±0.3

* Estimated based on extrapolation, see Figure A. 2.

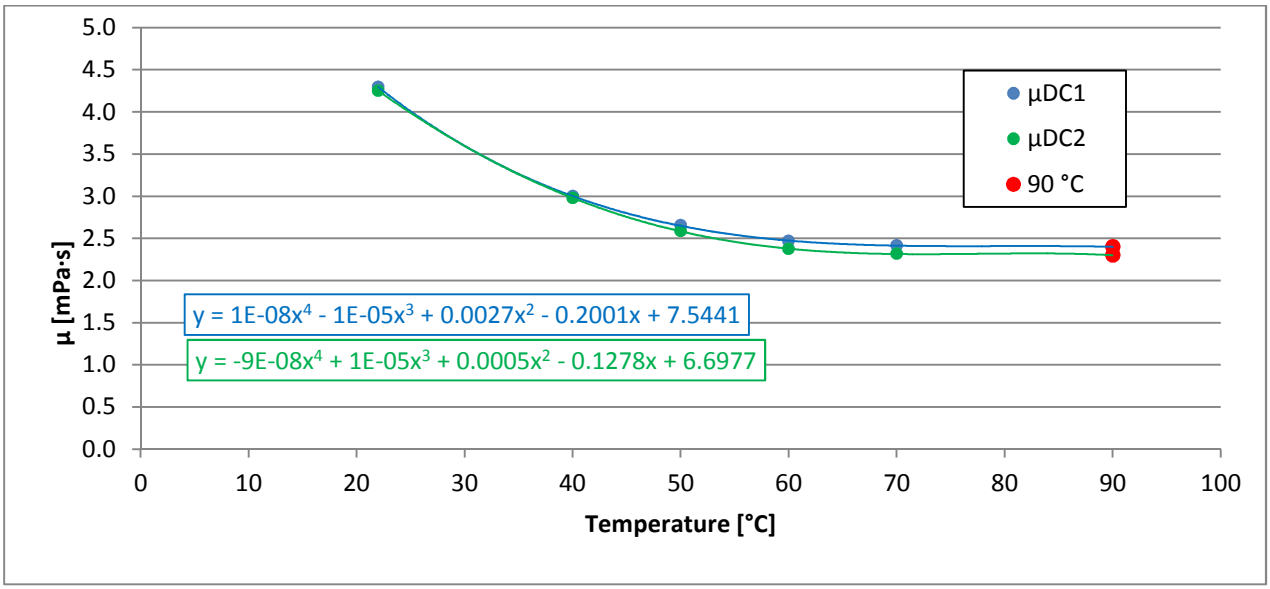

Figure A. 2 **The average viscosity (μ) at the different temperatures for both DC1 and DC2 are graphed as a function of temperature (T). Polynomial extrapolation (gave the best curve fitting of the data points) of the function to estimate μ at T = 90°C**

2) Viscosity of the aqueous solutions:

Table A. 4 **Measured viscosity data, μ, and average viscosity together with the uncertainty, Δμ, of the synthetic sea water (SSW), the low salinity (LS) and the low salinity surfactant solution (LS-S) at various temperatures. Two parallels were performed for each of the aqueous solutions.**

T [°C]	μ_{SSW} [mPa·s]	$\Delta\mu_{SSW}$ [mPa·s]	μ_{LS} [mPa·s]	$\Delta\mu_{LS}$ [mPa·s]	μ_{LS-S} [mPa·s]	$\Delta\mu_{LS-S}$ [mPa·s]
22	1.01	1.01	0.95	0.953	0.97	0.97
	1.01	±0.03	0.957	±0.03	0.97	±0.03
40	0.70	0.71	0.66	0.66	0.71	0.71
	0.71	±0.03	0.66	±0.03	0.71	±0.03
50	0.65	0.65	0.54	0.55	0.57	0.57
	0.65	±0.03	0.56	±0.03	0.57	±0.03
60	0.54	0.54	0.48	0.48	0.55	0.51
	0.54	±0.04	0.49	±0.04	0.51	±0.04
70	0.47	0.47	0.46	0.47	0.46	0.47
	0.46	±0.04	0.48	±0.04	0.47	±0.04
90	0.33*	0.33 ±0.05	0.33*	0.33 ±0.05	0.31*	0.31 ±0.05

* Estimated based on extrapolation, see Figure A. 3.

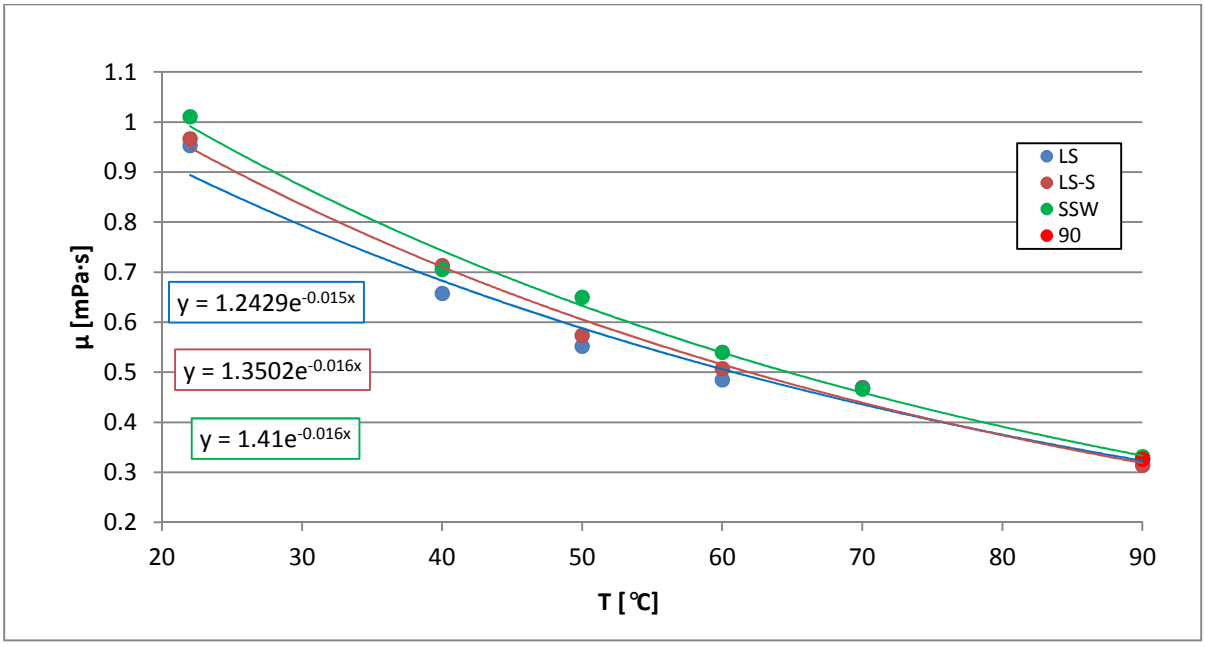

Figure A. 3 **The average viscosity (μ) at the different temperatures for synthetic sea water (SSW), low salinity brine (LS) and low salinity surfactant solution (LS-S) are graphed as a function of temperature (T). Exponential (gave the best curve fitting of the data points) extrapolation of the function to estimate μ at T = 90°C**

A.4 Length and diameter of the core samples

Table A. 5 Measured length and diameter of the core samples

Core ID	Length [cm]	Average length [cm]	Diameter [cm]	Average diameter [cm]
B1	9.910	9.92 ±0.01	3.775	3.775 ±0.005
	9.910		3.780	
	9.920		3.775	
	9.920		3.770	
B2	9.935	9.93 ±0.01	3.775	3.775 ±0.005
	9.940		3.770	
	9.930		3.780	
	9.940		3.775	
B3	9.930	9.92 ±0.01	3.770	3.776 ±0.005
	9.920		3.780	
	9.920		3.775	
	9.915		3.780	
B4	9.935	9.95 ±0.01	3.780	3.779 ±0.005
	9.945		3.775	
	9.960		3.780	
	9.960		3.780	

A.5 Mohr's titration

Table A. 6 Experimental data from Mohr's titration

Core ID	$m_{effluent}$ [g]	$V_{titrant}$ [mL]	c_{CL-} [mol/L]	V_w (in core) [mL]	S_{or} (±50%)
B1	135.7	140	1.0E-02	25	0.12
B2	137.0	100	7.3E-03	18	0.37
B3	135.1	130	9.4E-03	23	0.20
B4	136.0	130	9.5E-03	23	0.18

A.6 Waterflooding experimental data

Table A. 7 Experimental data obtain during waterflooding in B1

Rate [mL/min]	Total injected brine [PV]	Produced oil + dead volume [mL]	Produced oil originally from core sample [PV]	Oil Recovery [% OOIP]	Comments
		±0.1	±0.002	±0.05	
SSW injection					
0.1	0.51	10.7	0.369	43.23	WBT
0.1	3.96	14.8	0.520	61.00	
0.3	25.51	14.8	0.520	61.00	
1.0	31.83	14.8	0.520	61.00	
LS injection					
0.1	38.8	14.8	0.520	61.00	
0.3	40.5	14.8	0.520	61.00	
1.0	50.2	14.8	0.520	61.00	
LS-S injection					
0.1	62.5	14.8	0.520	61.00	
0.3	70.4	14.8	0.520	61.00	
1.0	110.7	16.6	0.587	68.86	

Table A. 8 Experimental data obtain during waterflooding in B2

Rate [mL/min]	Total injected brine [PV]	Produced oil + dead volume [mL]	Produced oil originally from core sample [PV]	Oil Recovery [% OOIP]	Comments
		±0.1	±0.002	±0.05	
SSW injection					
0.1	0.64	12.0	0.424	49.50	WBT
0.1	4.80	12.8	0.454	53.02	
0.3	8.58	12.9	0.458	53.46	
1.0	12.60	13.1	0.466	54.33	
LS injection					
0.1	16.7	13.1	0.466	54.33	
0.3	20.7	13.1	0.466	54.33	
1.0	25.6	13.1	0.466	54.33	
LS-S injection					
0.1	30.6	13.1	0.466	54.33	
0.3	43.8	16.4	0.590	68.82	
1.0	55.1	17.3	0.624	72.78	

Table A. 9 Experimental data obtain during waterflooding in B3

Rate [mL/min]	Total injected brine [PV]	Produced oil + dead volume [mL]	Produced oil originally from core sample [PV]	Oil Recovery [% OOIP]	Comments
		±0.1	±0.002	±0.05	
SSW injection					
0.1	0.53	11.9	0.409	48.53	WBT
0.1	4.94	13.6	0.473	56.08	
0.3	8.47	13.7	0.476	56.52	
1.0	11.72	14.0	0.488	57.85	
LS injection					
0.1	15.76	14.0	0.488	57.85	
0.3	21.15	14.0	0.488	57.85	
1.0	31.62	14.0	0.488	57.85	
LS-S injection					
0.1	52.26	19.9	0.706	83.81	
0.3	56.30	20.0	0.708	84.03	
1.0	63.40	20.0	0.708	84.03	

Table A. 10 Experimental data obtain during waterflooding in B4

Rate [mL/min]	Total injected brine [PV]	Produced oil + dead volume [mL]	Produced oil originally from core sample [PV]	Oil Recovery [% OOIP]	Comments
		±0.1	±0.002	±0.05	
SSW injection					
0.1	0.53	13.4	0.464	53.30	WBT
0.1	6.19	16.2	0.569	65.29	
0.2	10.76	16.8	0.591	67.87	
0.5	22.18	17.1	0.603	69.15	
1.0	27.15	17.2	0.606	69.58	
LS injection					
0.1	31.82	17.2	0.606	69.58	
0.2	35.53	17.2	0.606	69.58	
0.5	39.99	17.2	0.606	69.58	
1.0	50.99	17.6	0.621	71.29	
LS-S injection					
0.1	61.63	20.4	0.763	87.57	